

AFAPL-TR-75-110

12

FL

AD A 025921

# TRANSONIC TWO-DIMENSIONAL FLOW ANALYSIS OF COMPRESSOR CASCADE WITH SPLITTER VANES

*AIRESEARCH MANUFACTURING COMPANY  
A DIVISION OF THE GARRETT CORPORATION  
SKY HARBOR AIRPORT 402 SOUTH 36TH STREET  
PHOENIX, ARIZONA 85034*

DECEMBER 1975

TECHNICAL REPORT AFAPL-TR-75-110  
FINAL REPORT FOR PERIOD 2 JANUARY 1975 - 30 SEPTEMBER 1975

Approved for public release; distribution unlimited

D D C  
RECEIVED  
JUN 22 1976  
RUSSELL

Prepared for  
AIR FORCE AERO PROPULSION LABORATORY

NOTICE

When Government drawings, specifications, or other data are used for any purpose other than in connection with a definitely related Government procurement operation, the United States Government thereby incurs no responsibility nor any obligation whatsoever; and the fact that the government may have formulated, furnished, or in any way supplied the said drawings, specifications, or other data, is not to be regarded by implication or otherwise as in any manner licensing the holder or any other person or corporation, or conveying any rights or permission to manufacture, use or sell any patented invention that may in any way be related thereto.

Publication of this report does not constitute Air Force approval of the report's findings or conclusions. It is published only for the exchange and stimulation of ideas.

This final report was submitted by AiResearch Manufacturing Company of Arizona, under Contract F33615-75-C-1004. The effort was sponsored by the Air Force Aero Propulsion Laboratory, Air Force Systems Command, Wright-Patterson AFB, Ohio under Project 7065, Task 13, and Work Unit 27 with A. J. Wennerstrom/AFAPL/TBC as Project Engineer. P. R. Dodge of AiResearch Manufacturing Company of Arizona was technically responsible for the work.

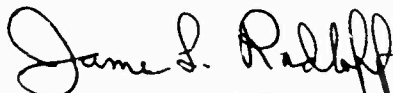
This report has been reviewed by the Information Office, (ASD/OIP and is releasable to the National Technical Information Service (NTIS). At NTIS, it will be available to the general public, including foreign nations.

This technical report has been reviewed and is approved for publication.

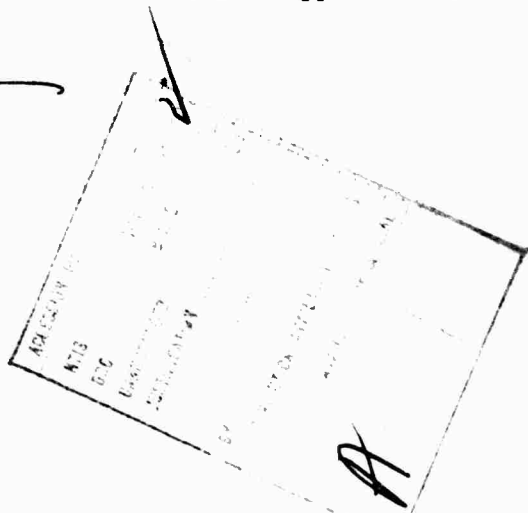


A. J. WENNERSTROM, GS-15  
Project Engineer

FOR THE COMMANDER



JAMES L. RADLOFF, MAJ., USAF  
Chief, Components Branch



Copies of this report should not be returned unless return is required by security considerations, contractual obligations, or notice on a specific document.

Unclassified

SECURITY CLASSIFICATION OF THIS PAGE (When Data Entered)

| REPORT DOCUMENTATION PAGE   |  | READ INSTRUCTIONS<br>BEFORE COMPLETING FORM        |
|---|--|--|
| 1. REPORT NUMBER<br>(15) AFAPL-TR-75-110  | 2. GOVT ACCESSION NO.  | 3. RECIPIENT'S CATALOG NUMBER                      |
| 4. TITLE (and Subtitle)<br>(6) TRANSONIC TWO-DIMENSIONAL FLOW ANALYSIS OF COMPRESSOR CASCADE WITH SPLITTER VANES.   | 5. TYPE OF REPORT & PERIOD COVERED<br>Tech. Report (Final)<br>2 Jan. 75 - 30 Sept 75                                     | 6. PERFORMING ORG. REPORT NUMBER<br>(14) 75-211839 |
| 7. AUTHOR(s)<br>(10) P. R. Dodge  | 8. CONTRACT OR GRANT NUMBER(s)<br>(15) F33615-75-C-1004 NEW  |  |
| 9. PERFORMING ORGANIZATION NAME AND ADDRESS<br>AiResearch Manufacturing Company of<br>Arizona, 402 South 36th Street<br>Phoenix, Maricopa, Arizona 85034  | 10. PROGRAM ELEMENT, PROJECT, TASK<br>AREA & WORK UNIT NUMBERS<br>Project 706513<br>Task 13<br>Work Unit 27 (16) AF-7065 |  |
| 11. CONTROLLING OFFICE NAME AND ADDRESS<br>USAF Air Force Systems Command Hq,<br>4950th Test Wing, 4950/PM ES<br>Wright-Patterson AFB, Ohio 45433   | 12. REPORT DATE<br>(11) Dec 1975   | 13. NUMBER OF PAGES<br>(12) 91p.                   |
| 14. MONITORING AGENCY NAME & ADDRESS (if different from Controlling Office)<br>Air Force Aero Propulsion Lab./TB<br>Wright Patterson Air Force Base,<br>Ohio 45433  | 15. SECURITY CLASS. (of this report)<br>Unclassified   | 16a. DECLASSIFICATION/DOWNGRADING<br>SCHEDULE      |
| 16. DISTRIBUTION STATEMENT (of this Report)<br><br>Approved for Public Release; Distribution Unlimited.   |  |  |
| 17. DISTRIBUTION STATEMENT (of the abstract entered in Block 20, if different from Report)<br>(9) Final technical report, 2 Jan - 30 Sep 75   |  |  |
| 18. SUPPLEMENTARY NOTES   |  |  |
| 19. KEY WORDS (Continue on reverse side if necessary and identify by block number)<br>Transonic relaxation<br>Compressor cascade,<br>Numerical analysis,<br>Inviscid flow,<br>Real flow<br>Aerodynamic analysis   |  |  |
| 20. ABSTRACT (Continue on reverse side if necessary and identify by block number)<br>→ A transonic relaxation program was utilized to analyze the inviscid flow through a cascade without splitters in order to verify the results of a previous experimental investigation. The analysis showed that viscous effects play a large part in the development of the flow field in the transonic flow regime. This was demonstrated by the following: (1) inviscid flow is guided far better by the blades than the real flow, |  |  |

4,4/19 next page

Unclassified

SECURITY CLASSIFICATION OF THIS PAGE(When Data Entered)

cont.

and (2) the blade surfaces are more highly loaded in the inviscid flow than in the experimentally observed viscous real flow.

Following the analysis of inviscid flow through a cascade without splitters, the program was modified to analyze the cascade flow with splitters. Splitter configurations had also been investigated experimentally in a previous program. The analysis was hampered by choking in the splitter passages which limited the range of application of the transonic flow program. The results of the analysis indicated that (1) viscous effects were more pronounced with splitters present in the flow field, and (2) flow conditions (incidence and flow split) at the splitter leading edge were different from those observed experimentally. This made optimization of the splitter location through inviscid analysis a matter of questionable utility.

A simplified scheme for deriving splitter passage flow areas to avoid choking was employed to develop two modified splitter configurations that were analyzed with use of the transonic relaxation program. A modified splitter of increased length exhibited choking problems when analyzed and no significant results were obtained. A much shorter splitter configuration was analyzed successfully, but the results are clouded by the viscous effects in the real flow field observed earlier.

Unclassified

SECURITY CLASSIFICATION OF THIS PAGE(When Data Entered)

## TABLE OF CONTENTS

|  | <u>Page</u> |
|--|-------------|
| SECTION I  |             |
| INTRODUCTION   | 1           |
| SECTION II   |             |
| TECHNICAL DISCUSSION                                     |             |
| 1. PHASE I - ANALYSIS OF CASCADES WITHOUT SPLITTER VANES | 3           |
| a. Objectives  | 3           |
| b. Inviscid Transonic Flow Calculation                   | 3           |
| c. Cascade Geometry and Test Data                        | 7           |
| d. Design Method   | 12          |
| 2. PHASE II - ANALYSIS OF CASCADES WITH SPLITTER VANES   | 15          |
| a. Objectives  | 15          |
| b. Cascade Geometry and Test Data                        | 15          |
| c. Program Modifications for Splitter Vanes              | 15          |
| d. Area Calculations                                     | 20          |
| 3. PHASES III AND IV - SPLITTER REDESIGN                 | 23          |
| SECTION III  |             |
| RESULTS  |             |
| 1. PHASE I - ANALYSIS OF CASCADES WITHOUT SPLITTERS      | 25          |
| a. Calculation Method - Surface Pressures                | 25          |
| b. Comparison of Analysis and Test Data                  | 26          |
| c. Effect of b-Width Variation                           | 46          |
| d. Pressure Surface Leading Edge                         | 51          |
| e. Exit Region   | 58          |
| f. Choking   | 58          |
| g. Conclusions - Phase I                                 | 59          |
| 2. PHASE II - ANALYSIS OF CASCADES WITH SPLITTER VANES   | 61          |
| a. Relaxation Solution                                   | 61          |
| b. Area Calculation                                      | 61          |
| c. Discussion of the Results                             | 71          |

TABLE OF CONTENTS (CONTD)

|  | <u>Page</u> |
|--|-------------|
| 3. PHASES III AND IV - SPLITTER REDESIGN | 75          |
| a. Methodology                           | 75          |
| b. Increased Length                      | 76          |
| c. Shortened Splitter                    | 76          |

SECTION IV

|                 |    |
|-----------------|----|
| CONCLUSIONS     | 87 |
| REFERENCES      | 89 |
| LIST OF SYMBOLS | 91 |

SECTION I  
INTRODUCTION

This document presents a detailed description of the work performed in the conduct of the "Compressor Cascades with Splitter Vanes Analysis Program" under USAF Aerospace Research Laboratories (ARL) Contract No. F33615-75-C-1004. The objectives of the program were:

- o To determine the most desirable configuration of a transonic splitter vane in a given cascade
- o To present the results in a manner which would permit their use for proper splitter vane selection in other cascade configurations

These objectives were pursued by the inviscid analysis of transonic flow through cascades. Calculations were performed with use of the methods defined in References 1 and 2.\*

The Program was divided into the following four phases:

- o Phase I - Analysis of Cascades Without Splitter Vanes
- o Phase II - Analysis of Cascades With Splitter Vanes
- o Phase III - Cascade/Splitter Vane Design Study
- o Phase IV - Generalization and Development of Design Rules

The addition of splitter vanes within a cascade is used, in general, to improve the turning of a blade row. However, due to the added surface area of the passage, the cascade with splitter vanes may be expected to suffer additional viscosity-induced losses. At present, there are no analytical means by which the designer may compare the potential gain in turning with the higher loss of the cascade so that the best splitter geometry may be chosen to accomplish a particular performance goal. When the complication of transonic operation is added, the designer has little experimental data for guidance.

Significant analytical methods used in each phase of the study are discussed in Section II, while the actual results for each phase are given in Section III.

---

\*References follow Section IV.

## SECTION II

## TECHNICAL DISCUSSION

## 1. PHASE I - ANALYSIS OF CASCADES WITHOUT SPLITTER VANES

## a. Objectives

The objectives for Phase I were to compare analytically determined blade loadings and turning angles with experimental data for the cascade tests described in Reference 3. The basic analytical tool used in this phase was the inviscid transonic flow program developed by AiResearch, which is described in Reference 1. The comparison was made first on the basis of the predictive ability of the numerical method, and second, on the design usefulness of the results of such a calculation.

## b. Inviscid Transonic Flow Calculation

The inviscid transonic flow calculation method used in this investigation required that transformation of the potential equation be made into a variable, non-orthogonal grid system within the cascade. The transformation resulted in an equation that involved both elliptical and hyperbolic operators. The coefficients of each of the operators depend upon the local Mach number and the local grid angle. For example, when the flow is supersonic and the grid angle is in the characteristic direction, the coefficient of the elliptic operator is zero.

The extent of the analysis of Phase I was limited to the following cascade flow conditions:

- o Cascade design inlet flow conditions ( $M_1 = 1.46$ ,  $\beta_1 = 66.85^\circ$  as determined by experiment).
- o Three values of the cascade outlet Mach number, which implied three different values of the overall static-pressure rise.

Specification of the inlet Mach number, inlet flow angle, and outlet Mach number for an inviscid flow implies a relation between the stream tube contraction across the cascade and the outlet flow angle. This relation, as shown in Equation (1), is

$$\frac{b_2}{b_1} \cos \beta_2 = \left( \frac{1 + \frac{\gamma-1}{2} M_2^2}{1 + \frac{\gamma-1}{2} M_1^2} \right)^{\frac{\gamma+1}{2(\gamma-1)}} \frac{M_1 \cos \beta_1}{M_2} \quad (1)$$

where the b-width is defined as the distance normal to the plane of potential flow calculation between the effective flow boundaries at the cascade end walls. Equation (1) is plotted for the specified inlet flow conditions in Figure 1 for a range of outlet Mach number. This figure shows that if it were possible to throttle a cascade through the subsonic discharge flow range, and maintain a constant outlet flow angle ( $\beta_2$ ), then  $b_2/b_1$  increases as  $M_2$  decreases. (Note, decreasing  $M_2$  is equivalent to increasing  $P_2/P_1$ .)

The b-width ratio can be related by the continuity equation directly to the axial velocity-density ratio (AVR) across the cascade.

$$\frac{b_2}{b_1} = \frac{1}{\text{AVR}}$$

where

$$\text{AVR} = \frac{\rho_2 V_{x2}}{\rho_1 V_{x1}}$$

The experimental observation that turning increases with increasing AVR (or, alternately expressed, turning increases with decreasing  $b_2/b_1$ ) is illustrated in Figure 2 (taken from Reference 4) for a typical low-speed compressor blade element. The same trend can be calculated with the use of an inviscid flow analysis coupled with an assumption concerning the Kutta condition. If the Kutta condition is used to fix the circulation of the cascade, reasonable agreement is obtained between the calculations and experiments (Reference 4). Two different inviscid calculations are illustrated in Figure 2 for a cascade having relatively small viscous effects. Experience has shown that when viscous effects become more important, agreement often breaks down.

At least two ways in which the inviscid transonic analysis method may be set up for comparison with experimental measurements may be used.

(1) The uniform flow angle ( $\beta_2$ ) at the far downstream station may be fixed to agree with the experimental value. When doing this, the normal stagnation point would change from that expected from the Kutta condition at the trailing edge. To obtain periodicity, a stagnation point and, therefore, the connection of the dividing streamline would have to be moved to the suction surface. This method was eliminated because of numerical difficulties imposed on the grid system.

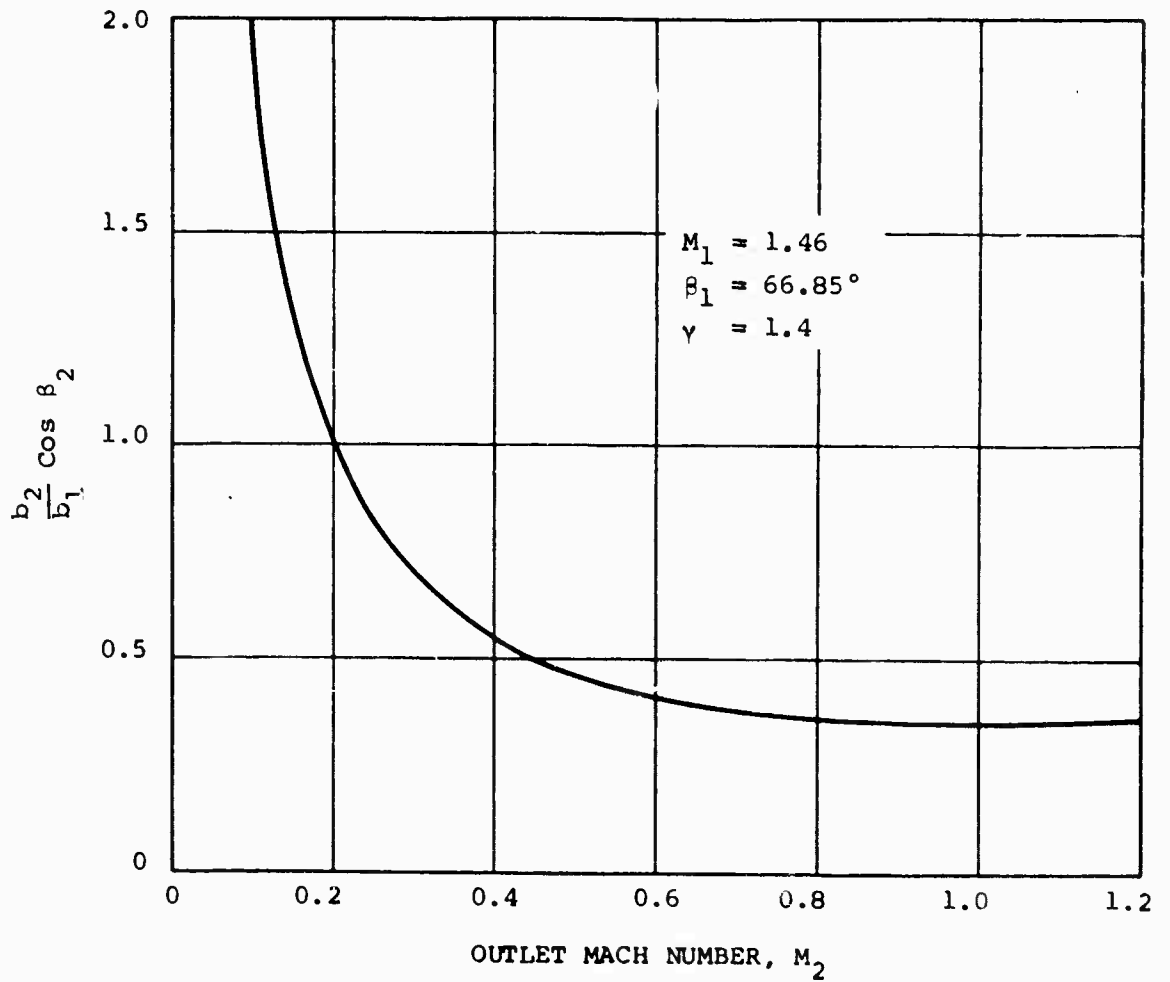


Figure 1. Variation of the Product of the b-Width Ratio and the Cosine of the Outlet Flow Angle with Outlet Mach Number.

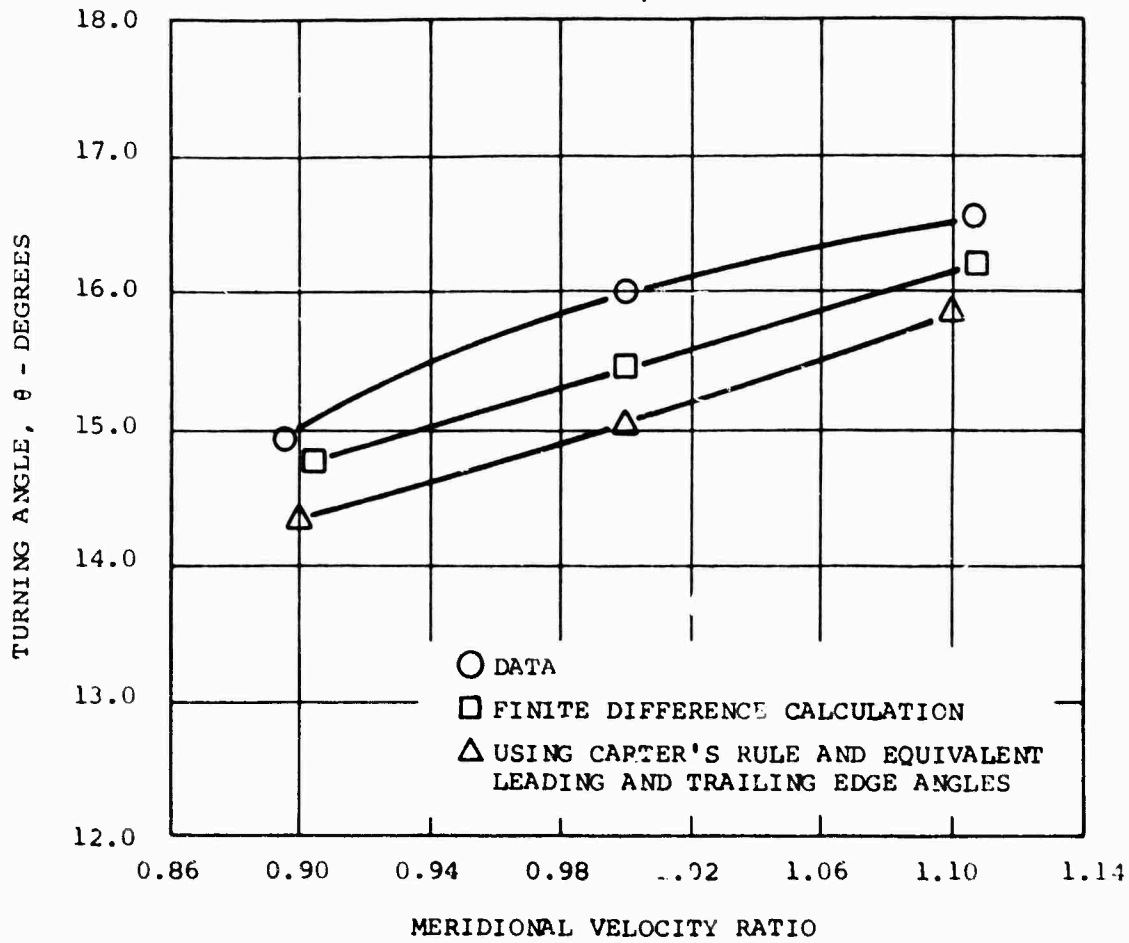


Figure 2. Turning Angle Versus Meridional Velocity Ratio [ $65(A_{10})06$ ,  $\sigma = 1.0$ ,  $\beta_1 = 50^\circ$ ,  $\alpha = 10^\circ$ ].

(2) The Kutta condition can be satisfied at the trailing edge by suitable choice of the outlet flow angle. Thus, an inviscid estimate of turning is obtained.

The second method is more suited to the program goals, but the first method often leads to better prediction of the blade surface pressure distribution.

### c. Cascade Geometry and Test Data

A summary of pertinent geometrical details of the cascade tested in Reference 3 is presented in Table I. The blade element is illustrated in Figure 3, which indicates the blade surface coordinate positions chosen to numerically represent the blade element in the present analysis.

TABLE I. CASCADE PHYSICAL CHARACTERISTICS.

|   |            |
|---|------------|
| Chord                                       | 3.004 in.  |
| Axial chord                                 | 1.8397 in. |
| Blade spacing                               | 1.5810 in. |
| Blade span - inlet plane                    | 2.861 in.  |
| Blade span - exit plane                     | 1.477 in.  |
| Maximum thickness/chord ratio               | 0.03614    |
| Metal angle - leading-edge pressure surface | 61.417°    |
| Metal angle - leading-edge suction surface  | 65.479°    |
| Mean camber angle - leading edge            | 63.448°    |
| Mean camber angle - trailing edge           | 22.534°    |
| Stagger angle                               | 52.316°    |
| Camber angle                                | 40.913°    |
| Solidity                                    | 1.9        |

The end walls of the cascade investigated experimentally in Reference 3 were convergent, so that the overall geometrical b-width ratio ( $b_2/b_1$ ) was 0.4871. The variation of the geometrical b-width with axial position through the cascade is illustrated in Figure 4.

Typical experimental data (from Reference 3) for the ARL supersonic compressor cascade is shown in Figures 5 and 6 in terms of wall static pressure ratio versus axial distance. Passage No. 4 of a seven-bladed cascade was instrumented with 10 static pressure taps on each sidewall to obtain this data. Pressure ratio is expressed as wall static pressure over the upstream total pressure. This pressure ratio and the corresponding isentropic flow relation were employed to obtain the experimental wall Mach numbers presented in Section III.

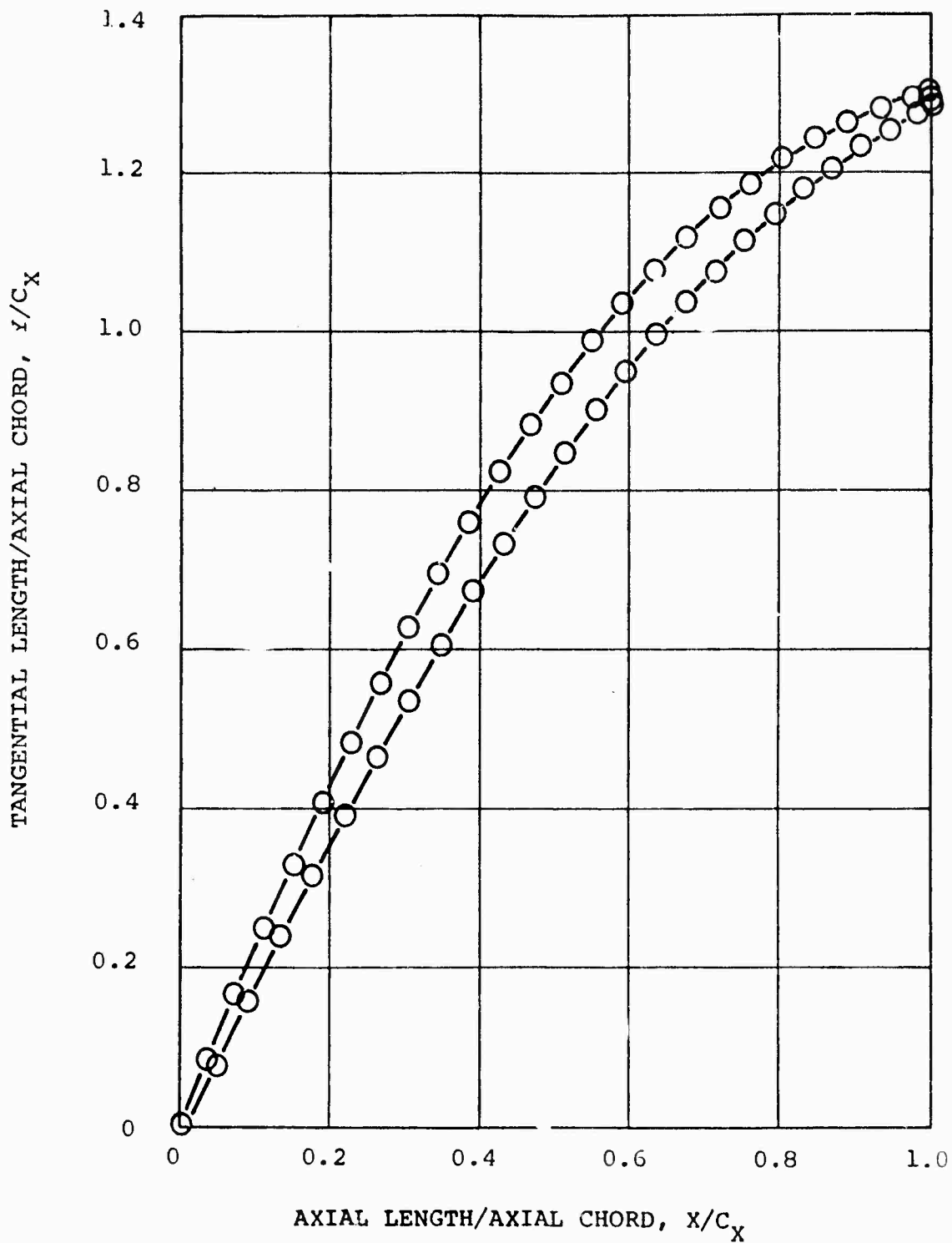


Figure 3. Blade Element and Surface Coordinate Points used to Numerically Represent the Blade Element.

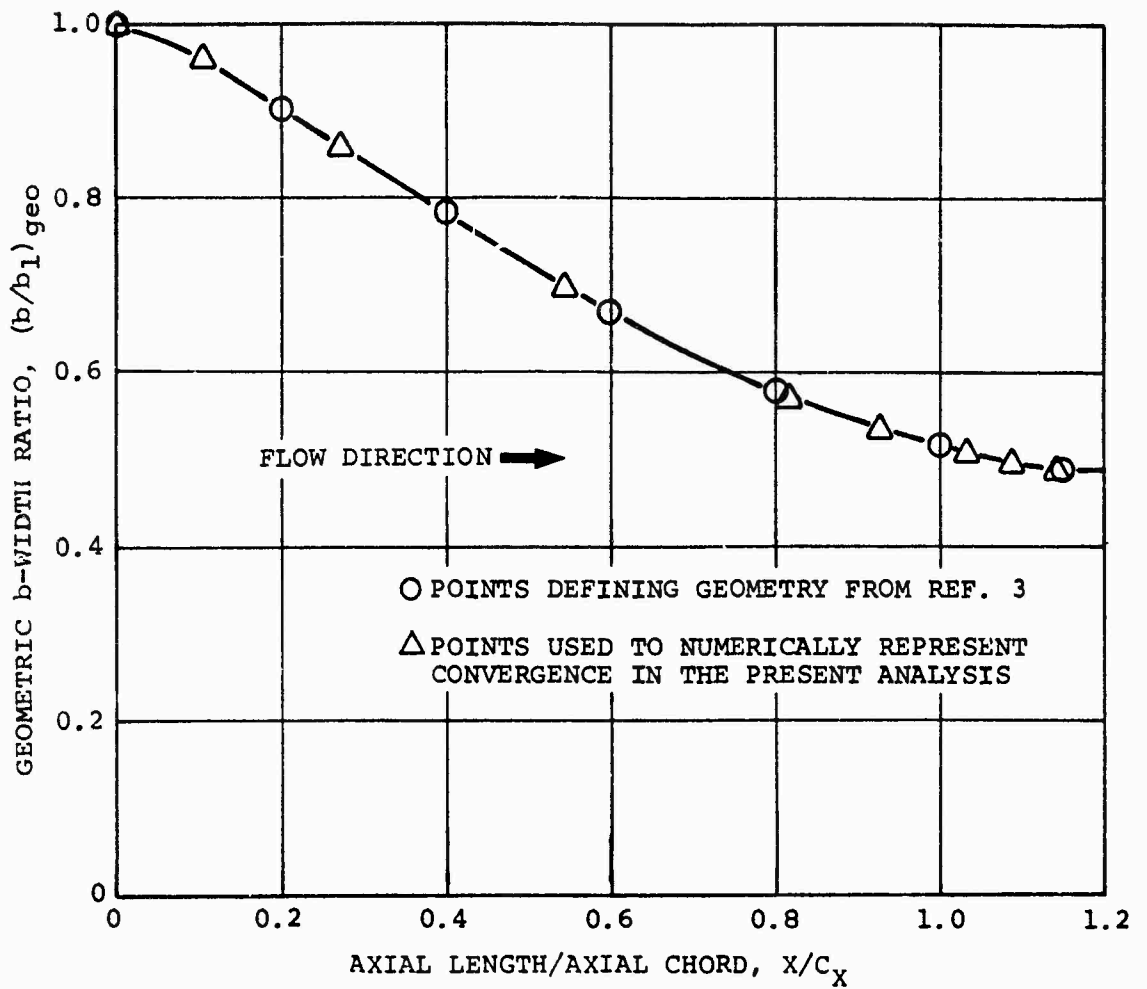


Figure 4. Variation of the Geometrical b-Width as a Function of Axial Distance Through the Cascade.

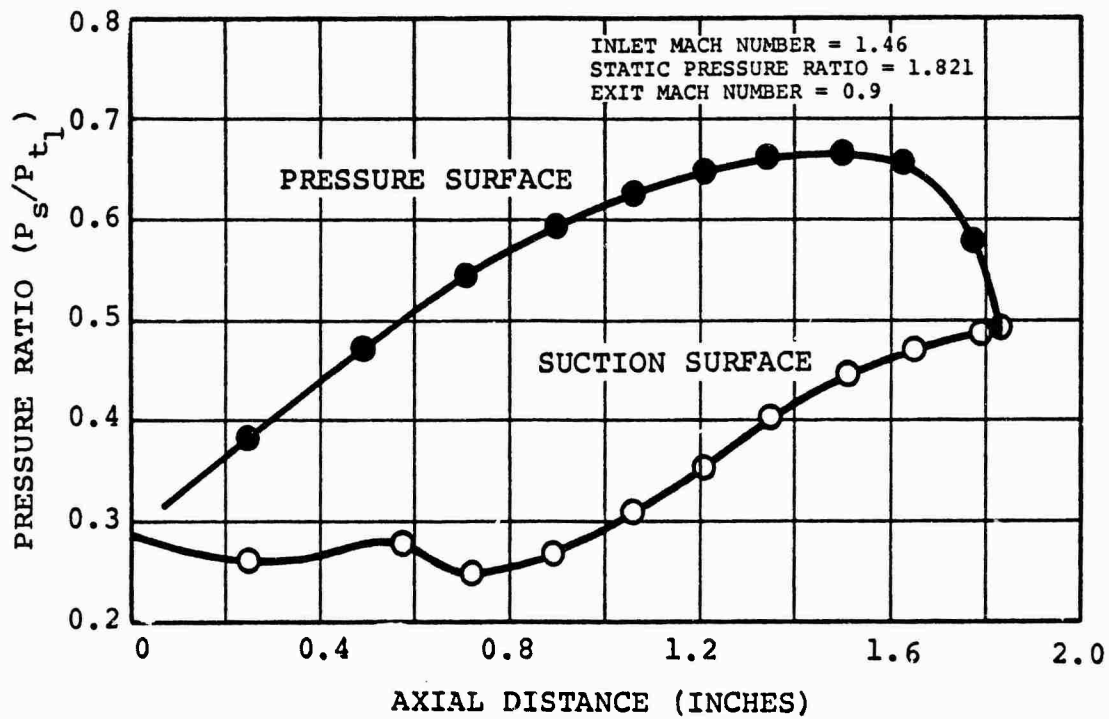


Figure 5. Experimental Data for Supersonic Compressor Cascade (Reference 3).

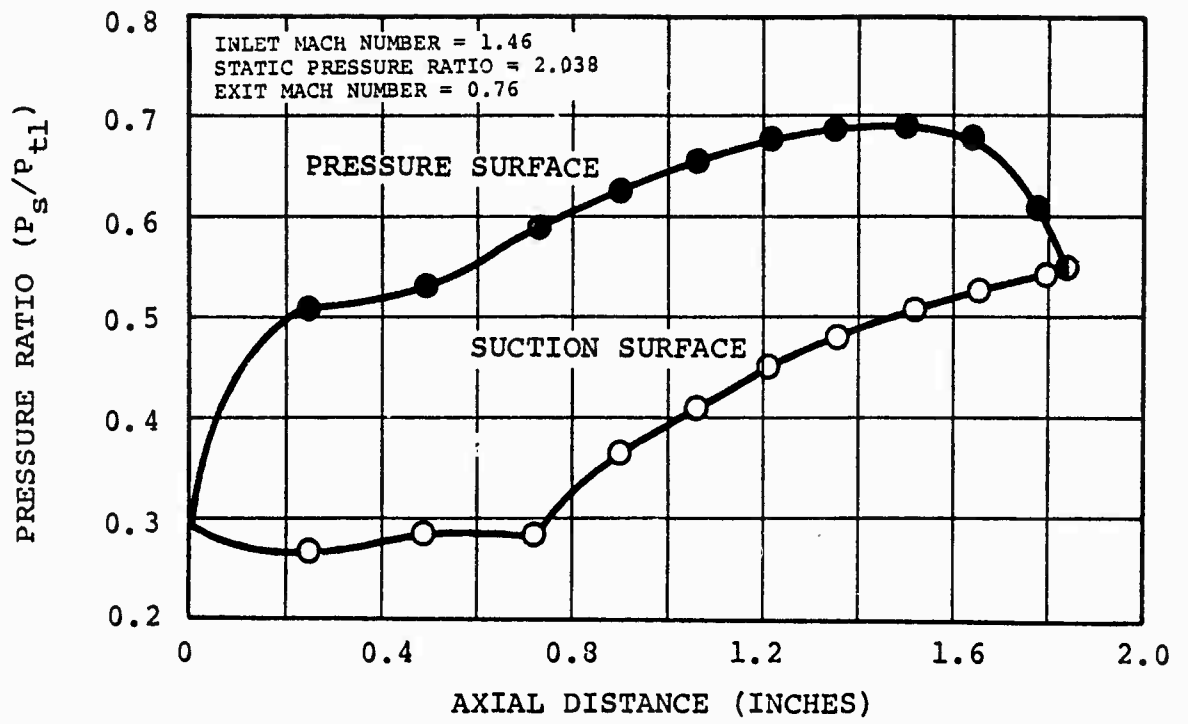


Figure 6. Experimental Data for Supersonic Compressor Cascade (Reference 3).

## d. Design Method

An inviscid calculation, no matter how accurately it predicts surface pressure distribution, does not by itself directly provide the results needed for design decisions. For the case in point, two principal aerodynamic criteria are used in design.

(1) A measure of the loss (or relative position on a loss scale) of the section relative to other possible sections.

(2) A measure of the increase in turning obtainable by the section.

A useful estimate of the relative performance of one configuration versus others has been obtained from inviscid calculations. Total losses can be estimated with use of a boundary layer/loss calculation. However, to rate a set of similar cascades, a reasonable criterion can be constructed with the maxima and minima of a blade static pressure distribution (Reference 4).

Based on the parameter of Reference 4, Equation (2) yields a value to compare the performance of a cascade with similar cascades.

$$\Delta s_{\text{total}} = \Delta s \Big|_{\substack{\text{principal} \\ \text{blade}}} + \Delta s \Big|_{\substack{\text{splitter} \\ \text{vane}}} \quad (2)$$

$$\text{where } \Delta s = \frac{(P_{\text{max}} - P_{\text{min}})_{\substack{\text{suction} \\ \text{surface}}} + (P_{\text{max}} - P_{\text{min}})_{\substack{\text{pressure} \\ \text{surface}}}}{q_1}$$

In order to determine if this criterion is reasonable, the data presented in References 3 and 7 is utilized to plot the experimental loss coefficient,  $\bar{w}$ , versus  $\Delta s$ . This is shown in Figure 7. As can be observed, the data is well correlated with an increasing  $\Delta s$  yielding an increasing loss. Even the introduction of a splitter does not seriously alter the correlation. Thus, this parameter can be utilized to correlate cascade losses for the configurations investigated.

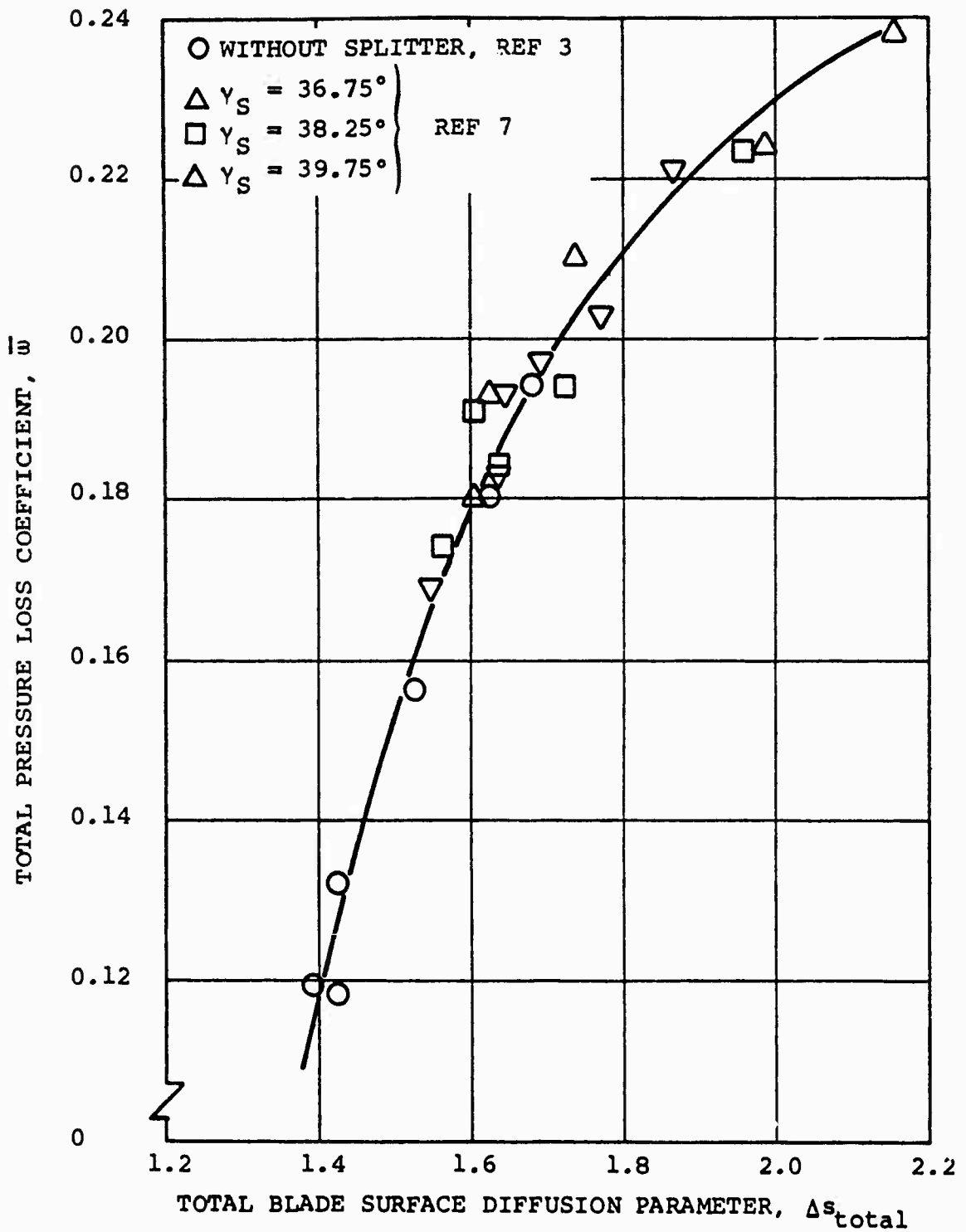


Figure 7. Total Pressure Loss Parameter Versus Total Blade Surface Diffusion Parameter from Measurements for a Compressor Cascade With and Without Splitter Vanes.

The turning performance represents a separate problem. An inviscid calculation is not complete without a specification of total turning. This is often done by imposing a viscous condition on the trailing edge called the Kutta condition (see Reference 4). Simply stated, the Kutta condition prescribes that the stagnation streamline must attach to a sharp trailing edge. This condition, along with the requirement of periodicity, is sufficient to establish an exit flow angle for a cascade having subsonic flow at the exit. The practical method of establishing the validity of this varies, depending on what is viewed to be convenient or accurate by the user of an inviscid program. Excellent results are obtained when the cascades have sharp trailing edges and moderate boundary layers. Unfortunately, the cascade of this study violates, to some degree, both of these criteria. The result is that the deviation angle prediction should be less accurate than that noted in Reference 4.

The majority of the calculations for the transonic relaxation program utilized the following exit boundary conditions:

- o The stagnation point on the trailing edge is specified.
- o The shape of the stagnation streamline is adjusted periodically throughout the calculation procedure in an attempt to enforce periodicity.
- o A far-downstream flow angle is specified. Stagnation streamlines are forced to this angle at a selected distance from the trailing edge.

In light of the uniqueness of turning with a specified stagnation point, it is clear that the boundary conditions are overspecified. Unless the specified far-downstream angle is the unique angle for this cascade, periodicity is not obtainable no matter how much adjustment is attempted. Consequently, some iteration is required to determine the proper inviscid turning for a particular cascade.

If it is desired to match data other than that yielding an ideal Kutta condition, the stagnation point can be moved from the trailing edge to either the suction or pressure surfaces. However, excess movement of this type will cause an irregularity in the grid system and hence, numerical difficulty. Consequently, turning has been restricted to ideal Kutta conditions.

## 2. PHASE II - ANALYSIS OF CASCADES WITH SPLITTER VANES

### a. Objectives

The objectives of this phase of the program were to modify the transonic-relaxation program to accept a splitter of arbitrary geometry and to compare the splitter analysis with experimental data. The experimental data employed in this comparison was obtained from Reference 7. In the test program, the setting angle of the splitter vanes could be altered plus or minus 3 degrees. Therefore, the analysis was expanded to include an investigation of the effect of splitter rotation on calculated splitter loadings.

### b. Cascade Geometry and Test Data

Geometrical details of the main blades are summarized in Section II.1.c. Splitter coordinates chosen to numerically represent the blade element are shown in Figure 8. This figure also contains pertinent physical characteristics for the splitter vane.

Experimental data for the ARL supersonic cascade with splitters is presented in Figures 9, 10, and 11 in terms of wall static pressure versus axial distance. The cases addressed in these figures are:

- o A nominal vane setting angle of  $39.75^\circ$
- o Rotated by plus  $3^\circ$  or a vane setting angle of  $42.75^\circ$
- o Rotated by minus  $3^\circ$  or a vane setting angle of  $36.75^\circ$

When the cascade was operated with splitters, the vane was instrumented with pressure taps to obtain a limited number of surface static-pressure measurements. Information such as main blade and splitter static-pressure is included in these figures.

### c. Program Modifications for Splitter Vanes

The basic program for computing inviscid transonic flows in a cascade is described in Section II.1.b. That program was modified to incorporate splitter vane geometry. A total of 22 coordinate points on each surface were selected to represent the splitter. These are input to the program as surface boundary points.

The splitter vane is handled like any other solid wall in that the normal component of fluid velocity is zero, or the derivative of the potential in the normal direction is zero. The coordinate system downstream of the splitter is set up as a dividing streamline with no flow across the surface. Initially, this streamline is assumed to have a linear distribution of flow angle from the trailing edge to the far downstream angle. With each major iteration, the curvature along the dividing streamline is adjusted to equalize the fluid velocities on each side.

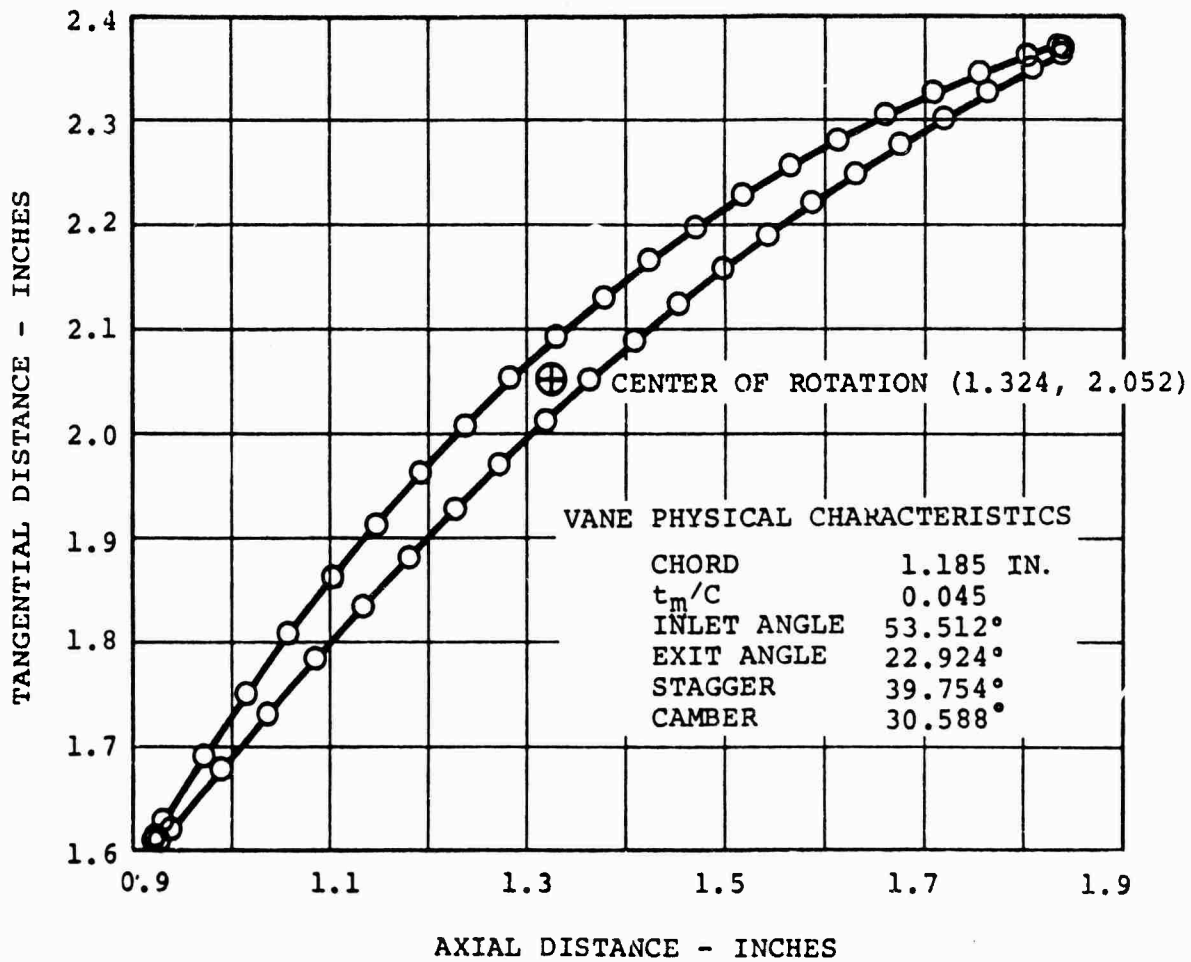


Figure 8. Splitter Vane Coordinates.

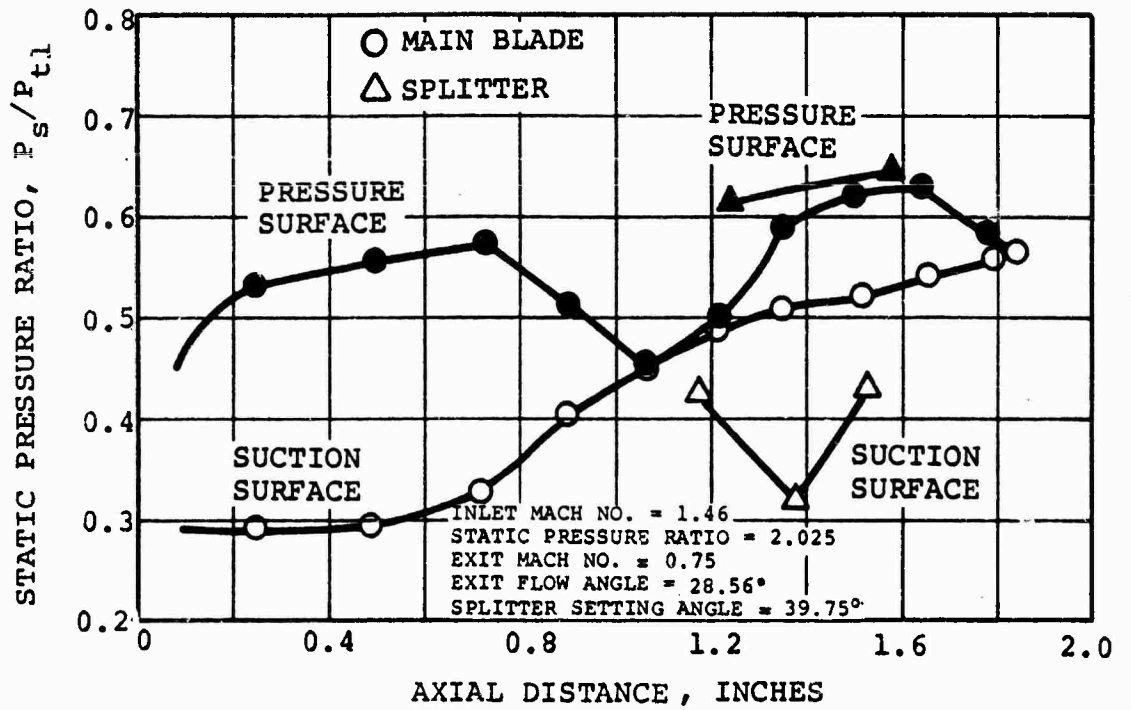


Figure 9. Experimental Data for Cascade With Splitter Vanes, 0° Rotation.

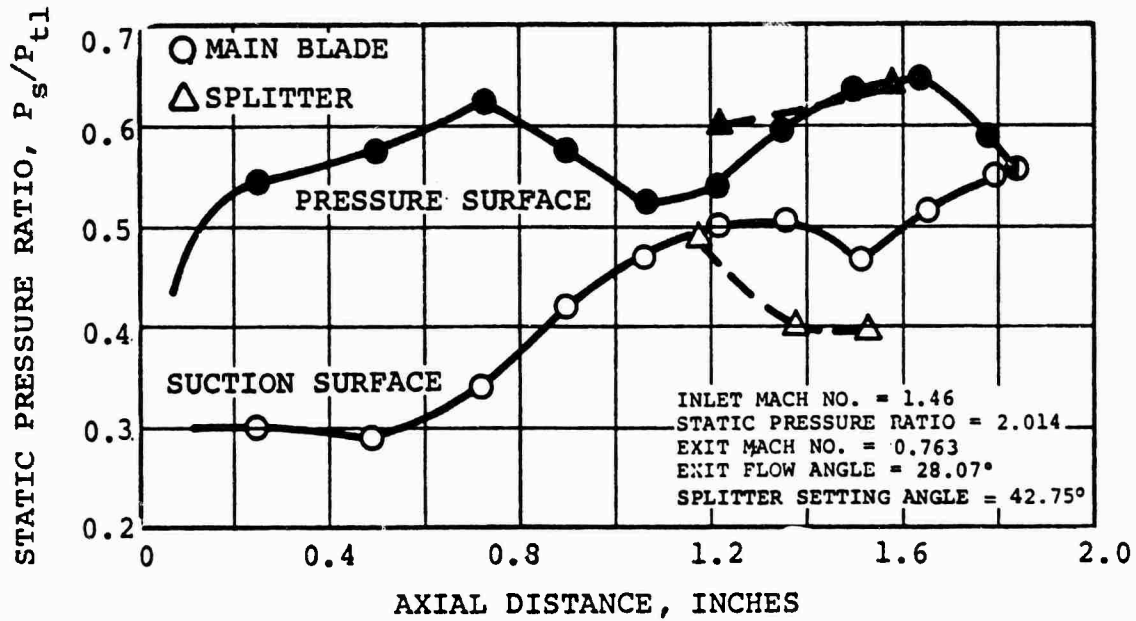


Figure 10. Experimental Data for Cascade With Splitter Vanes, +3° Rotation.

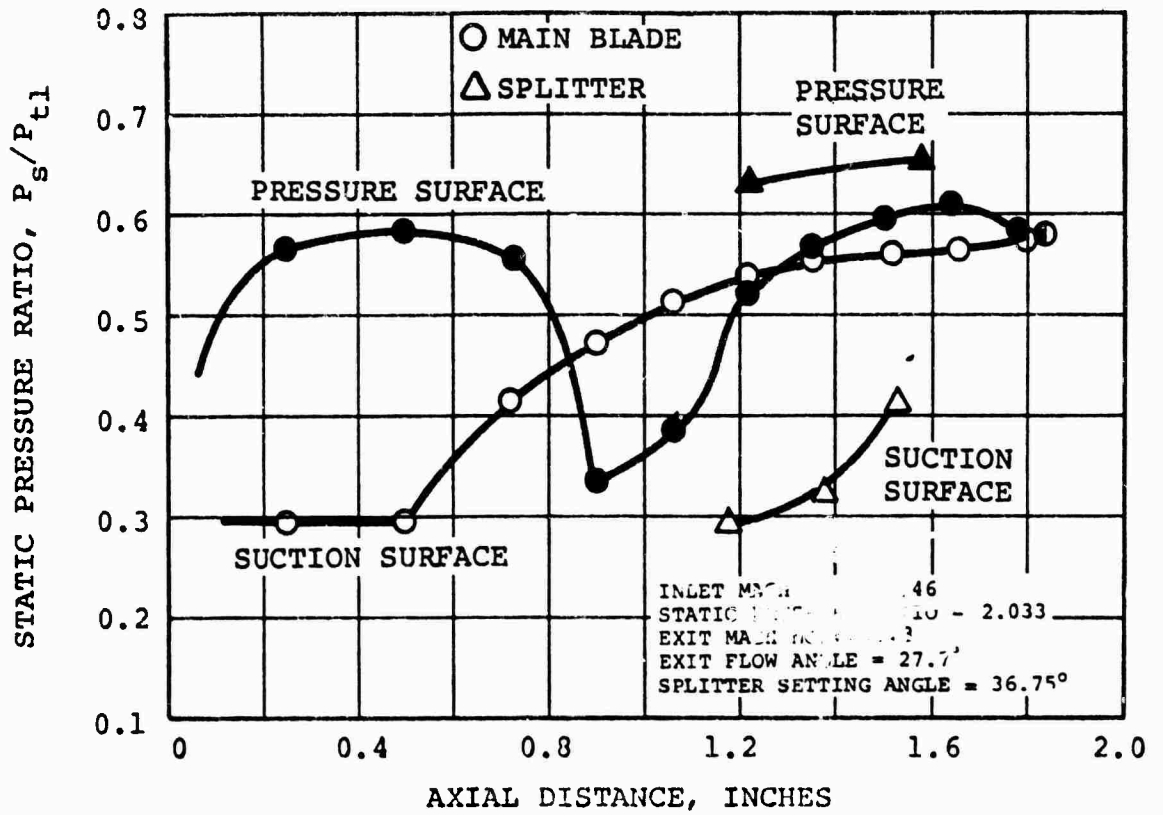


Figure 11. Experimental Data for Cascade With Splitter Vanes,  $-3^\circ$  Rotation.

In essence, the two passages above and below the splitter vane are isolated and treated separately beyond the splitter leading-edge station except for this curvature correction to the dividing streamline. The exit grid pattern is often uneven because the total number of grid rows is constant and grid spacing changes between passages. However, this does not pose a problem, since the far downstream exit conditions include essentially constant flow angles and velocity at each grid intersection.

A typical grid pattern for the transonic cascade with splitters is shown in Figure 12. Difficulty was experienced in defining the grid in the vicinity of the splitter leading edge due to the interpolation scheme for locating the first upper boundary point on the splitter surface. Under certain circumstances, the intersection occurs upstream of the leading edge station and the program fails. This is remedied by changing the upstream grid spacing to remove the upper grid intersection from the vicinity of the splitter leading edge.

Storage schemes had to be modified throughout the program because the location of the leading edge in the grid system was unknown. In the conventional case, odd and even rows of grid points are different. Even rows do not have surface intercepts, and have one less point than odd rows, as illustrated in Figure 13a. However, when a splitter is introduced, surface intercepts may occur on either odd rows (Figure 13b) or even rows (Figure 13c). As the calculation proceeds, the grid system is periodically updated. At one of these updates, splitter intercept patterns may change from even to odd rows. This causes an unavoidable discontinuity in what would otherwise be a suitable iteration process. If splitter intercepts are on an even row, exit boundary conditions must also be modified since the last row is odd but does not contain a splitter surface intercept as is the case with standard grid systems.

#### d. Area Calculations

Area calculations were performed to aid in the interpretation of the results obtained with the inviscid transonic program. Areas were obtained geometrically by finding a circle tangent to the blade surfaces. The location of the center of this circle was used to obtain a b-width. The area was then determined by applying Equation (3).

$$A = 2rb \quad (3)$$

This process involves some inaccuracy. First, the flow direction can be approximated by assuming that one-half of it is parallel to one surface and, the other half is parallel to the remaining surface. The process also assumes that a proper average b-width can be assigned by utilizing a single value correlated to the circle center. The level of this inaccuracy is clearly visible in the results presented in Section III.

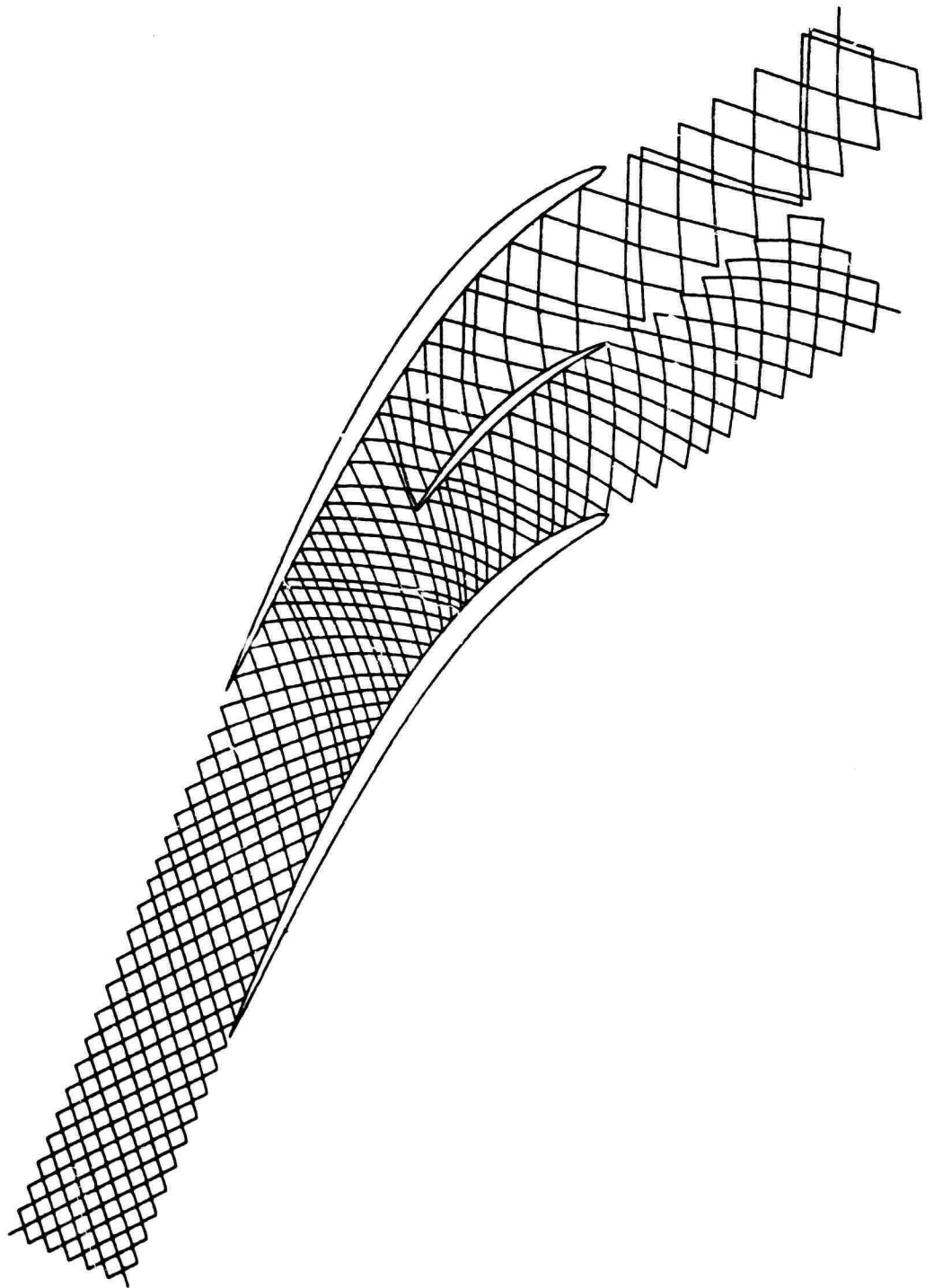


**Figure 12. Non-Orthogonal Grid System for Cascade With Splitters.**

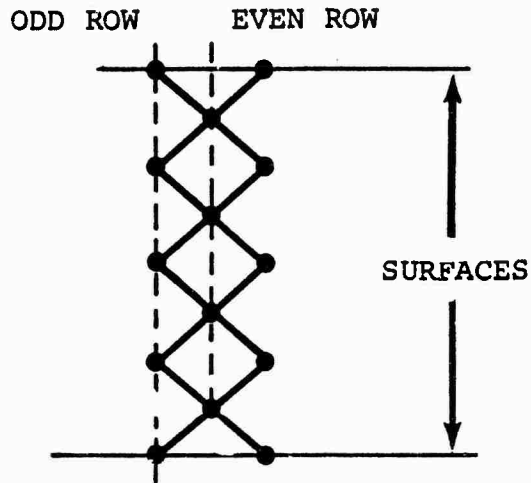


Figure 13a. Grid System Without Splitter.

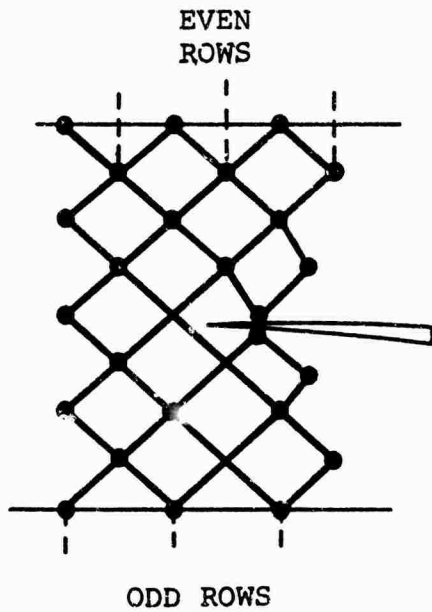


Figure 13b. Intercept of Splitter on Odd Row.

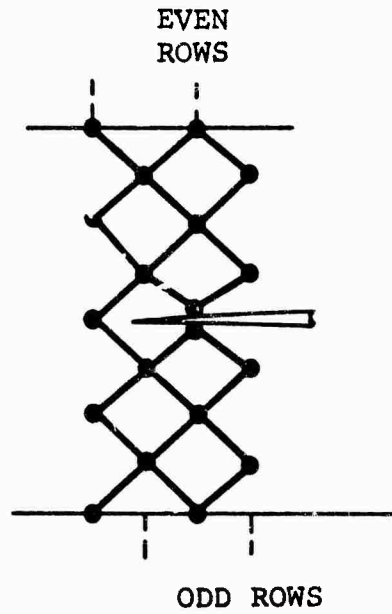


Figure 13c. Intercept of Splitter on Even Row.

### 3. PHASES III AND IV - SPLITTER REDESIGN

A useful approach for constructing new candidate geometries was to begin with a solution for the cascade without a splitter. Since choking is a major problem, all candidate configurations must be selected so as to provide an adequate area distribution. At the same time, incidence at the splitter leading edge can be estimated from free streamlines. To obtain free streamlines, a program was written to utilize the data stored on disk file that resulted from the inviscid transonic calculation. This program integrated flow from surface to surface along successive rows of data. The location of a streamline was then determined and velocities were interpolated to this streamline. Pressure and suction surface shapes are represented by well reasoned deviations from the streamline shape. This technique was applied along with the numerical fluid dynamic solutions discussed in Sections I and II to redesign splitter configurations.

## SECTION III

## RESULTS

## 1. PHASE I - ANALYSIS OF CASCADES WITHOUT SPLITTERS

## a. Calculation Method - Surface Pressures

The analyses performed in this investigation assume an inviscid flow field. In order to compare measurements of blade surface pressures with the calculations, a Mach number is calculated for the blade surface pressure from the following isentropic relation:

$$M = \left[ \frac{2}{\gamma-1} \left\{ \frac{P_{t1}}{P} \frac{\gamma-1}{\gamma} - 1 \right\} \right]^{1/2} \quad (4)$$

where  $P$  is the local static pressure on the blade surface and  $P_{t1}$  is the upstream total pressure.

The utilization of this ideal Mach number rests on two assumptions.

(1) A core flow with essentially no total pressure loss

(2) A boundary layer with no appreciable normal pressure gradients

As regards the first assumption, cascade data taken for this configuration indicates that considerable loss in core flow total pressure occurs at most static pressure ratios. The second assumption is probably true in unseparated regions. No experimental evidence exists, however, to positively establish the size and extent of separations on the blade surface. It can be inferred that they must exist by examining both ideal and experimental levels of diffusion.

To approximately correct the value of Mach number computed from Equation 4 for total pressure loss, the following expression is also utilized.

$$M = \left[ \frac{2}{\gamma-1} \left\{ \frac{P_t}{P} \frac{\gamma-1}{\gamma} - 1 \right\} \right]^{1/2} \quad (5)$$

where

$$P_t = (C_X - X)(P_{t1} - P_{t2})/C_X + P_{t2}$$

and where

$P_{t1}$  and  $P_{t2}$  are the experimental inlet and exit total pressures of the core flow

Several subsequent figures show both methods of converting experimental pressure distributions into equivalent Mach numbers for comparison to inviscid calculations.

b. Comparison of Analysis and Test Data

It is difficult to compare inviscid flow calculations with experimental results where viscous effects are so evident. It is not possible to make a single comparison of all the important parameters across the transonic cascade. The following table summarizes the problem and indicates how the final comparisons are made.

TABLE II. PARAMETERS SELECTED FOR PHASE I ANALYSIS.

| Analytical Data              |                          |           |  |                                  | Experimental Data        |           |  |                                  |
|------------------------------|--------------------------|-----------|--|----------------------------------|--------------------------|-----------|--|----------------------------------|
| $M_2$<br>Exit<br>Mach<br>No. | $\theta$<br>Turn-<br>ing | $\beta_2$ | AVR-Axial<br>Velocity-<br>Density<br>Ratio | Static<br>Pres-<br>sure<br>Ratio | $\theta$<br>Turn-<br>ing | $\beta_2$ | AVR-Axial<br>Velocity-<br>Density<br>Ratio | Static<br>Pres-<br>sure<br>Ratio |
| 0.6                          | 34.65                    | 32.20     | 2.08                                       | 2.72                             | --                       | --        | --   | --                               |
| 0.76                         | 42.35                    | 24.00     | 2.53                                       | 2.36                             | 36.90                    | 29.95     | 2.07                                       | 2.038                            |
| 0.808                        | 45.05                    | 21.80     | 2.62                                       | 2.26                             | 37.39                    | 29.47     | 2.15                                       | 1.968                            |
| 0.9                          | 46.30                    | 20.55     | 2.67                                       | 2.05                             | 37.25                    | 29.60     | 2.24                                       | 1.821                            |

Initial conditions for the analysis were fixed at an inlet Mach number of 1.46 and an inlet flow angle of 66.85 degrees as in the experimental setup. Analyses were then conducted for three exit Mach numbers; the latter two cases ( $M_2 = 0.76$  and  $0.9$ ) corresponded to experimental conditions. The  $0.6$  Mach number case corresponds to inviscid flow with no aerodynamic blockage.

This case has an axial velocity-density ratio similar to the experimental condition at  $M = 0.76$  and, therefore, provides an additional means for comparing the two results. As indicated in Table II, the turning, axial velocity-density ratio, and static pressure ratio are different when analytical and experimental results are compared at the same exit Mach number. However, by comparing cases with similar axial velocity-density ratios, the turning is more nearly the same but exit Mach numbers and static pressure ratios are different. Thus, the former comparison (equal  $M_2$ ) is employed to match analytical and experimental blade loadings while the latter comparison (Equal AVR) is made to evaluate the flow turning conditions. This is illustrated in Figure 14.

Analytical results for exit Mach numbers of 0.6, 0.76, 0.808, and 0.9 are shown on the subparts of Figures 15 through 18 respectively. These figures are divided into: (a) surface Mach number, (b) the grid system, (c) the variation of Mach numbers along quasi-streamlines and, except for Figure 15, (d) contours of constant Mach number. Surface Mach numbers are calculated directly with use of the program described in Section II. Experimental values are calculated using one of the two methods described in (a) above. The grid system shows Mach lines in the supersonic region. This permits interpretation of the effects of reflections of one surface on another. The streamline curves represent an exploded plot of Mach number along lines obtained by connecting grid points in a streamwise fashion. The number imprinted at the start of each line is an adder used to spread the curves. The Mach number read is equal to the true Mach number plus the adder. The last plot is a plot of lines of constant Mach number within the cascade. No experimental Mach numbers are shown for the 0.6 Mach number case since it represents the b-width distribution of the cascade end wall without any aerodynamic blockage effects.

A comparison with time-dependent methods was made to verify the accuracy of the relaxation method. The surface Mach number distributions resulting from this comparison are shown in Figure 19. Two different b-width distributions are shown. As one of its boundary conditions, the time-dependent calculation always satisfies an ideal Kutta condition. The exit Mach number, however, will vary with the downstream flow angle required to meet the Kutta condition. Thus, to precisely match data when using the time-dependent method, a variety of axial velocity-density ratios must be applied until one is found that yields the exit Mach number desired. Table III summarizes the results of the comparison of the two calculation methods with test data. The numerical smoothing of the time-dependent method provides a much smoother surface Mach number distribution than that of the relaxation solution. However, the general features of the relaxation process are all confirmed. In particular:

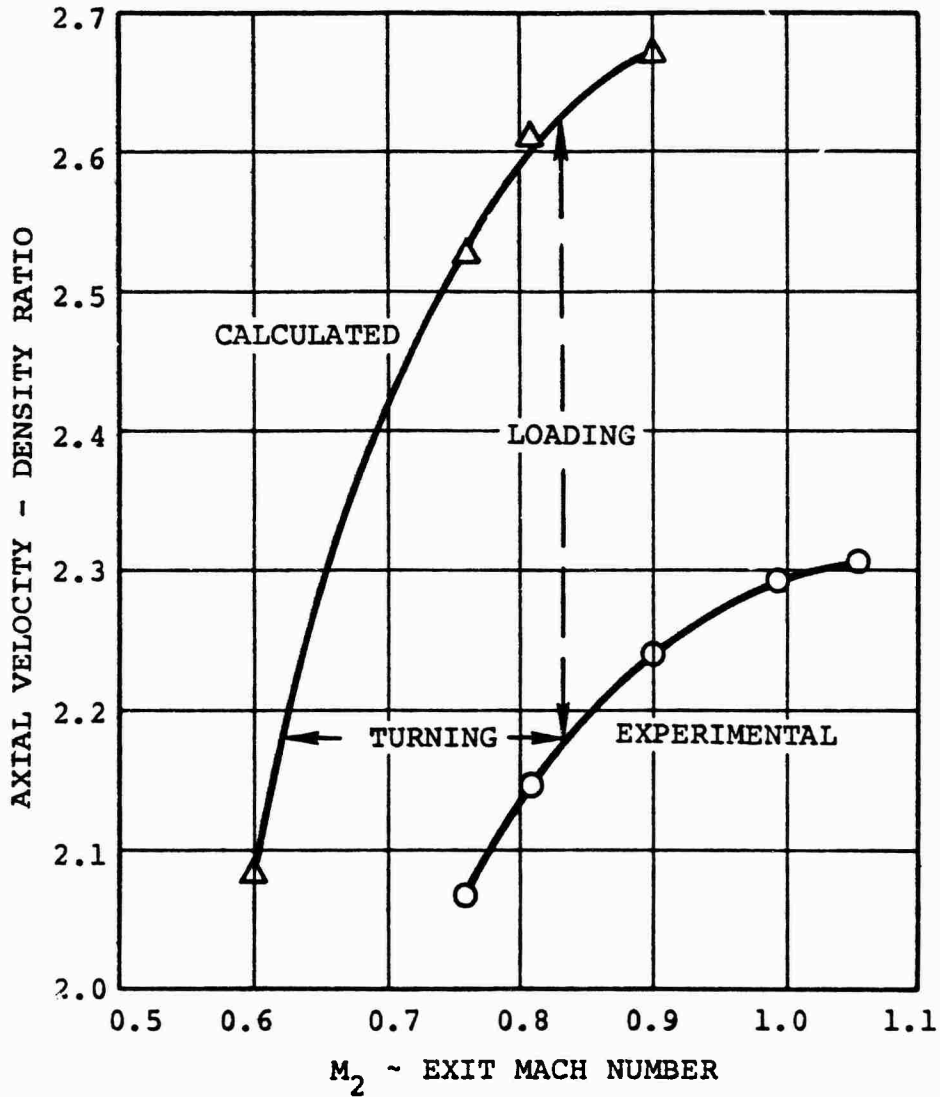


Figure 14. Inviscid Simulation of Real Fluid Conditions in a Cascade.

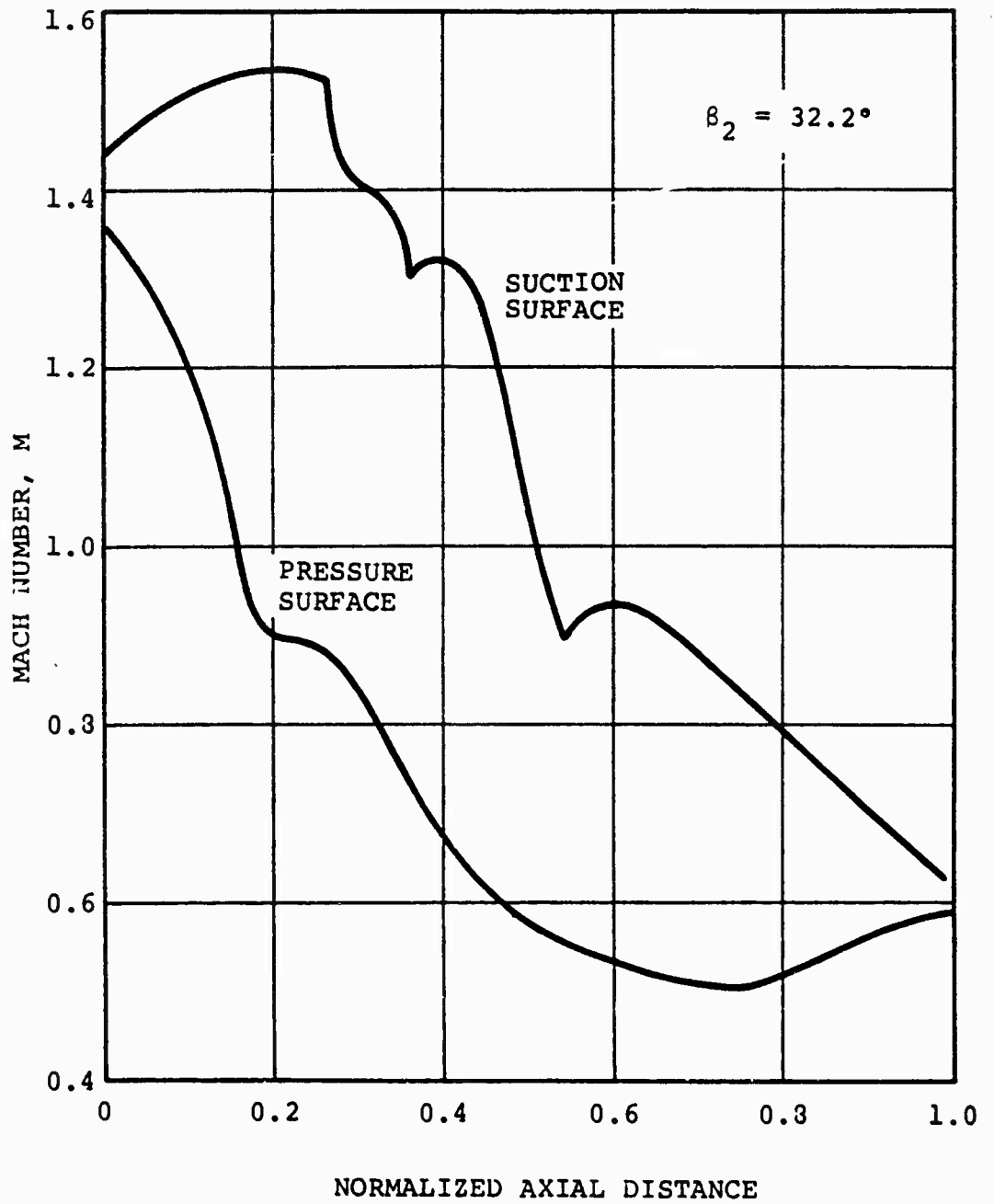


Figure 15a. Surface Mach Number Distribution for Compressor Cascade at  $M_2$  of 0.6.

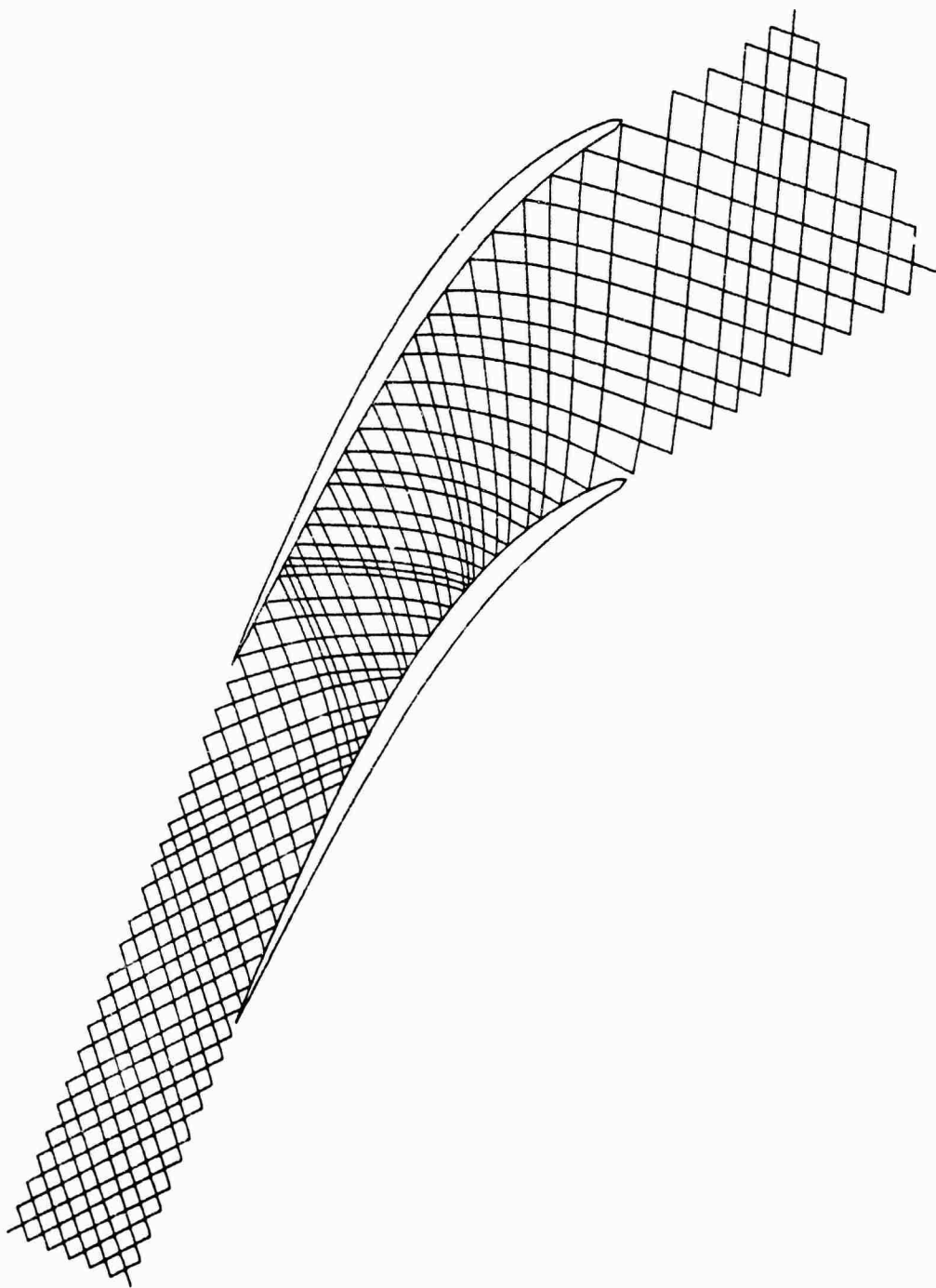


Figure 15b. Non-Orthogonal Grid System for Compressor Cascade at  $M_2$  of 0.6.

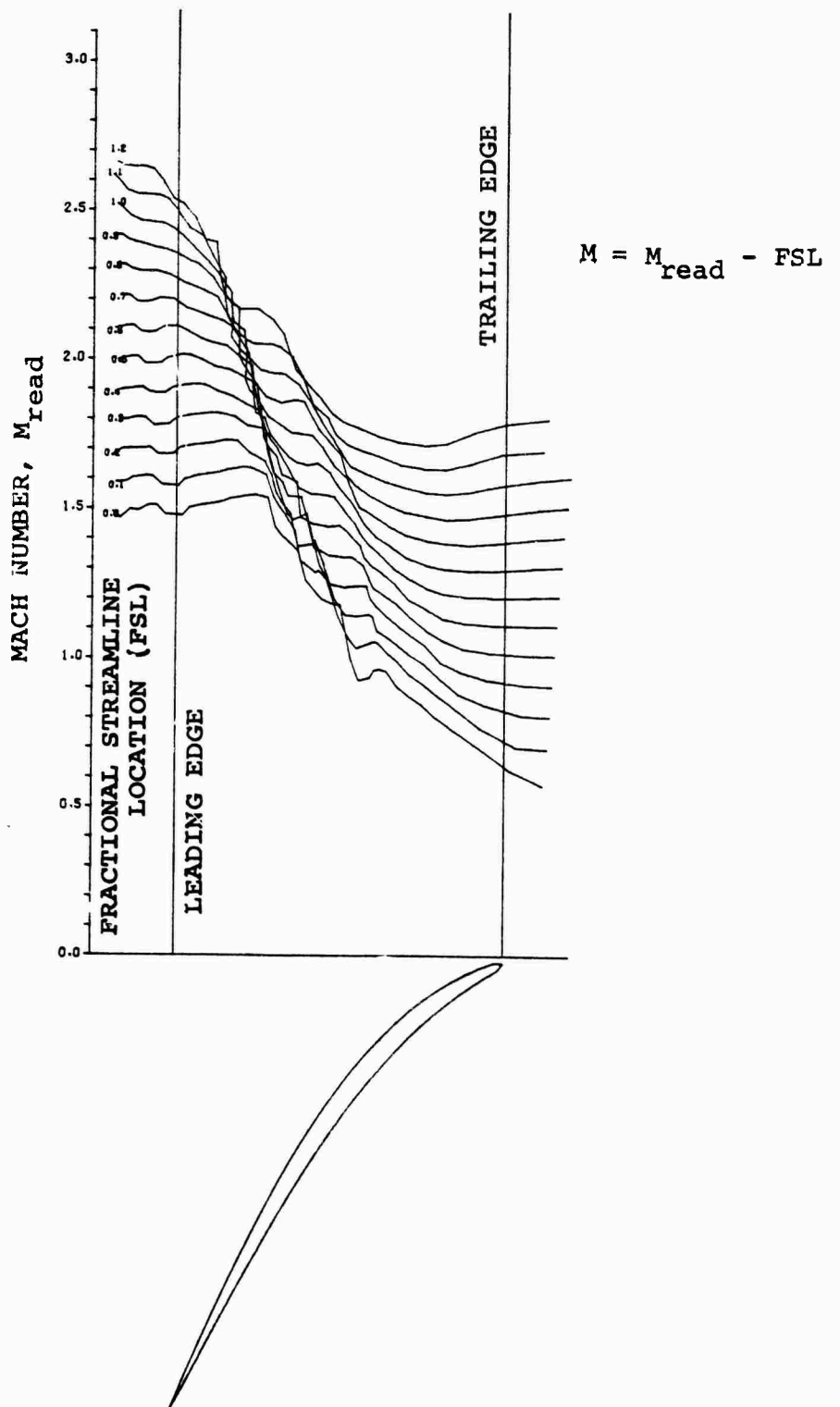


Figure 15c. Flowfield Mach Number Distribution for Compressor Cascade at  $M_2$  of 0.6.

OUTLET FLOW CONDITIONS

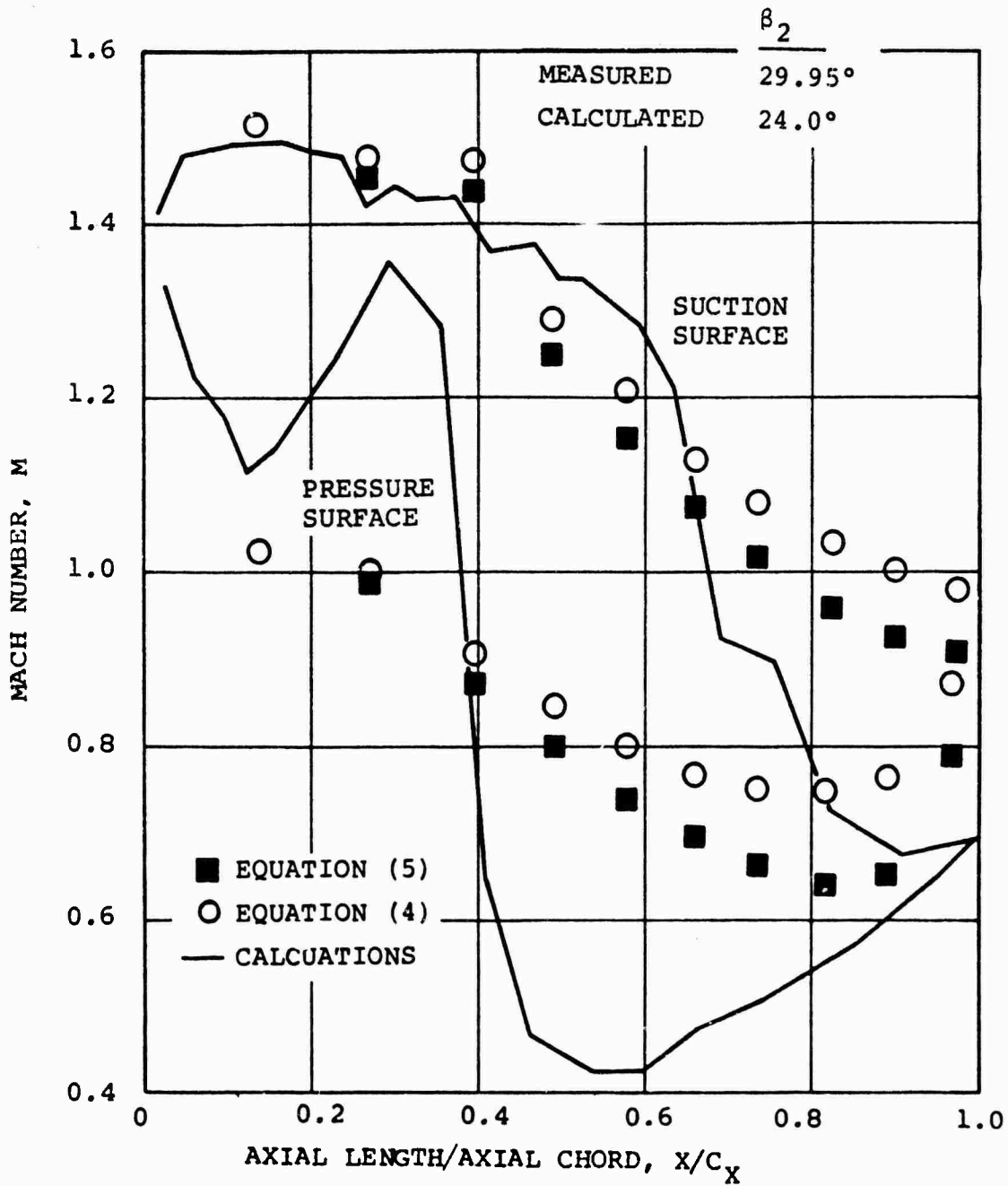


Figure 16a. Comparison of Experimental Blade Surface Mach Number Distribution with Results of Calculation for  $M_2 = 0.760$ .

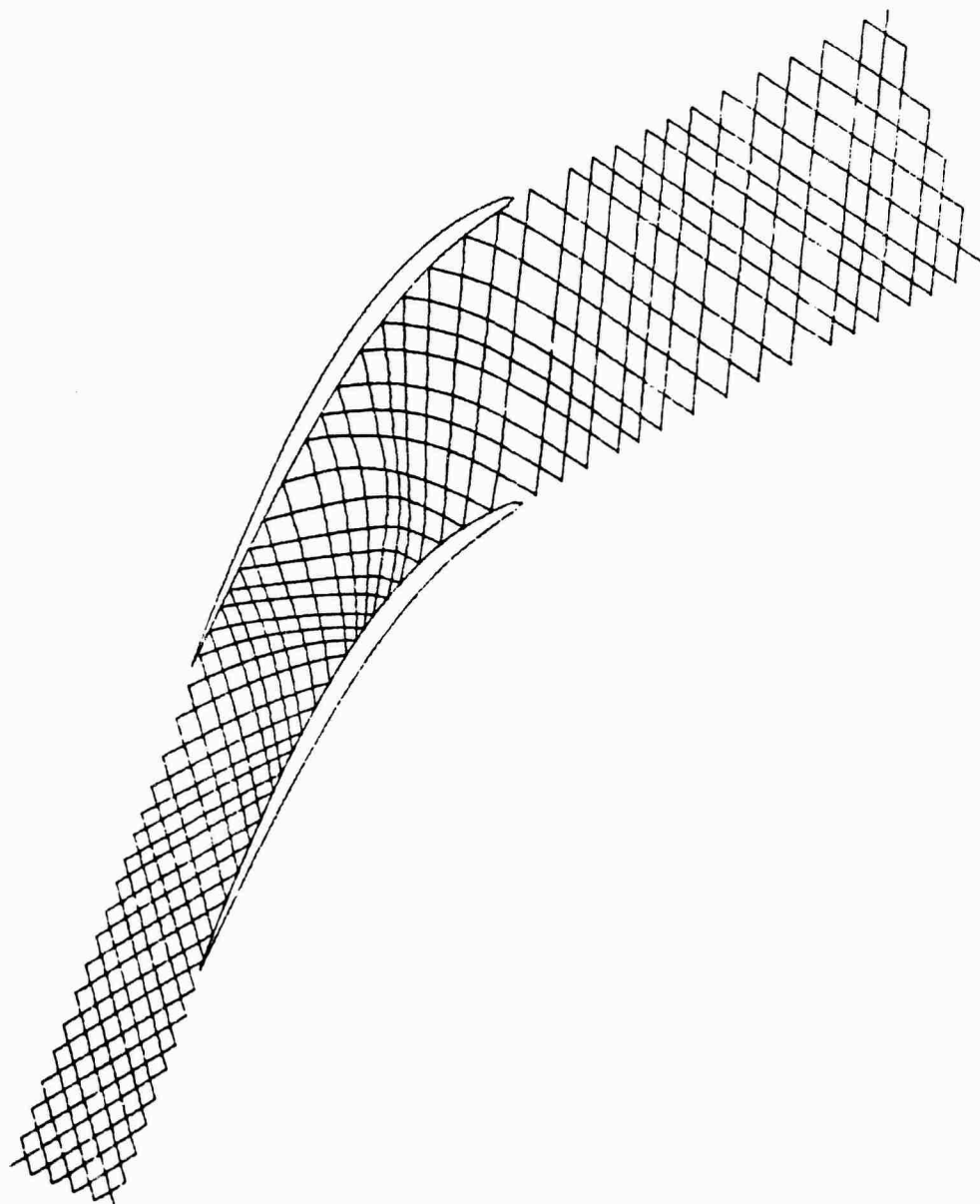


Figure 16b. Non-Orthogonal Grid System for Compressor Cascade at  $M_2$  of 0.760.

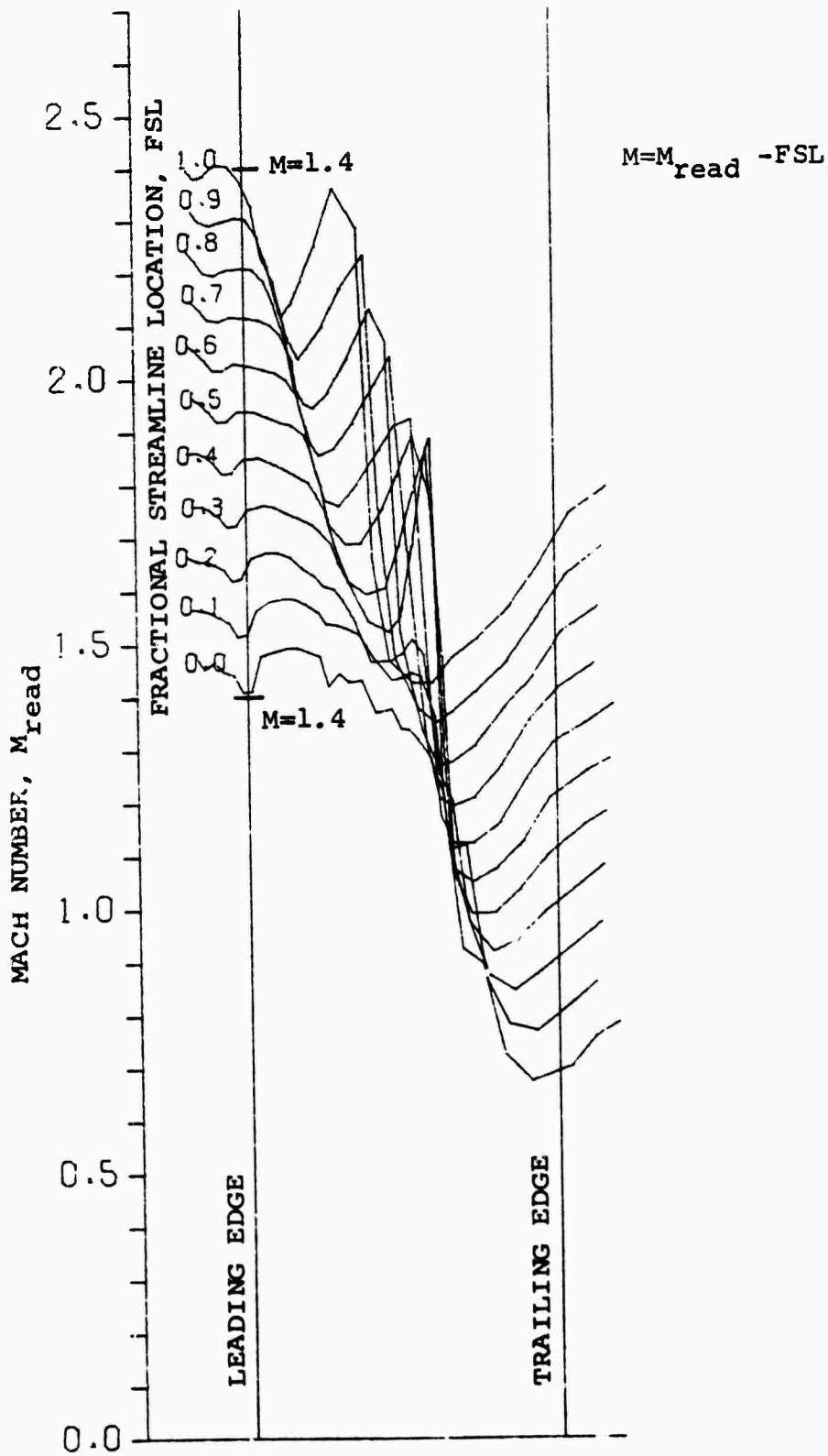


Figure 16c. Variation of Mach Number Along Streamlines at  $M_2$  of 0.760.

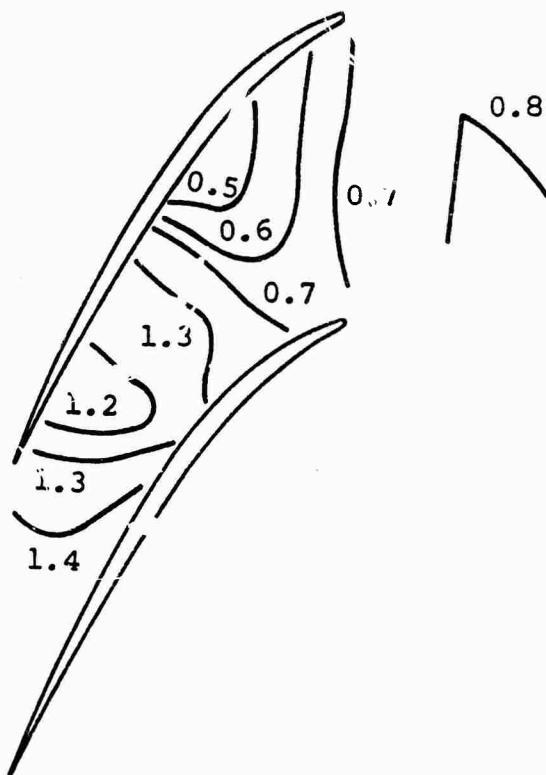


Figure 16d. Contours of Constant Mach Number at  $M_2$  of 0.760.

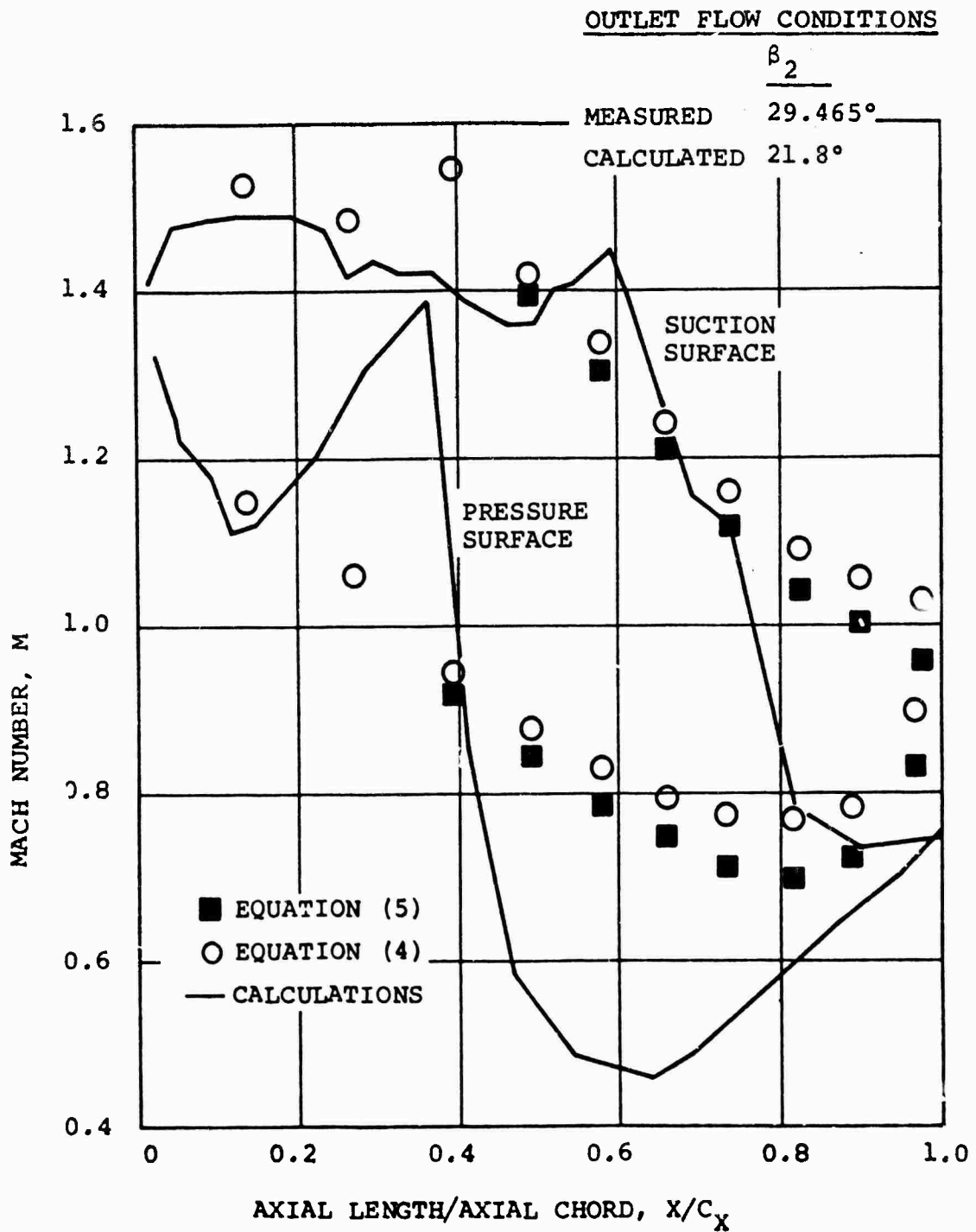


Figure 17a. Comparison of Experimental Blade Surface Mach Number Distribution with Results of Calculation at  $M_2$  of 0.808.

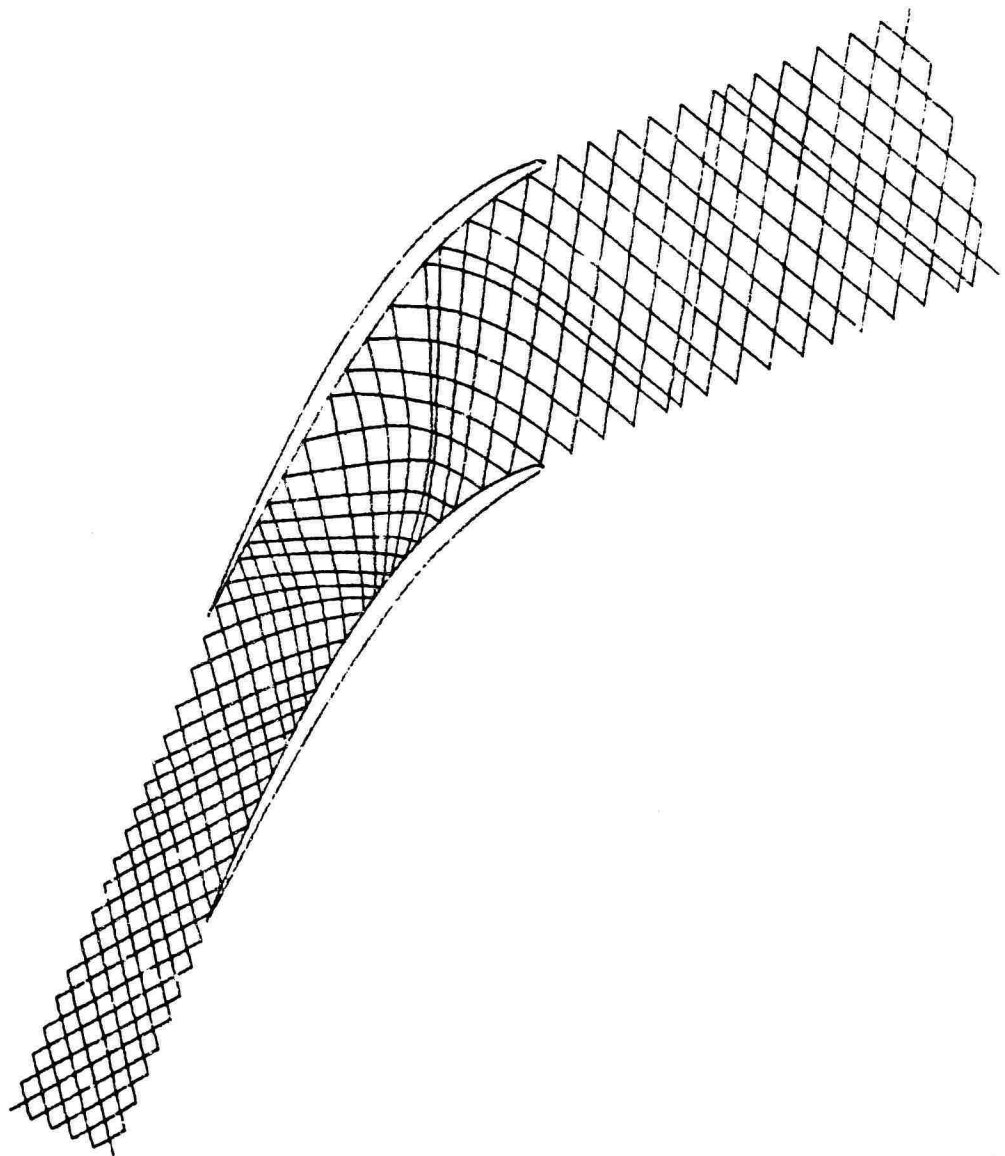


Figure 17b. Non-Orthogonal Grid System for Compressor Cascade at  $M_2$  of 0.808.

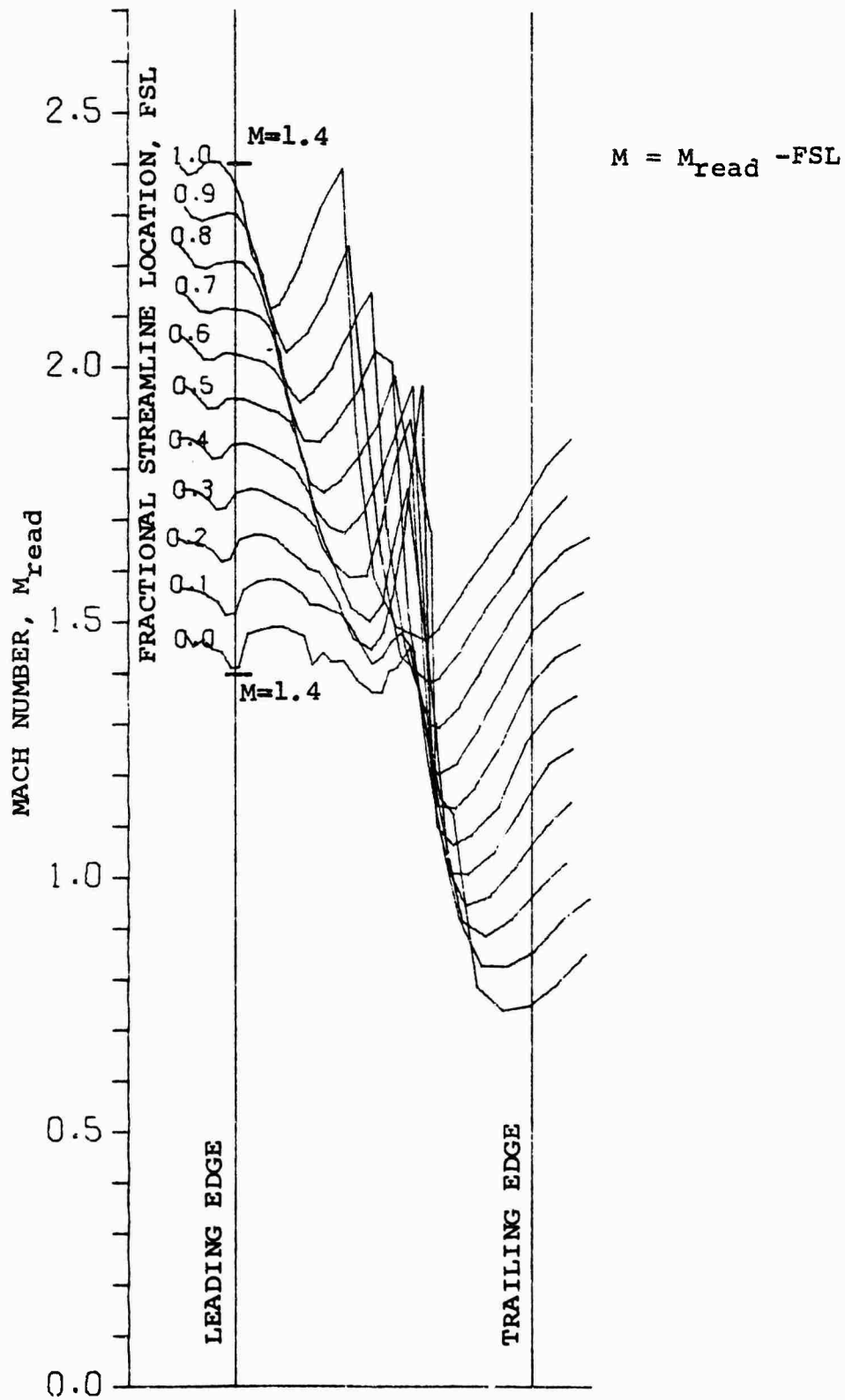


Figure 17c. Variation of Mach Number Along Streamlines at  $M_2$  of 0.808.

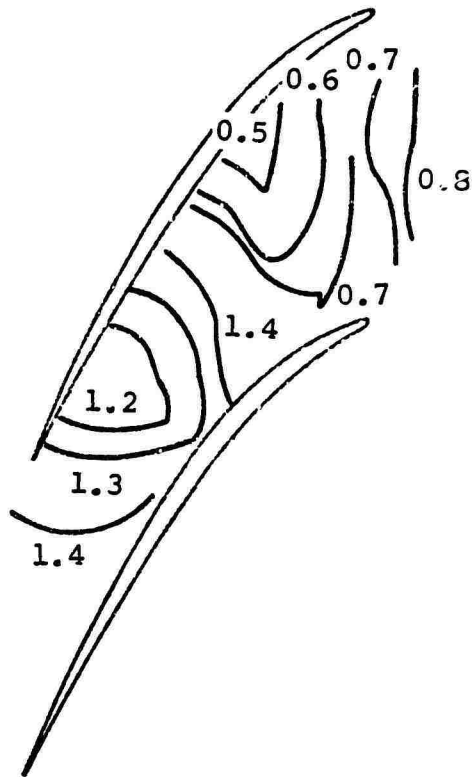


Figure 17d. Contours of Constant Mach Number at  $M_2$  of 0.808.

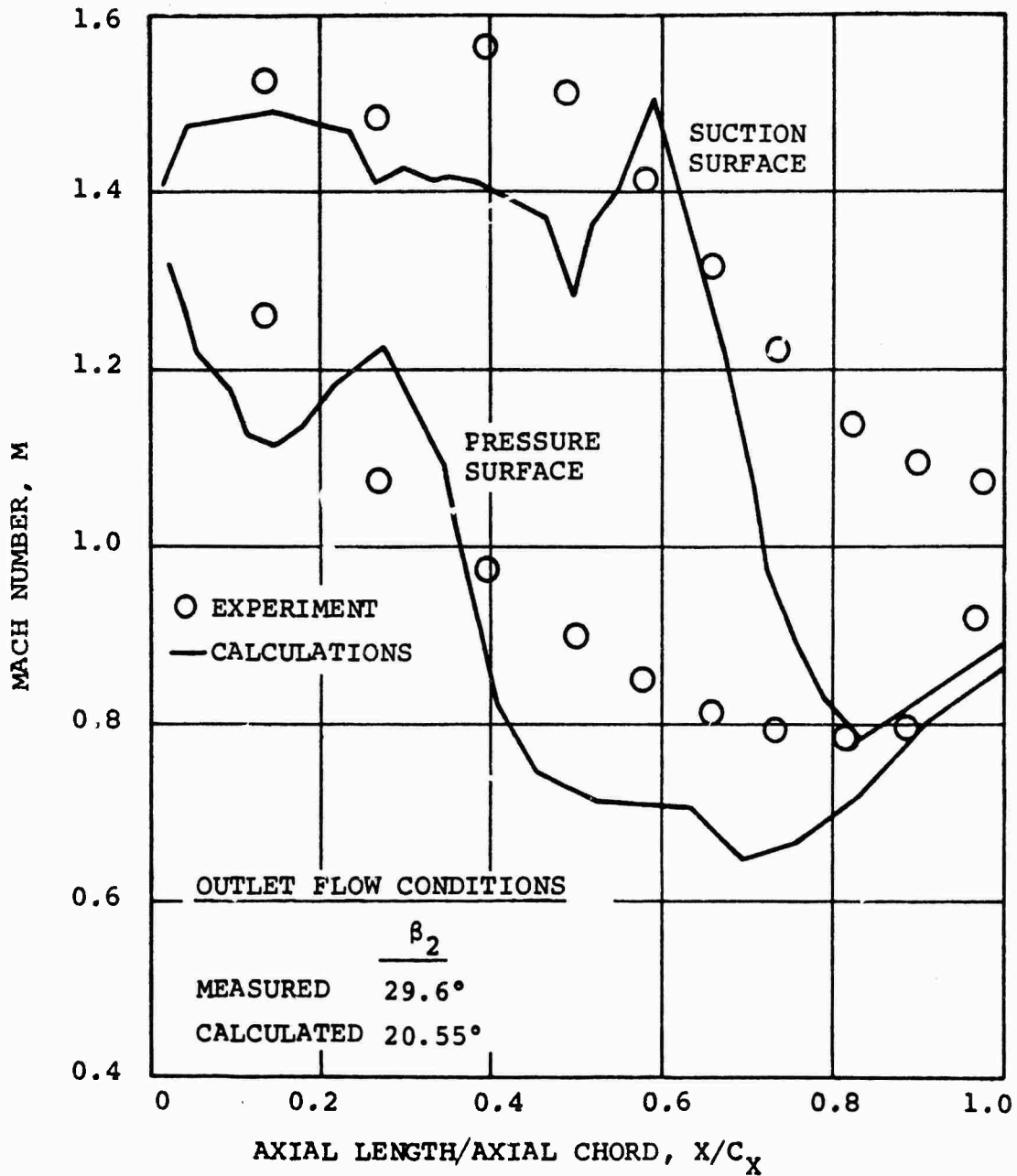


Figure 18a. Comparison of Experimental Blade Surface Mach Number Distribution with Results of Calculation at  $M_2$  of 0.900.

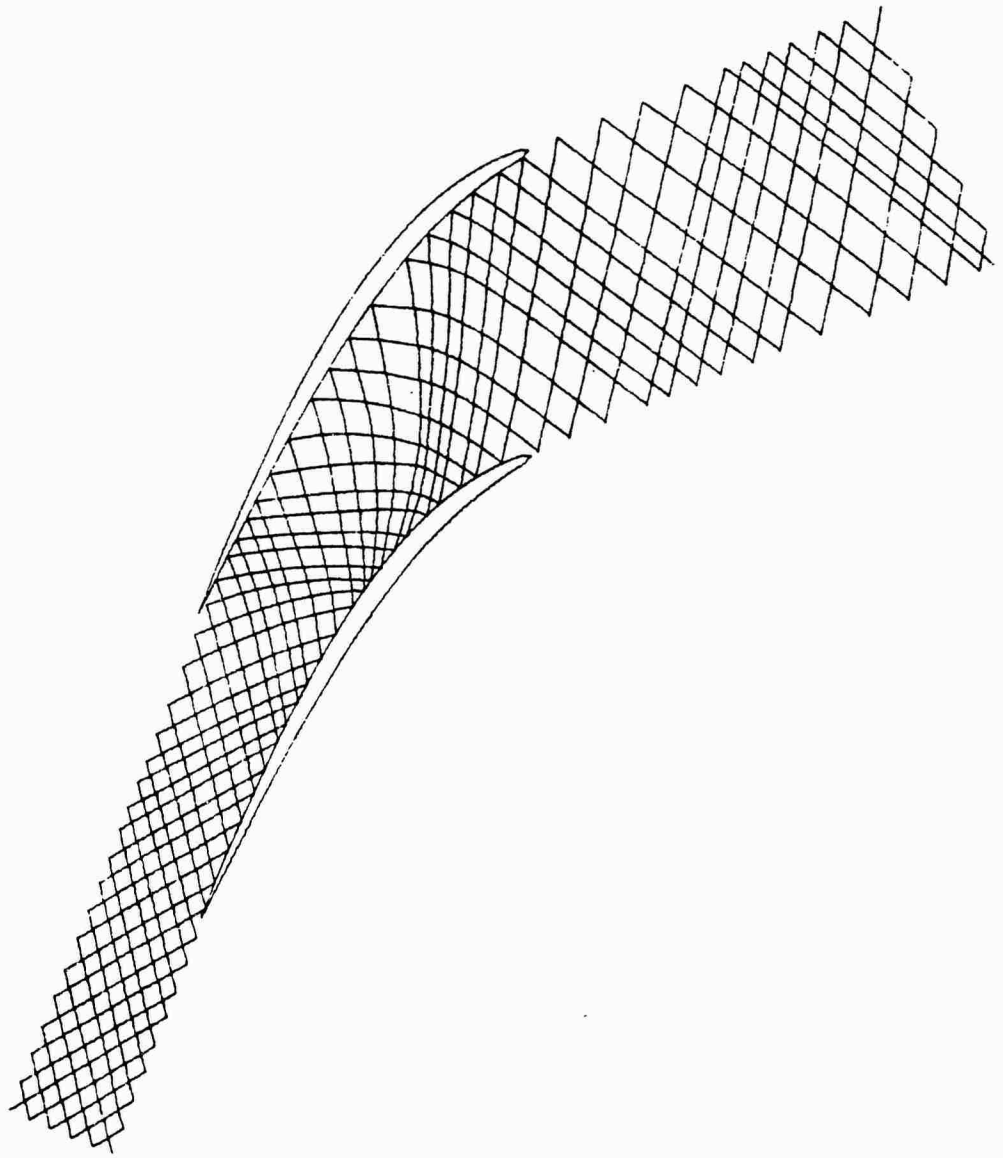


Figure 18b. Non-Orthogonal Grid System for Compressor Cascade at  $M_2$  of 0.900.

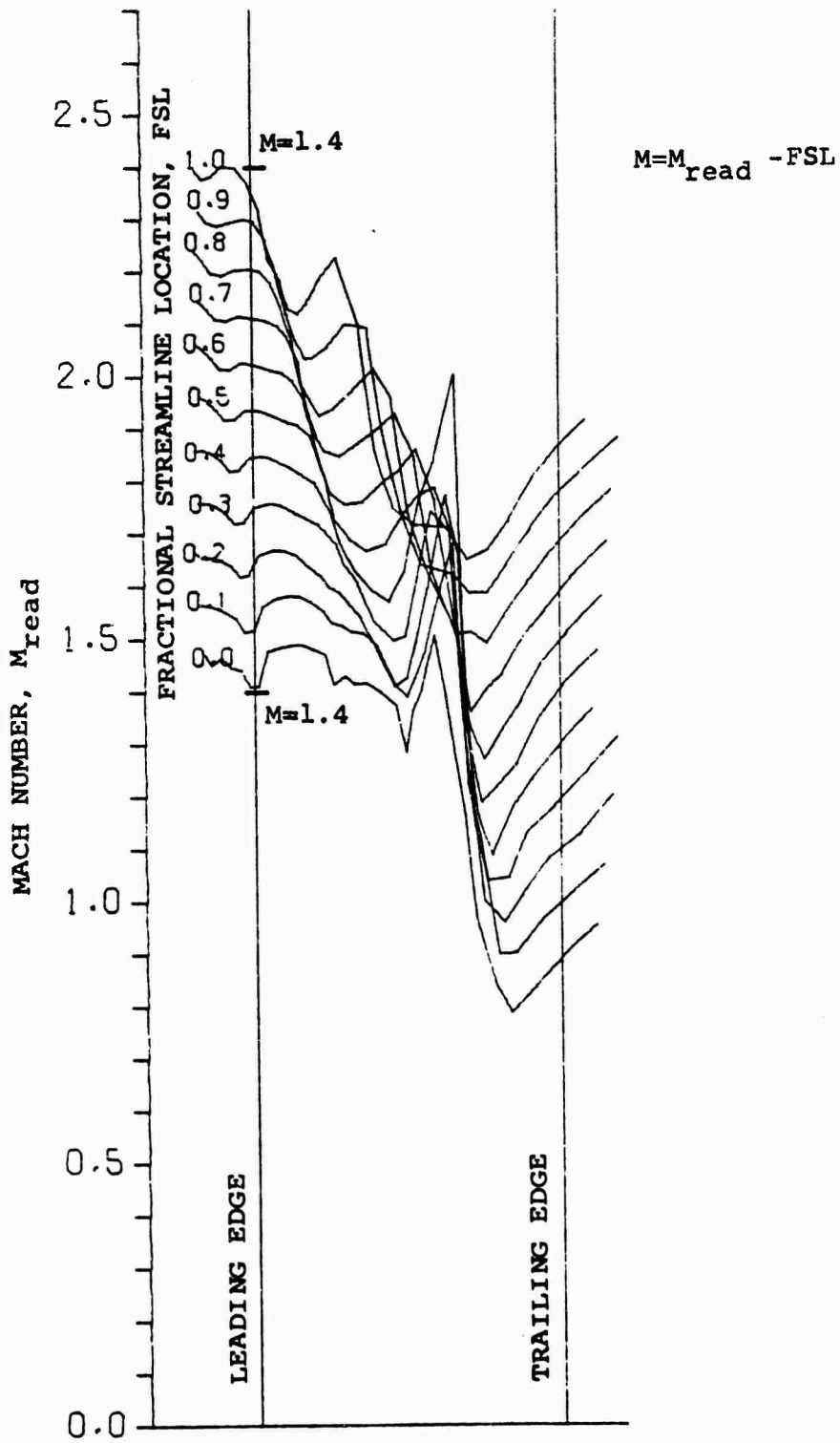


Figure 18c. Variation of Mach Number Along Streamlines at  $M_2$  of 0.900.

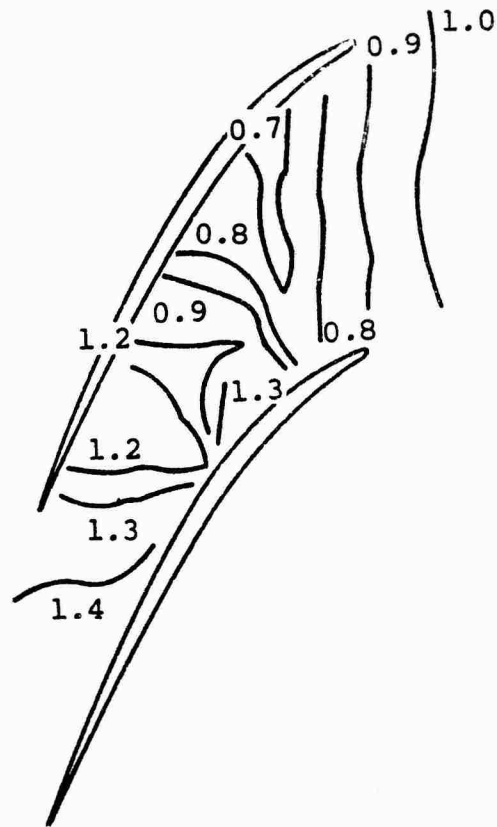


Figure 18d. Contours of Constant Mach Number at  $M_2$  of 0.900.

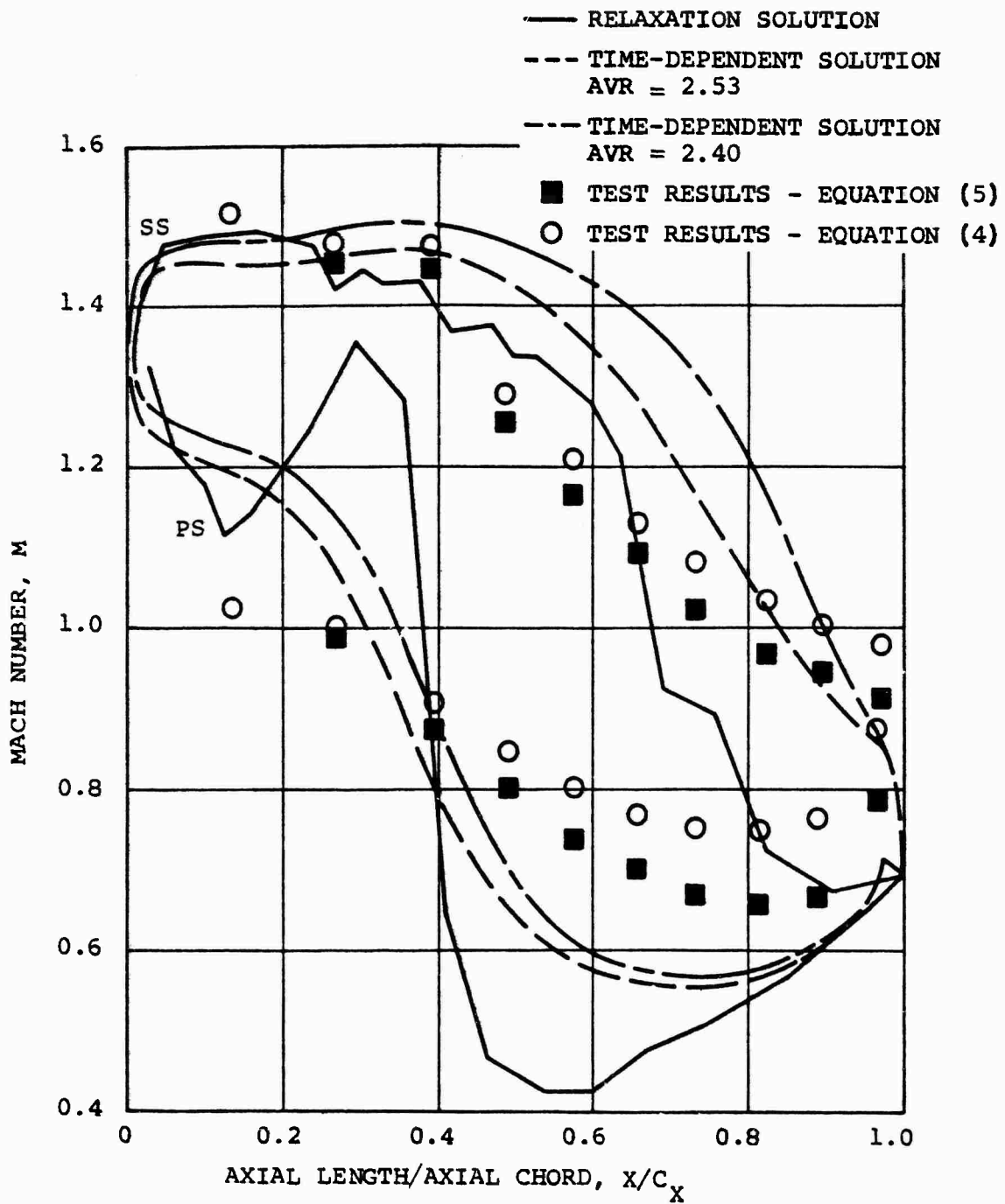


Figure 19. Comparison of the Relaxation Solution With the Time-Dependent Solution for a Compressor Cascade.

TABLE III. COMPARISON OF RELAXATION AND TIME DEPENDENT SOLUTIONS.

| Solution Type  | $M_1$ | $\beta_1$ | $\bar{M}_{TE}$ | $\beta_{TE}$ | $M_2$  | $\beta_2$ | Comments  |
|--|-------|-----------|----------------|--------------|--------|-----------|---|
| Experiment   | 1.460 | 66.85     | --             | --           | 0.760  | 29.95     | AVR = 2.07  |
| Relaxation   | 1.460 | 66.85     | 0.6956         | 27.355       | 0.7858 | 24.0      | $b_2/b_1$ based on $M_2 = 0.760$ ,<br>$\beta_2 = 24.0^\circ$      |
| Time-dependent comparable to relaxation              | 1.455 | 67.27     | 0.7075         | 29.71        | 0.7905 | 26.34     | b-width was the same as for the relaxation solution<br>AVR = 2.53 |
| Time-dependent satisfying measured outlet conditions | 1.457 | 66.83     | 0.6868         | 29.90        | 0.7595 | 27.21     | $b_2/b_1$ based on measured $M_2$ , $\beta_2$<br>A/R = 2.40       |

(1) The Mach numbers at the leading edge pressure surface are similar to the relaxation results, and definitely higher than experimental values.

(2) The Mach numbers near the trailing edge pressure surface are significantly below experimental values, but agree with relaxation calculations.

(3) Suction surface Mach number distributions over the first 60 percent of the blade agree reasonably well with both relaxation and experimental values.

(4) The relaxation solutions indicate a stronger compression on the latter 40 percent of the suction surface than does the time-dependent method. However, the time-dependent method is still stronger than the experimental values.

In addition, time-dependent methods predict larger turning than actually occurs although it is not quite as large as that indicated by relaxation solutions. See Table III.

#### c. Effect of b-Width Variation

In order for the computations to achieve the measured outlet Mach number for specified values of inlet Mach number and flow angle, the effective outlet b-width must be less than the geometrical b-width. This is physically a consequence of boundary layer growth through the cascade.

Equation (1) is the continuity equation for the overall flow between the inlet Station 1 and the downstream Station 2. For the ratio of specific heats,  $\gamma$ , equal to 1.4 and the specified inlet flow test conditions ( $M_1 = 1.460$ ,  $\beta_1 = 66.850$ )\*, Equation (1) becomes

$$\frac{b_2}{b_1} = 0.197810 \frac{(1 + 0.2M_2^2)^3}{M_2 \cos \beta_2} \quad (7)$$

This equation shows that for values of  $M_2$  specified by test conditions, the overall effective b-width ratio depends upon the value of  $\beta_2$  required to satisfy the Kutta condition.

---

\*The lack of periodicity in the analyses showed that periodic upstream flow was not obtained with these conditions.

The overall change in the effective b-width does not yield sufficient information to determine the variation of the b-width within the cascade. Instead, assumptions are required concerning the variation of the b-width. It was assumed that the b-width variation was primarily controlled by the variation of the geometrical b-width through the cascade. Then, the change in local b-width from its geometrical value can be expressed by

$$\Delta b(X) \equiv \frac{b(X) - b_{\text{geo}}(X)}{b_1} = f(X) \left[ \frac{b_2}{b_1} - \left( \frac{b_2}{b_1} \right)_{\text{geo}} \right]$$

where  $f(X)$  is some function of the axial coordinate,  $X$ , through the cascade expressing the local change in b-width in relation to the overall change in b-width.

The following three assumptions for  $f(X)$  were investigated:

Assumption 1:  $f(X) = a_0 + a_1 X$

with boundary conditions

- o  $f(X) = 0$  at  $X = -0.0546 C_x$  (0.1-inch axially upstream of leading edge)
- o  $f(X) = 1$  at  $X = 1.1458 C_x$  (approximately 0.5% of  $C_x$  forward of the region of contraction of cascade end walls)

Assumption 2:  $f(X) = a_0 + a_1 X$

with boundary conditions

- o  $f(X) = 0$  at  $X = 0.5 C_x$
- o  $f(X) = 1$  at  $X = 1.1458 C_x$

Assumption 3:  $f(X) = a_0 + a_1 X + a_2 X^2 + a_3 X^3$

with boundary conditions

- o  $f(X) = 0$  at  $X = -0.0546 C_x$
- o  $df(X)/dX = 0$  at  $X = -0.0546 C_x$
- o  $f(X) = 1$  at  $X = 1.1458 C_x$
- o  $df(X)/dX = 0$  at  $X = 1.1458 C_x$

The variation of  $f(X)$  is illustrated in Figure 20 for these three assumptions.

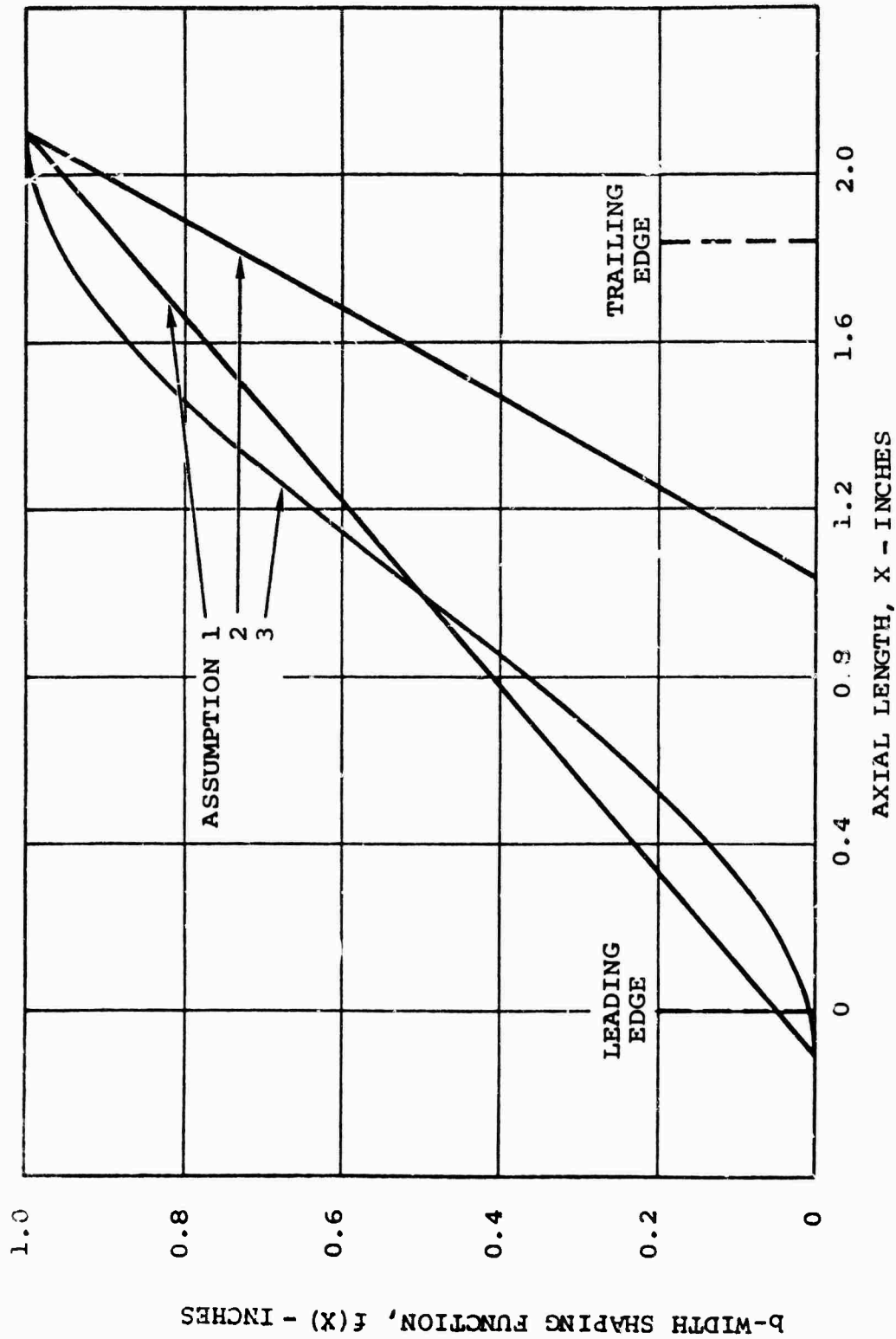


Figure 20. Curves Describing  $f(x)$ .

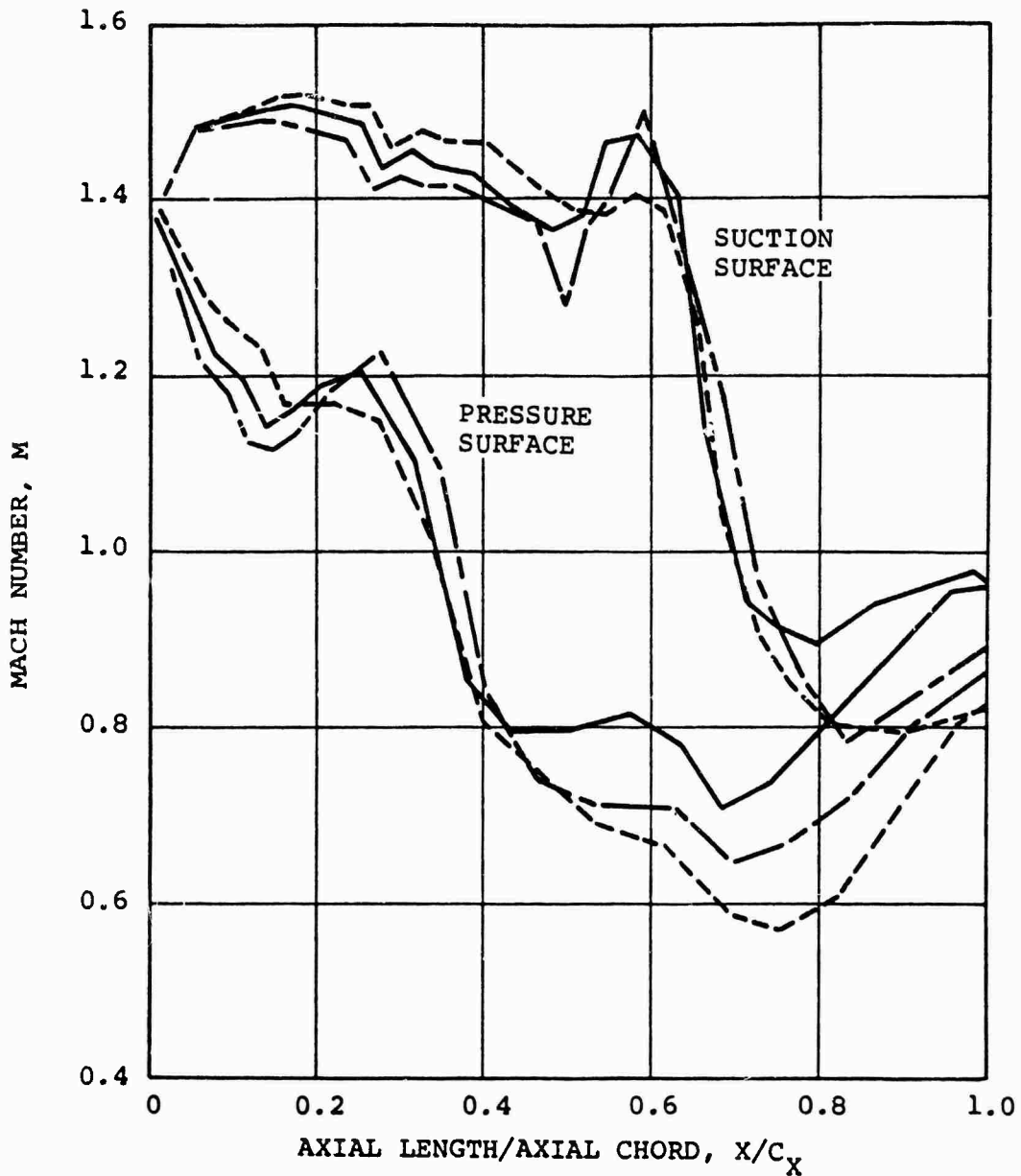
Examples of the blade surface Mach number distributions resulting from the three assumptions of the functional form of  $f(X)$  are illustrated in Figure 21. The results are for the outlet flow angles that approximately satisfy the Kutta condition. Significant differences are noted in the trailing edge region and on the pressure surface from  $X/C_x \approx 0.5$ . The calculation results yield different values for the flow angle at the trailing edge as indicated in Table IV. As may be seen, the deviation angle at the trailing edge varies from near zero to 2.5 degrees, depending upon the manner in which  $f(X)$  is represented.

TABLE IV. ESTIMATES OF FLOW ANGLE AT THE TRAILING EDGE PLANE UNDER THE INFLUENCE OF b-WIDTH DISTRIBUTION.

| Description  | $\beta_2$ | $M_2$  | $\bar{M}_{TE}$ | $\bar{\beta}_{TE}$ |
|--|-----------|--------|----------------|--------------------|
| Experimental results<br>( $P_2/P_1 = 1.821$ )          | 29.600°   | 0.900  | -              | 22.534°*           |
| Linear $f(X)$ from $X/C_x =$<br>-0.0546 (Assumption 1) | 20.55°    | 0.9514 | 0.8766         | 22.3°              |
| Linear $f(X)$ from $X/C_x =$<br>0.5 (Assumption 2)     | 21.0°     | 0.9581 | 0.8281         | 24.5°              |
| Smooth $f(X)$ (Assumption 3)                           | 25.0°     | 0.9617 | 0.9597         | 25.1°              |

\*Trailing edge blade angle on mean camber line (see Table I).

The choice between the three assumed functions  $f(X)$ , as well as any other that may be chosen, is purely arbitrary since no means exist for determining the variation of the effective b-width. Furthermore, comparison of the calculated blade surface Mach number distributions with measured values is not likely to confirm a choice since the measured values necessarily include the viscous effects of the real flow (i.e., blade boundary layer growth due to shock-boundary layer interaction--an effect that leads to smoothing the blade surface pressure distributions in comparison to inviscid flow calculations). For this reason, the simplest assumption (Assumption 1) was used in this investigation.



| $\beta_2$    | $M_2$          |   |
|--------------|----------------|---|
| — 25.0°      | 0.9617 (0.900) | SMOOTH b-WIDTH VARIATION                |
| - - - 21.0°  | 0.9581         | LINEAR b-WIDTH CHANGE FROM $0.5c_x$     |
| - · - 20.55° | 0.9514         | LINEAR b-WIDTH CHANGE FROM $-0.0546c_x$ |

Figure 21. Comparison of Blade Surface Mach Number Distributions for Various Assumptions on the Behavior of  $f(x)$ .

## d. Pressure Surface Leading Edge

On both a qualitative and quantitative basis, the Mach number distribution near the pressure surface leading edge differs markedly from that of the data. All relaxation calculations show a compression over the first 10 percent of the blade followed by a sharp but brief re-acceleration and a strong shock wave. Test data shows a compression near the leading edge that is a strong function of cascade back pressure without any re-acceleration such as that observed by the calculation. The time-dependent calculation falls between the data and the relaxation calculation, indicating a weaker compression but no re-acceleration.

Analysis of the area distribution through the cascade indicates that the area continuously decreases from the leading edge until a minimum is reached midway through the cascade. This minimum has approximately 8 percent less area than exists at the leading edge. Figure 22 shows the approximate location of this minimum. The minimum lies between the pressure surface at approximately 0.31 axial chord and the suction surface at 0.72 axial chord. The calculated strong compression occurs just downstream of this location. Correspondingly, the strong compression evidenced on the suction surface occurs very near 0.72 of axial chord. The presence of a strong, nearly normal wave in this region (shown in Figures 16d, 17d, and 18d) seems to be related to this minimum passage area. The lack of a similar strong compression in the data is evidence of strong viscous action in this region.

A comparison of Mach numbers calculated by relaxation and derived from experimental data is shown in Figure 23. The oblique shocks going from upstream conditions ( $M = 1.460$ ,  $\beta = 66.85^\circ$ ) to the local surface angle are shown in Figure 23 to permit a reasonable compression value to be estimated. Two branches, a strong oblique and weak oblique, are indicated. The relaxation analysis shows compressions reasonably consistent with the weak oblique shock relations. At the maximum static pressure ratio, the data yields a substantially stronger compression than either the relaxation analysis or the oblique shock relations. A compression of this magnitude would require an oblique shock yielding in excess of 10.5 degrees of deflection. This is 5 degrees of deflection past the local metal angle. Such a deflection is possible, since the static pressure ratio exceeds that needed to separate a boundary layer (static pressure from far upstream to the first point measured on the pressure surface for the  $M_2 = 0.76$  case is 1.78). However, other effects could also be responsible since this case is far more complex than those usually treated by simple oblique shock relations. Waves generated abreast of the blade should be weak since the unique inlet flow angle is nearly the suction surface angle. The

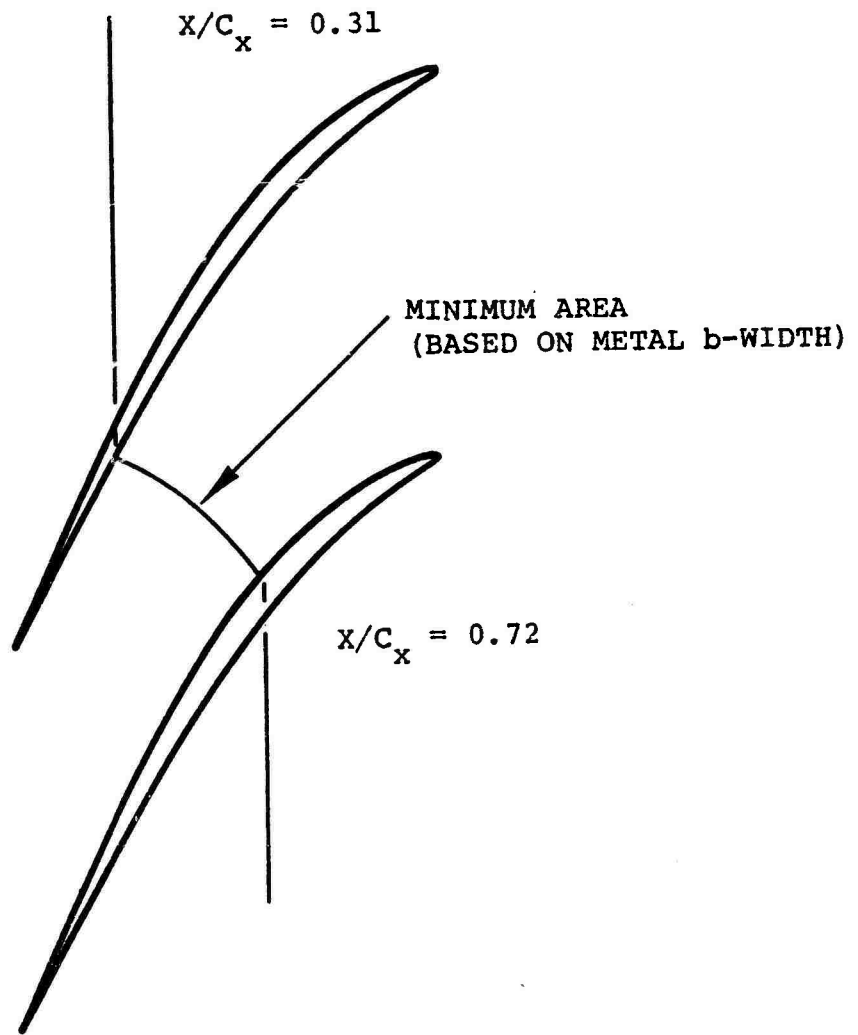


Figure 22. Location of Minimum Area Section.

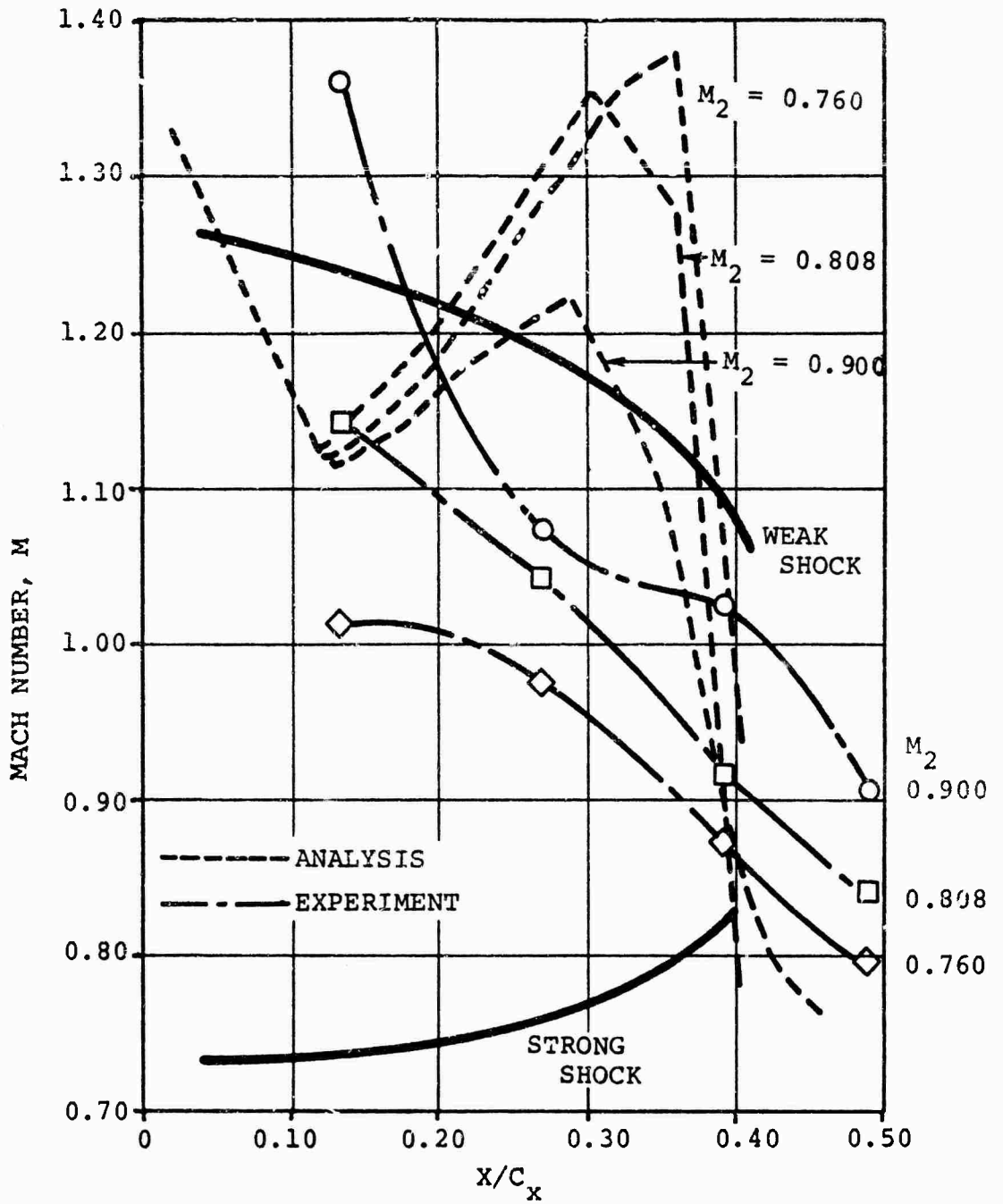


Figure 23. Pressure Surface Mach Number Distribution.

relatively strong contraction in b-width complicates the understanding of the phenomenon in the leading edge region. For example, an unloaded streamline should have nearly constant Mach number along it. When there is no change of b-width, such a streamline is straight. When b-width is not constant, the following relations can be applied:

$$\rho V \cos\beta b = \rho_1 V_1 \cos\beta_1 b_1 \quad \begin{array}{l} \text{Continuity} \\ \text{of flow} \end{array} \quad (6)$$

$$V \sin\beta = V_1 \sin\beta_1 \quad \begin{array}{l} \text{Constant} \\ \text{tangential} \\ \text{momentum} \end{array} \quad (7)$$

The result is that an unloaded streamline will have a flow angle given by Equation (8)

$$\tan\beta = \frac{\rho b}{\rho_1 b_1} \tan\beta_1 \quad (8)$$

Often, when  $\beta$  is large, the density ratio is near unity and Equation (7) becomes dominantly geometric. Thus, the suction surface even though curved, provides almost constant velocity near the leading edge. If the pressure surface has a radius of curvature less than that of a free streamline, it will be compressive (curve b of Figure 24). If it has a radius of curvature greater than a free streamline, it will be expansive (curve c of Figure 24). A streamline approaching from far upstream must be compressive as illustrated by Figure 25 (note the suction surface lies fairly close to a free streamline and is only slightly expansive). If the density variations are neglected, Equation (8) can be differentiated simply to yield Equation (9).

$$\frac{d(\tan\beta)}{d(x/c_x)} = \frac{\tan\beta_1}{b_1} \frac{d(b)}{d(x/c_x)} \quad (9)$$

This equation can be used to estimate whether a surface should be compressive or expansive. A plot of Equation (9) compared to the actual derivative of  $\tan\beta$  on the pressure surface is shown in Figure 26. Note that if the flow upstream were aligned with the pressure surface, it would expand along the pressure surface until a point in excess of 20 percent of chord is reached, whereupon it would compress. This indicates that it is reasonable to expect the following on the pressure surface.

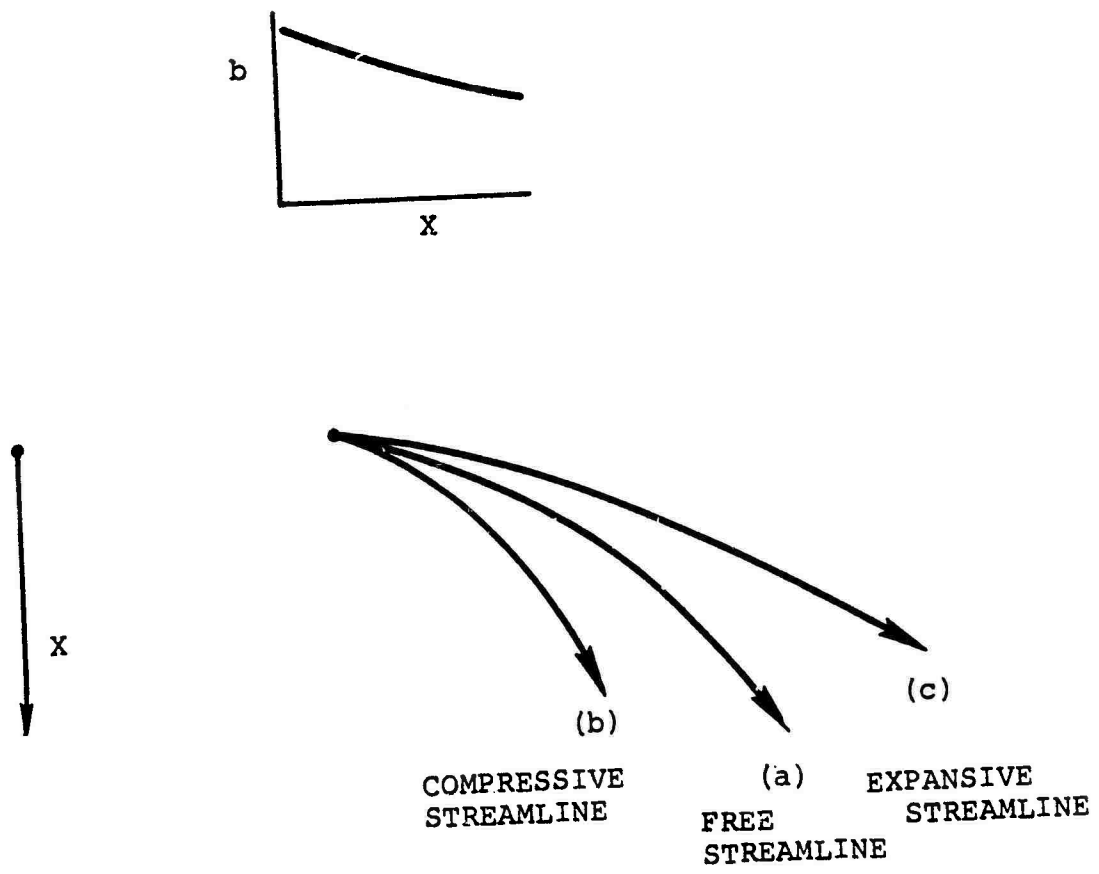


Figure 24. Streamline Curves Relative to the Neutral.

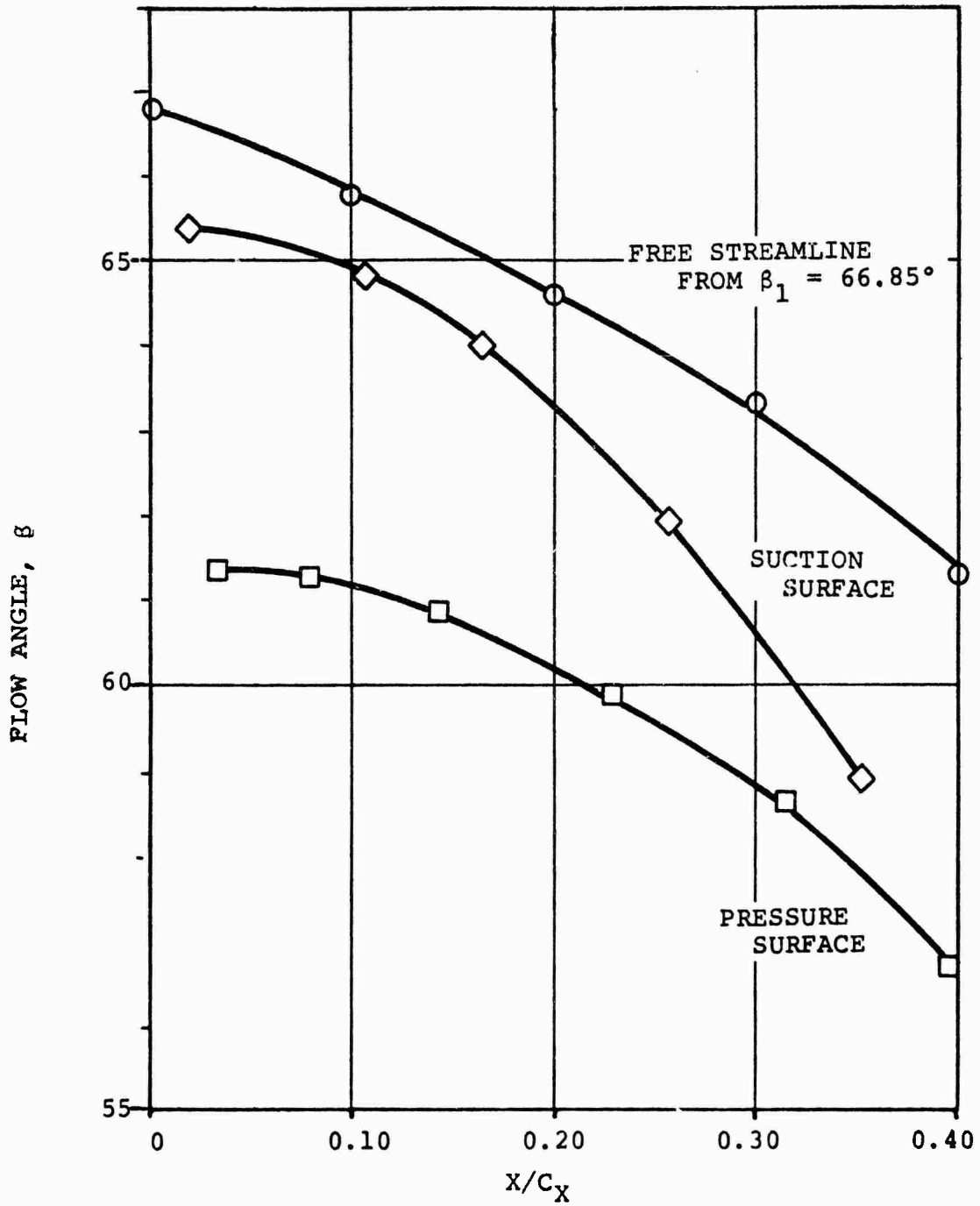


Figure 25. Flow Angles Along Suction Surface, Pressure Surface, and a Free Streamline.

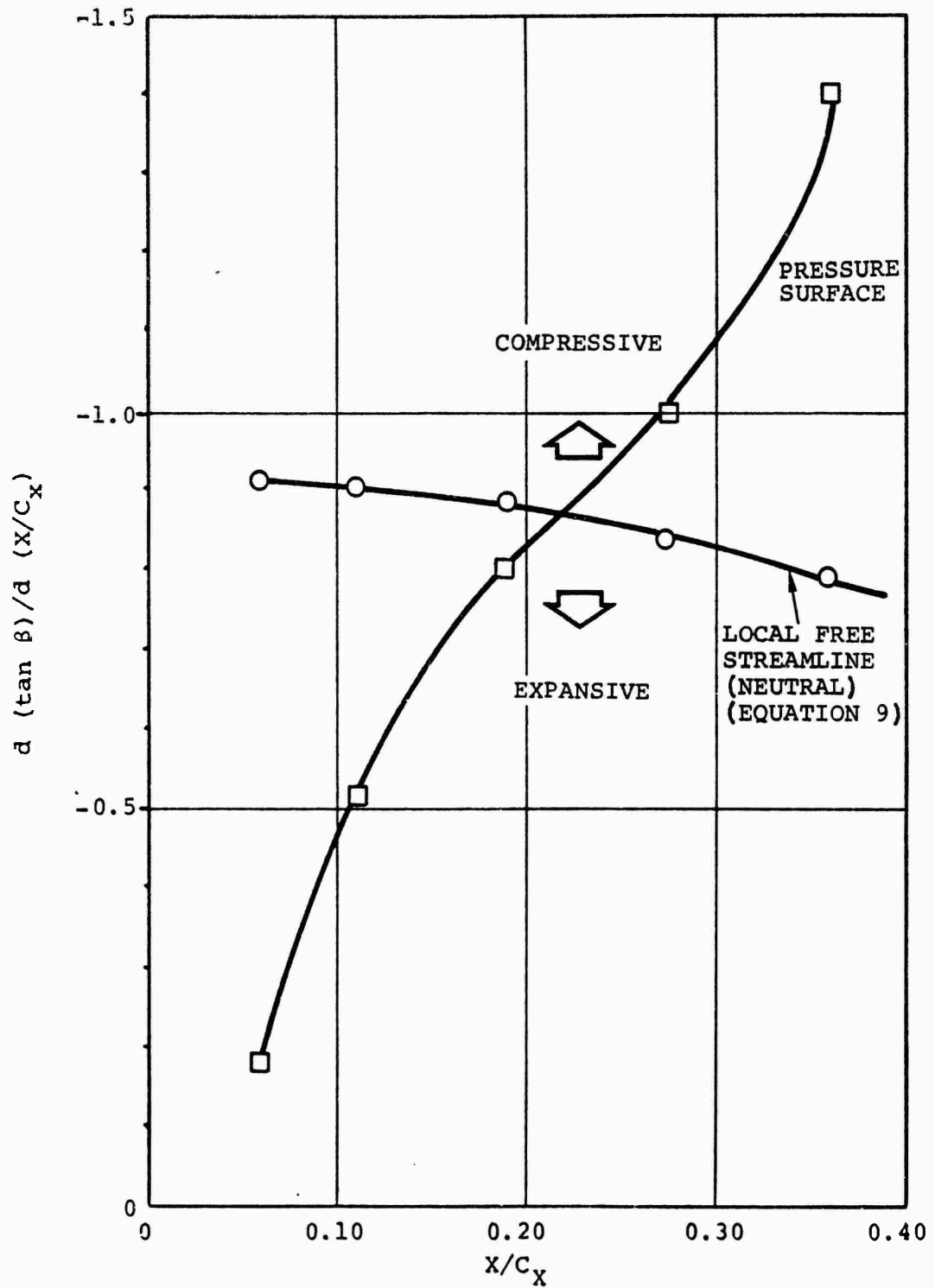


Figure 26. Derivative of Pressure Surface Angle Versus Axial Position.

(1) Compression from the upstream direction to the local flow direction at leading edge

(2) Expansion behind the compression due to the sharp b-width reduction on a surface of low curvature

(3) Subsequent compression due both to increased surface curvature and a decrease in available flow area

This general structure is exactly what was computed. Its absence in the data is attributed to strong viscous effects in the leading edge region. The effect on design could be significant because the inviscid calculation predicts high Mach numbers immediately ahead of the splitter. The data indicates a much lower level of Mach number, at least on the pressure surface.

e. Exit Region

It has been established experimentally that an important parameter for determining exit deviation angle is axial velocity density ratio. At the same time, exit deviation angle is largely independent of Mach number when large viscous effects are not present. Consequently, to predict turning, axial velocity density ratio should be matched. When losses are high, an inviscid calculation cannot match the axial velocity-density ratio and the static pressure rise of the cascade even approximately. Adjustment of b-width will reproduce either exit Mach number or axial velocity-density ratio, but not both. Consequently, when b-width distributions are adjusted to match exit Mach number, the calculated turning is greater than is observed experimentally. The result is more turning near the trailing edge and rather large discrepancies in loading distribution in the latter portion of the blade.

f. Choking

It is important, when considering the application of splitters, to determine the ability of the prediction method to predict choke. Boundary conditions for the inviscid transonic relaxation are such that a constant flow rate is forced into the cascade. If this exceeds the flow capacity, a "spill" in the choked region will occur which causes the coefficient matrix to become singular and the relaxation solution to diverge. Study of several cascades indicates that this "choking" failure takes place when the flow is just less than that yielding a local  $A/A^*$  of unity.

For the cascade under study in Phase I, the area decreases to a minimum (approximately 8 percent less than the inlet). Since the  $A/A^*$  for an inlet Mach number of 1.460 is 1.1501 this is not sufficient to cause choking. The area then increases to the trailing edge. The minimum passage b-width occurs downstream of the trailing edge. Figure 27 shows the combination of turning and axial-velocity-density ratio that results in choking ( $A/A^* = 1.0$ ) at this downstream station. Relaxation calculations were possible at axial velocity-density ratios up to at least 2.67. Calculations were not possible when axial velocity-density ratios were increased beyond a certain point. During the calculations to determine the Kutta condition, results were obtained to an exit Mach number of 0.98. Normal calculations to determine the Kutta condition consisted of varying the exit angle with a constant axial velocity density ratio. Variations below the Kutta line (Figure 27) were observed to be severely restricted by "choking" failures.

#### g. Conclusions - Phase I

A review of the analysis completed in Phase I suggests the following:

(1) The transonic relaxation solution represents a reasonable approximation to the inviscid flow within the cascade.

(2) Substantial deviations between experimental data and inviscid calculations were observed. Principal deviations, from a design point of view, are:

- o The lack of a strong pressure surface re-acceleration followed by compression. The inviscid solution implies relatively high Mach number abreast of the location of a splitter leading edge
- o Larger turnings than those observed at a given exit Mach number
- o Less diffusion on the pressure surface
- o The exit flow angle at the Kutta condition was appreciably influenced by b-width shape and distribution

(3) There is general agreement between the experimental data and the calculations along the suction surface.

It should be possible, with use of the inviscid solution, to determine the configuration offering the lowest overall surface diffusion. Consequently, the lowest loss configuration could also be determined. However, a reasonable design estimate of deviation angle probably cannot be based on the inviscid solution.

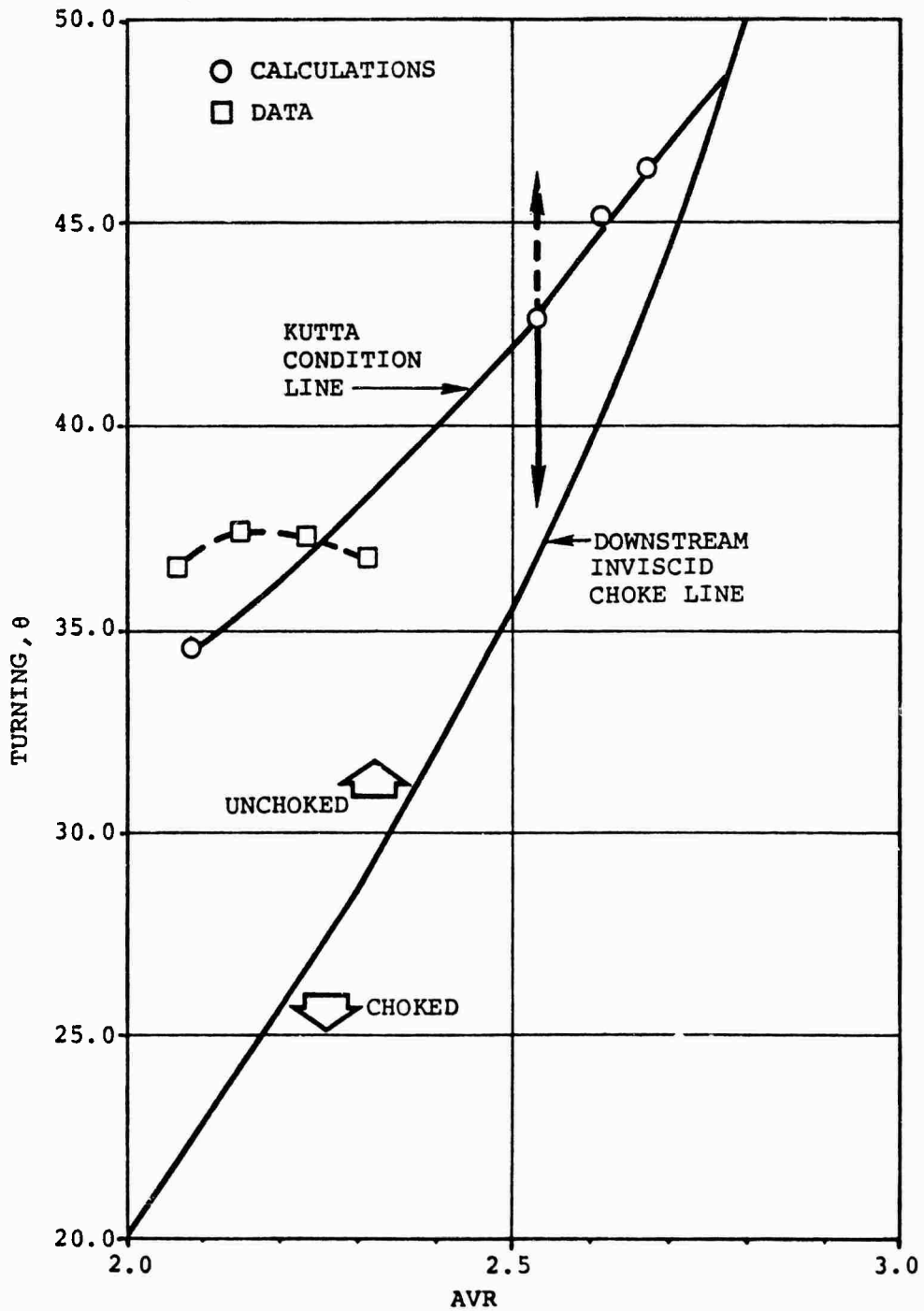


Figure 27. Choking Characteristic, Single Bladed Cascades.

## 2. PHASE II - ANALYSIS OF CASCADES WITH SPLITTER VANES

### a. Relaxation Solution

The results of relaxation calculations with the ARL splitter at two different splitter settings are presented in Figures 28a through 28d, and 29a through 29d. The following information is shown in each figure.

28a and 29a - Final grid system

28b and 29b - Mach number distribution along quasi-streamlines

28c and 29c - Lines of constant Mach number

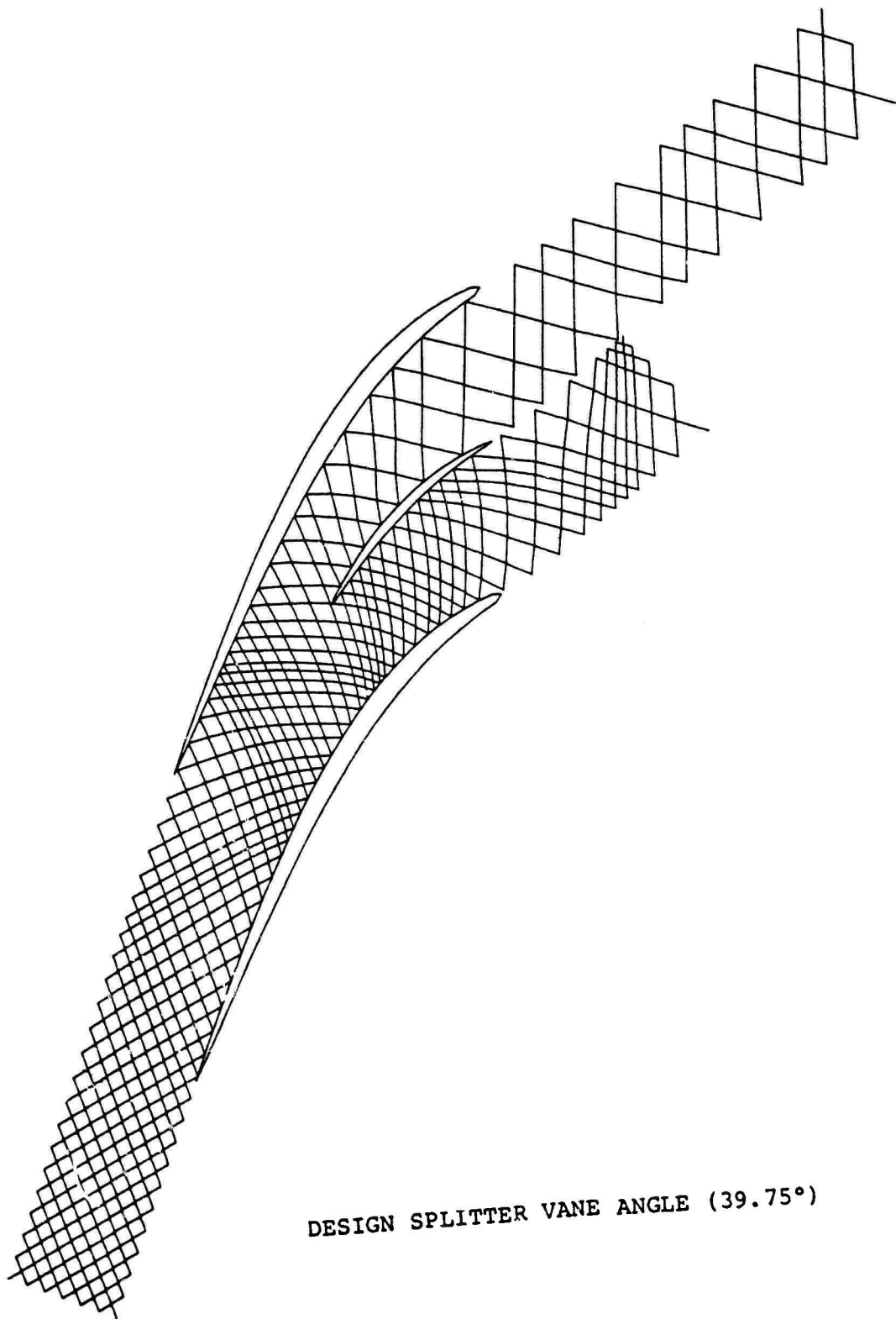
28d and 29d - Surface static pressures

Relaxation calculations were performed with a b-width distribution that corresponds to the cascade test metal dimensions. Mach number distributions are for the highest experimental static-pressure ratio, even though the experimental exit Mach number is always higher than the 0.6 exit Mach number computed.

All calculations with the exit Mach number near the experimental values indicated that the cascade was choked. These calculations were performed with a natural flow split. That is, the one with the continuous potential across the downstream boundary between the upper and lower passages. Attempts were made to modify the calculated flow split between upper and lower passages. This could be done by increasing the potential on the far downstream boundary of one passage relative to the other. However, it would also result in higher velocities in one passage than it would in the other. This complicates the calculation of the shape of the boundary between passages since the curvature of this slip line is adjusted to yield a static pressure balance on the common contour between passages downstream of the splitter. The changes required to accomplish this modified flow split correctly were extensive and outside the scope of the present program. The observed choking led directly to the examination of flow area, which is discussed in Paragraph b.

### b. Area Calculation

The overall area distribution through the passage, with and without splitters is shown in Figure 30. The introduction of the splitter results in a 2-percent reduction of the minimum flow area. However, the overall area is well above the 15-percent contraction required to choke the cascade. Individual passage areas yield a quite different result. An estimate of the flow split can be obtained by observing the streamline (without the splitter) passing through the location of the splitter leading edge. This is done using the flow solution without splitter discussed in



DESIGN SPLITTER VANE ANGLE ( $39.75^\circ$ )

Figure 28a. Grid System for Converging Cascade With Splitters,

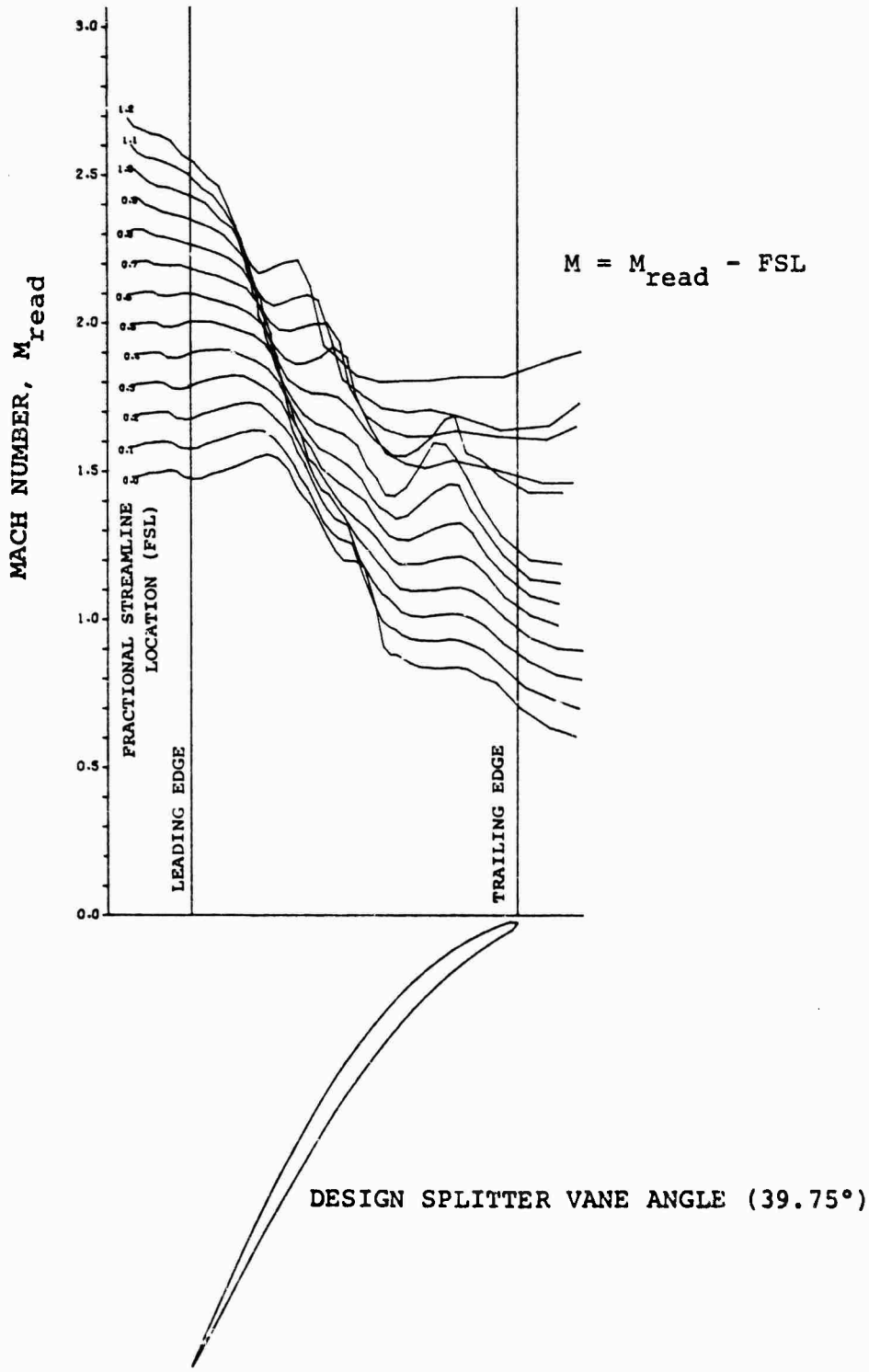


Figure 28b. Streamline Mach Number Distribution for Converging Cascade With Splitters.

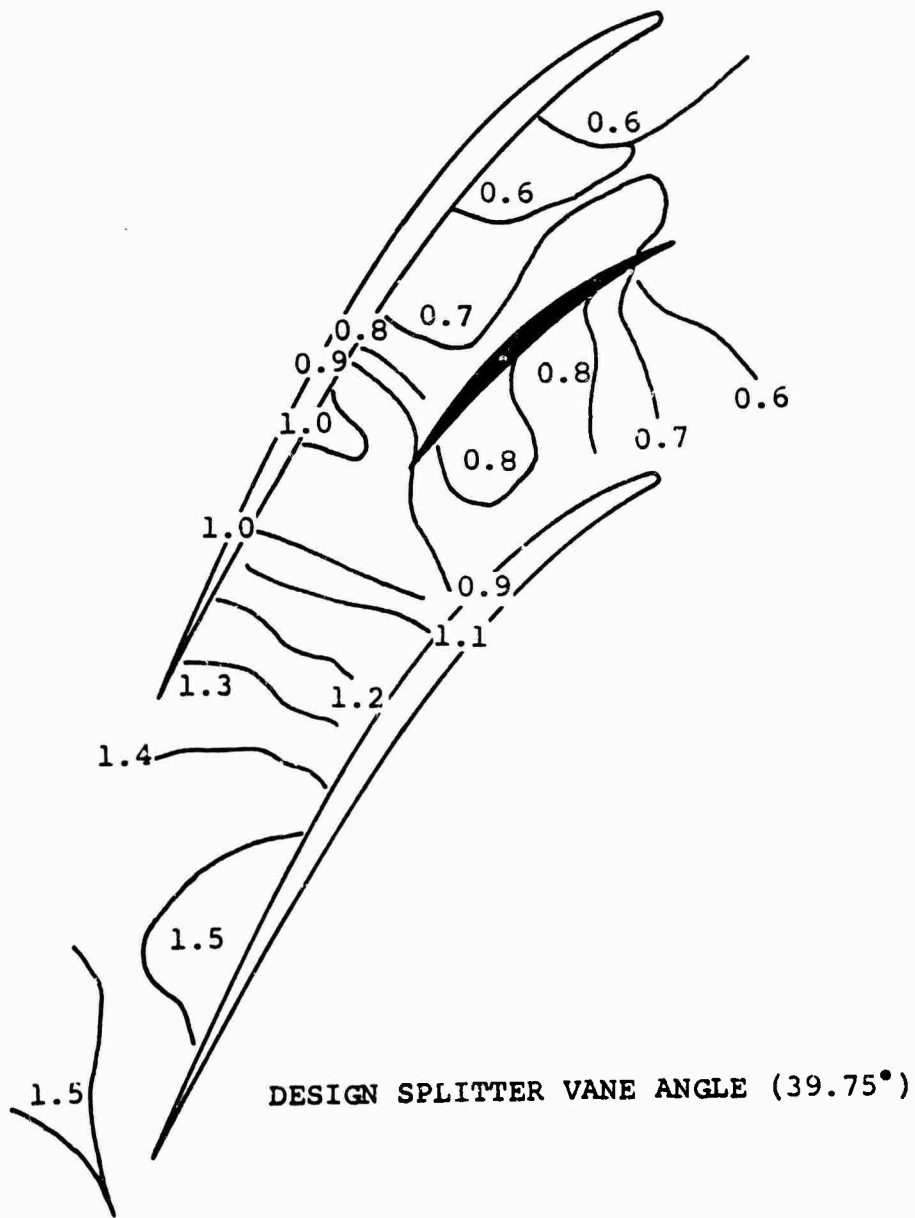


Figure 28c. Internal Mach Number Distribution for Cascade With Splitters.

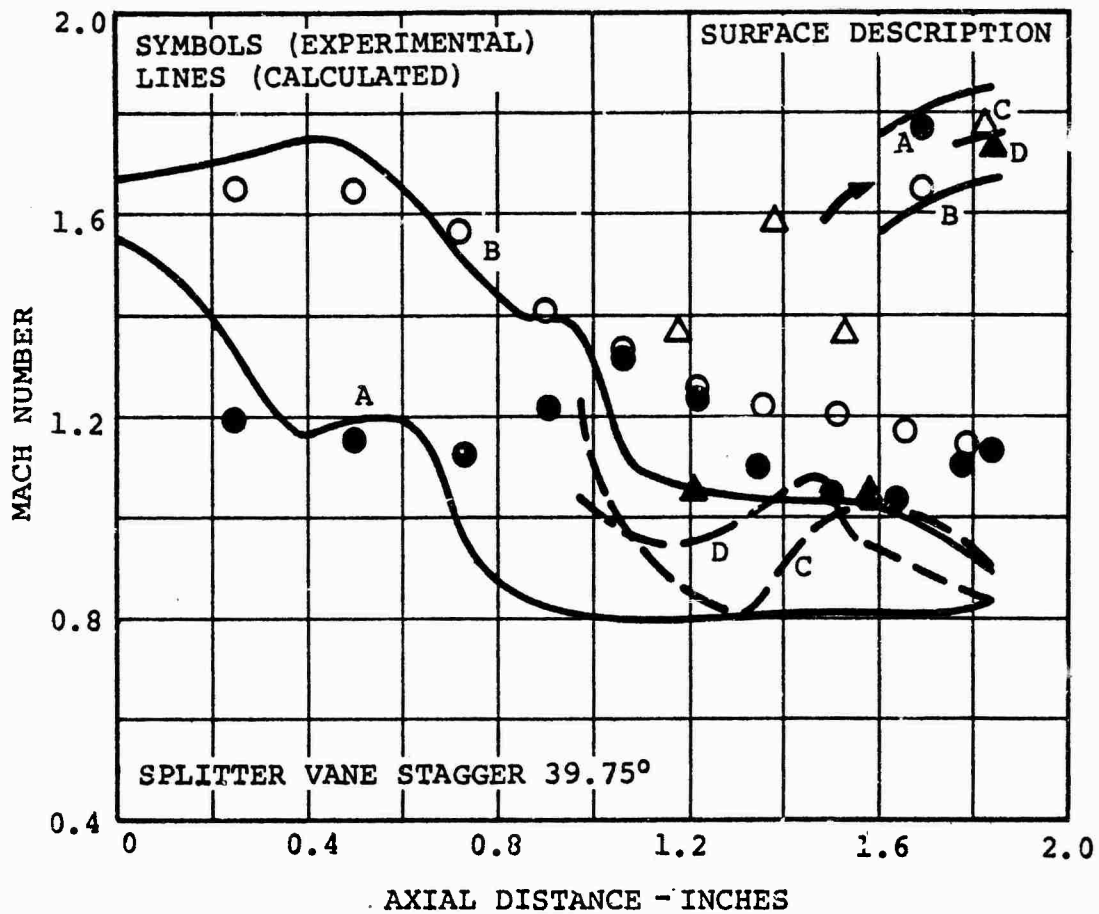


Figure 28d. Analytical and Experimental Wall Mach Numbers.

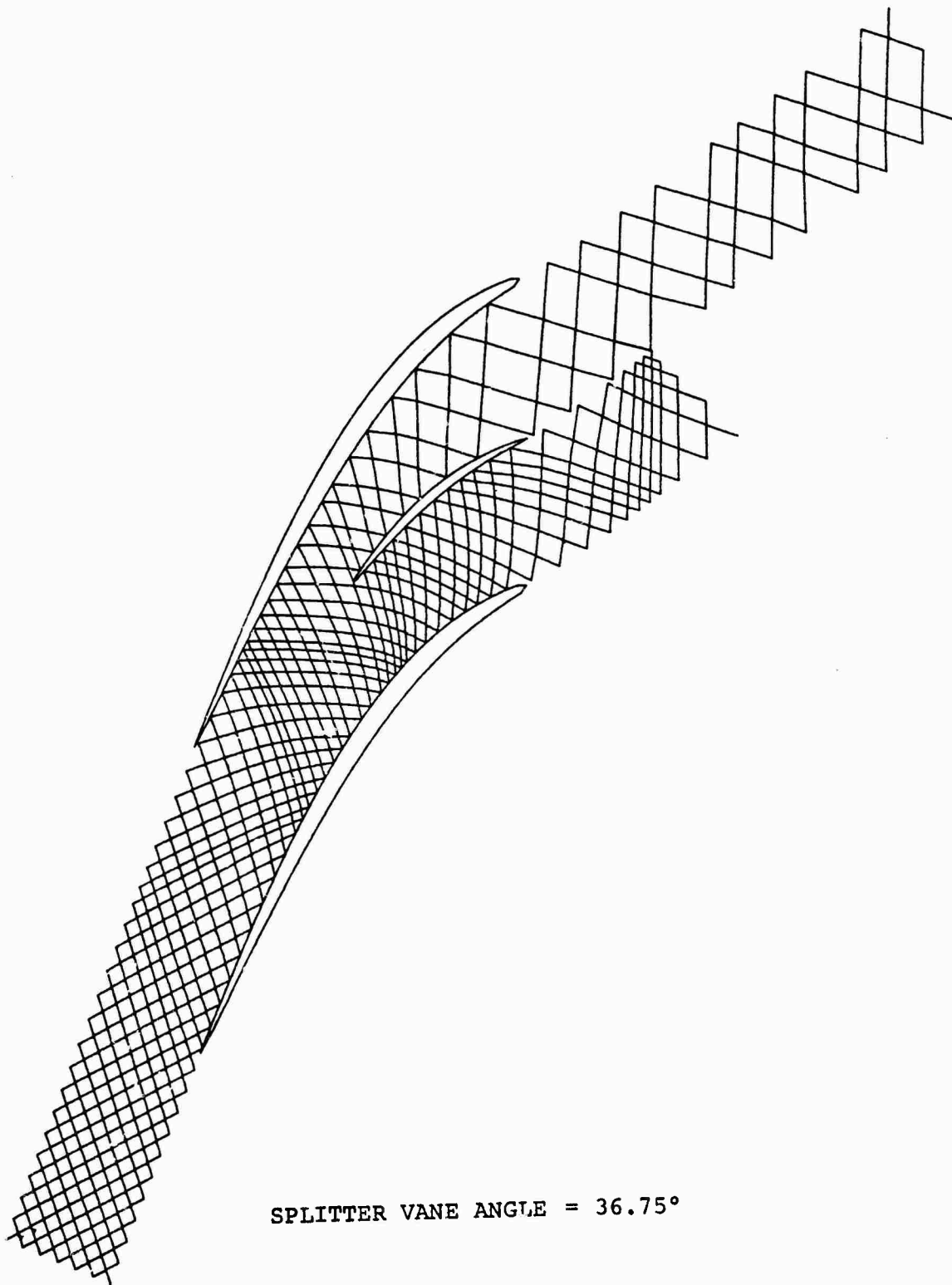


Figure 29a. Grid System for Converging Cascade  
With Splitters Rotated Minus 3°.

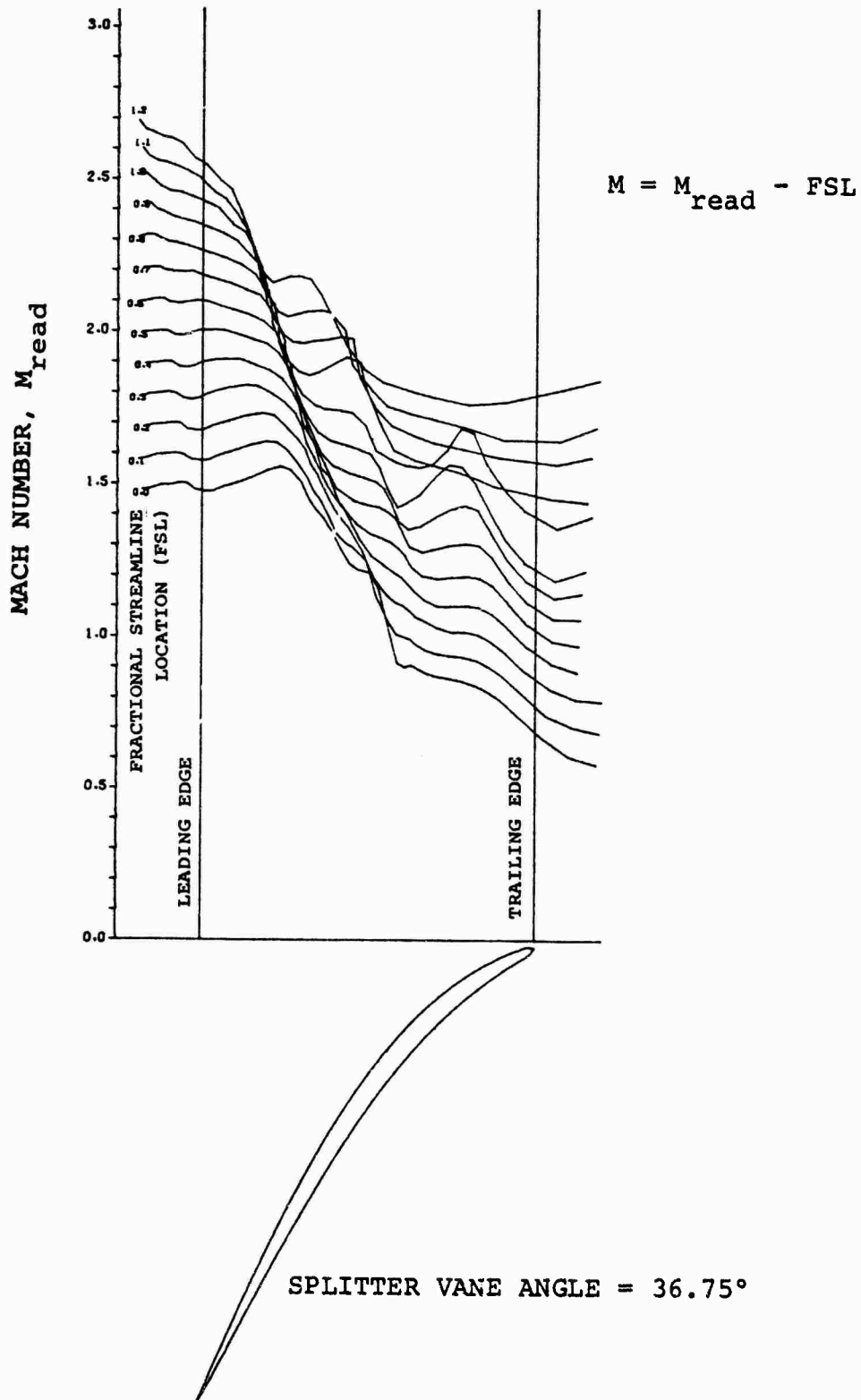
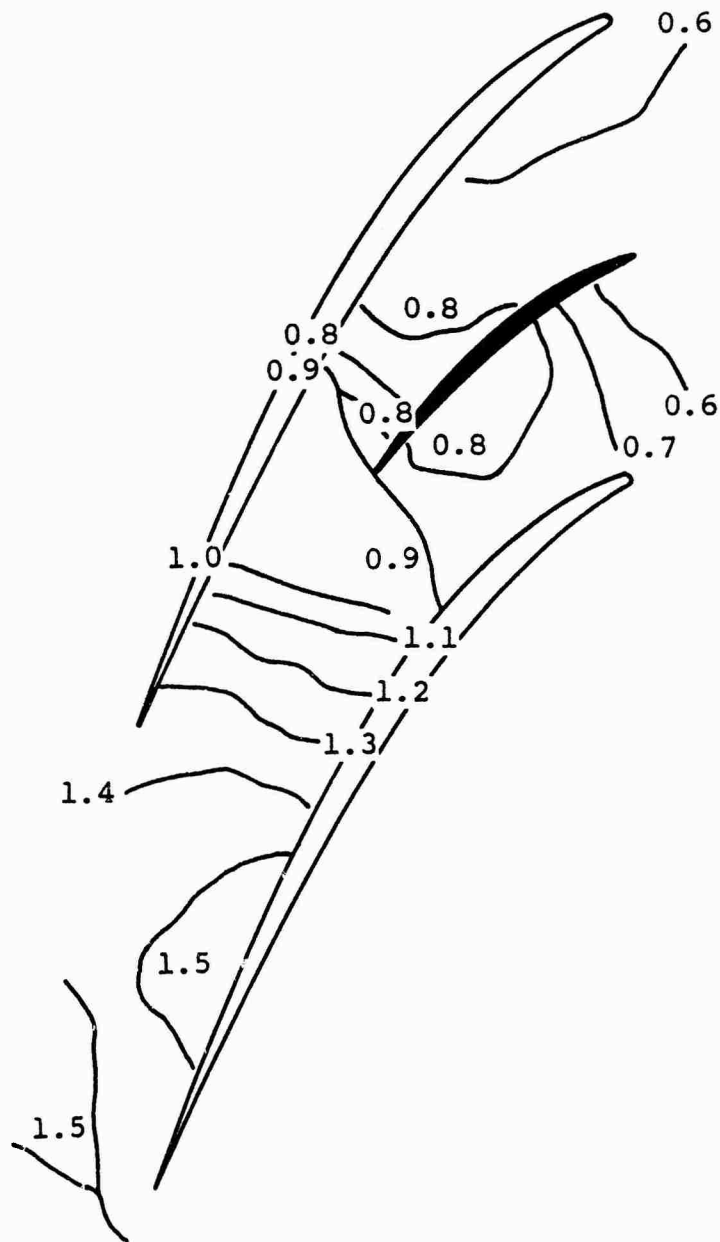


Figure 29b. Streamline Mach Number Distribution for Converging Cascade With Splitters Rotated Minus 3°.



SPLITTER VANE ANGLE =  $36.75^\circ$

Figure 29c. Internal Mach Numbers for Cascade With Splitters Rotated Minus  $3^\circ$ .

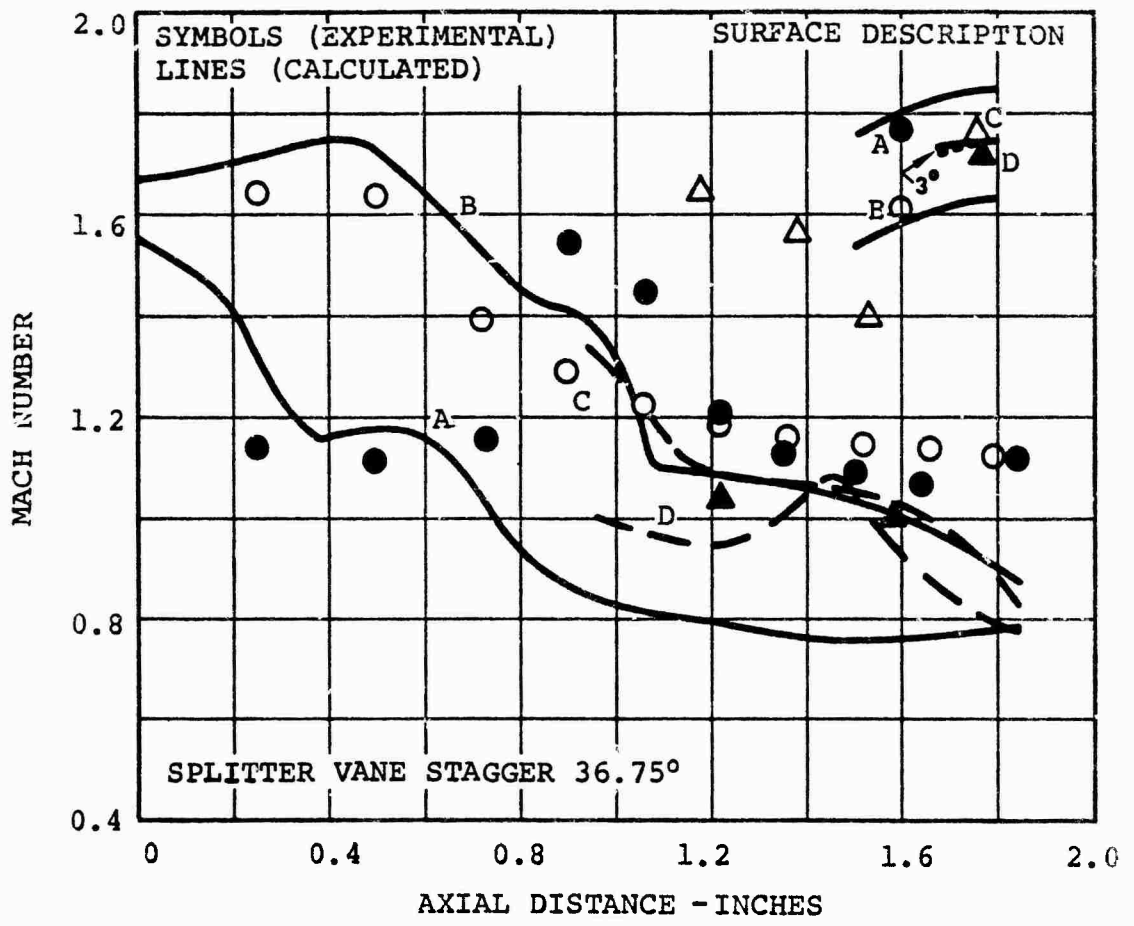


Figure 29d. Analytical and Experimental Wall Mach Numbers With Splitters Rotated Minus  $3^\circ$ .

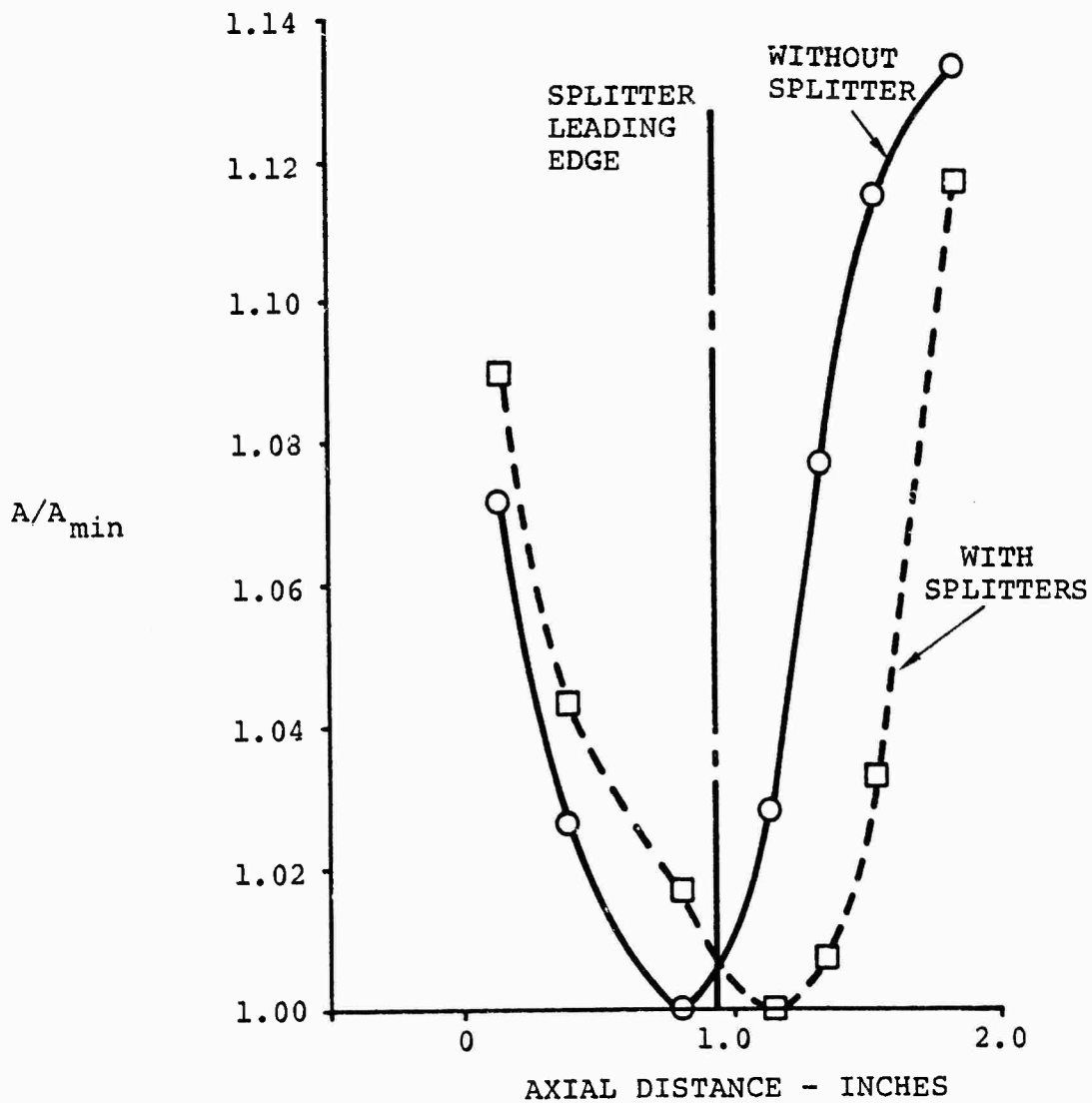


Figure 30. Area Distribution Through Cascade.

Section II. The result, given in Figure 31, shows approximately 60 percent of the flow passing between the splitter leading edge and the main blade suction surface. The area calculated for each streamtube relative to  $A^*$  (the choking area) of the upstream flow is shown in Figure 32. The net error in the geometric approach to area calculation is evident, since  $A/A^*$  should never be less than unity. This is true since the area comes from a solution that actually passed the flow. Nonetheless, the result is clear. The lower passage (between the splitter pressure surface and the main blade suction surface) is extremely deficient in area, while very large areas are available in the upper passage. An analysis of this indicates that the lower passage utilizes a  $b$ -width based on an average  $X$  that is larger than the upper passage. Since  $b$ -width converges rapidly with  $X$ , the result is a choked-lower passage.

### c. Discussion of the Results

The effect of choking the lower passage is markedly different between the experimental data and the calculation. In the relaxation calculation, a solution is not possible once the passage becomes choked. In the experiment, losses rise sharply in the choked (lower) passage and a flow shift towards higher upper passage flow results. This yields an incidence on the splitter that is quite different. Except at the highest stagger, the data indicates a positive incidence on the splitter. Calculations show a slight negative incidence at design stagger. The incidence shifts to positive as the stagger is decreased, indicating a neutral incidence between 39.75-degrees and 36.75-degrees splitter stagger. Comparison of the data indicates that experimental incidence was approximately 3-degrees higher than calculated incidence.

Further evidence of this choking can be obtained from the main blade pressure distributions. Pressure surface Mach numbers show a sharp rise in the vicinity of the splitter leading edge, which is not present when the splitter is removed. This is consistent with an increase in flow in the upper passage over what would normally be experienced. Since the method used will not calculate any case beyond the choke point, none of these effects are visible in the calculation. An attempt was made to modify the flow split away from one yielding lines of constant potential at the exit. However, the coding changes required to do this were beyond the scope of the program.

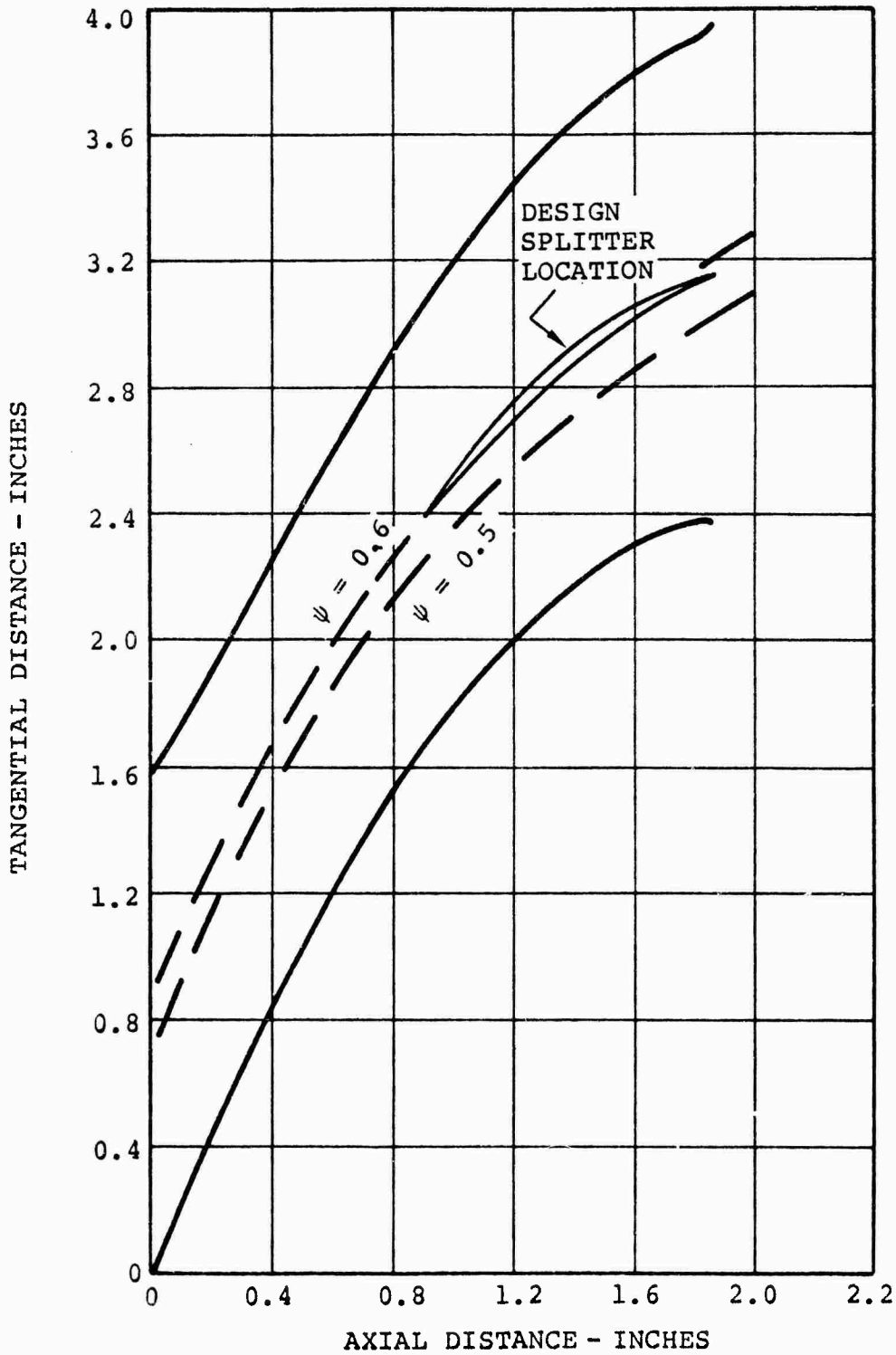


Figure 31. Inviscid Streamlines for Supersonic Cascade Without Splitters.

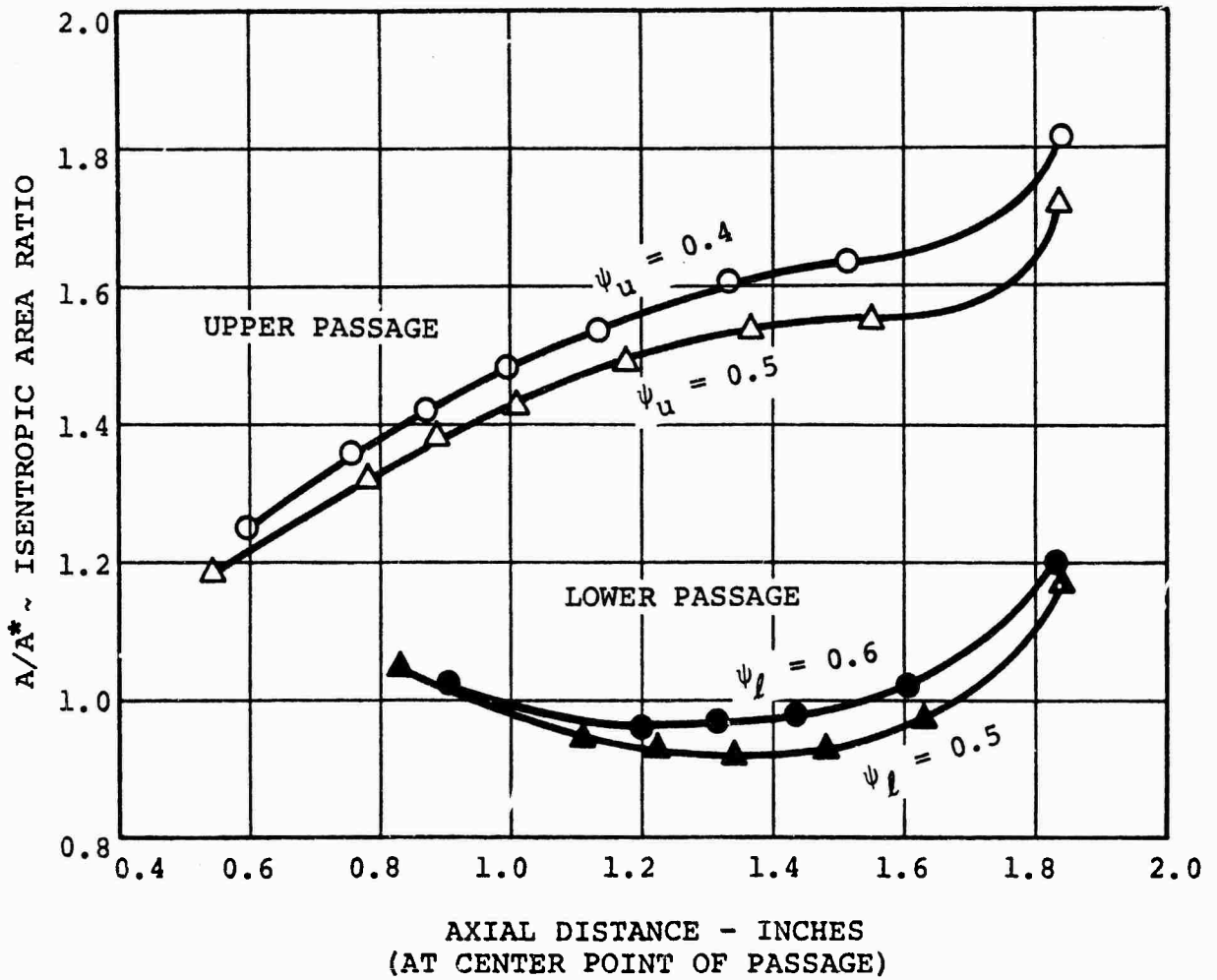


Figure 32. Area Ratio Conditions for Different Streamtubes in the Cascade.

### 3. PHASES III AND IV - SPLITTER REDESIGN

#### a. Methodology

Based on the results of Phases I and II, the following conclusions were achieved.

(1) Viscous effects are large enough to reduce the quality of agreement between the calculation and the experiment.

(2) The current cascade has a splitter configuration that (because of loss and boundary layer buildup) appears to operate with a choked lower passage.

(3) The choked lower passage causes a higher than predicted incidence on the splitter of approximately 3 degrees.

(4) A comprehensive comparison of experimental data and calculations is not possible with tested splitter configurations due to the absence of calculations beyond choke.

Even though comprehensive comparisons were not possible in Phase II, a redesign was attempted in Phase III. The choking condition observed in Phase II must be detrimental to cascade performance since it creates high losses in the lower passage and large over-velocities on the splitter suction surface due to the induced positive incidence. If a configuration exists that possesses adequate area and reasonable splitter pressure distributions, its performance should be better.

An examination of solutions without splitters (Figure 32) indicates that simply moving the splitter closer or further away from the suction surface will not help. The alternatives seem to be restricted to one of the following:

(1) Increasing splitter length until larger flow area is encountered

(2) Shortening the splitter until larger flow area is encountered

(3) Changes in camber line shape

(4) Changing b-width distribution

(5) Changing main blade shape

Alternatives (4) and (5) are changes to the entire rotor and, thus, are outside the scope of feasible changes. Consequently, Alternatives (1), (2), and (3) were investigated. Shortening the splitter is of more academic interest than practical value, since it would probably yield a rotor with stress and vibration problems. Lengthening the splitter would move the splitter leading edge into high Mach number regions, which would increase the loss of the splitter through increased dynamic head.

Changes in camber line might be effective, as a result of improved passage area, except that the splitter is very close to the minimum cascade area.

b. Increased Length

It would be desirable to place the splitter on a streamline at a position where adequate flow area would occur both above it and below it. The shape of the pressure surface would then be adjusted so that the area distributions would never fall below a certain minimum value. Such a design is shown in Figure 33. The leading edge is located at the 55-percent flow streamline. The pressure surface is selected to provide a constant  $A/A^*$  of 1.05. The resulting area distribution is shown in Figure 34. The grid system is shown in Figure 35. Unfortunately, this configuration results in a large negative incidence. The calculation indicates a large expansion in the lower passage, rising Mach number near the splitter leading edge, and a choked lower passage. This choking occurs even though on a one-dimensional basis, sufficient area exists to pass the flow. The expansion was strong enough to dominate the flow field and raised the Mach number to a point where the lower passage effective  $A/A^*$  was less than the actual geometric  $A/A^*$  available. This could result in a normal shock in front of the splitter along with a flow shift toward the upper passage in an actual cascade test. Clearly, this would be an undesirable condition.

To avoid this, the leading edge would need to be moved forward and the camber line established in a more gradual S-shape to control the expansion necessary for a contour with sufficient area to avoid choking. This problem is complicated by the decreasing b-width which serves to increase expansion levels further than would be the case with a two-dimensional cascade. As a result of this study, it did not appear that increased splitter length would yield a practical solution even with a change in splitter shape.

c. Shortened Splitter

A somewhat shortened splitter is illustrated in Figure 36. An area distribution is shown in Figure 37. Examination of Figure 37 indicates that the lower passage area distribution is relatively flat up to the trailing edge. Consequently, for a large improvement, an extremely shortened splitter would be needed. Little improvement would be expected with the shortened splitter shown in Figure 36. Figures 38a through 38d show the results of a calculation with no aerodynamic blockage. More severe b-width distributions yielded a choked lower passage as was the case with the design splitter. Further efforts along this line were abandoned since the splitter would need to be impracticably short to avoid a lower passage choke.

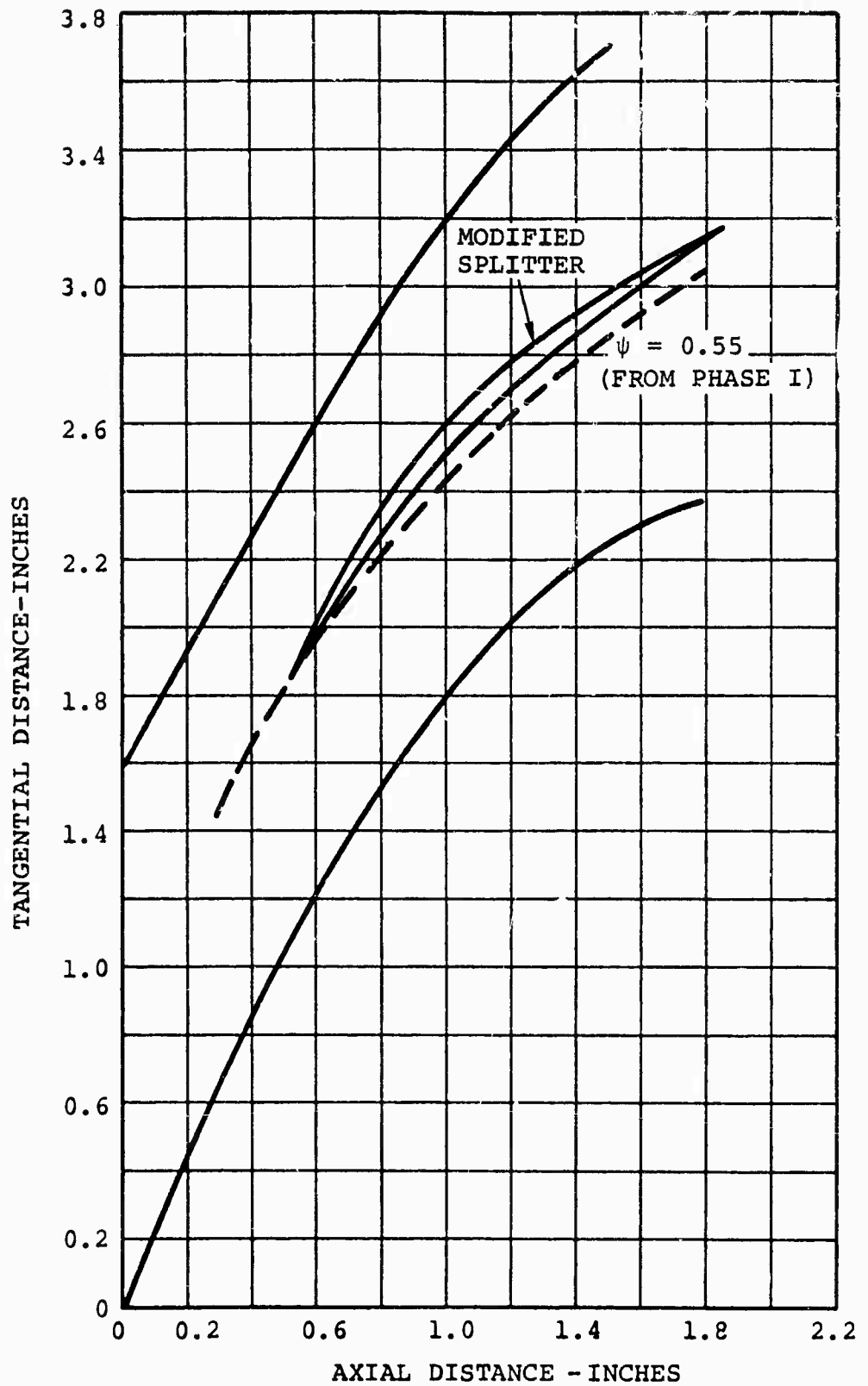


Figure 33. Modified Splitter for Cascade (Increased Length).

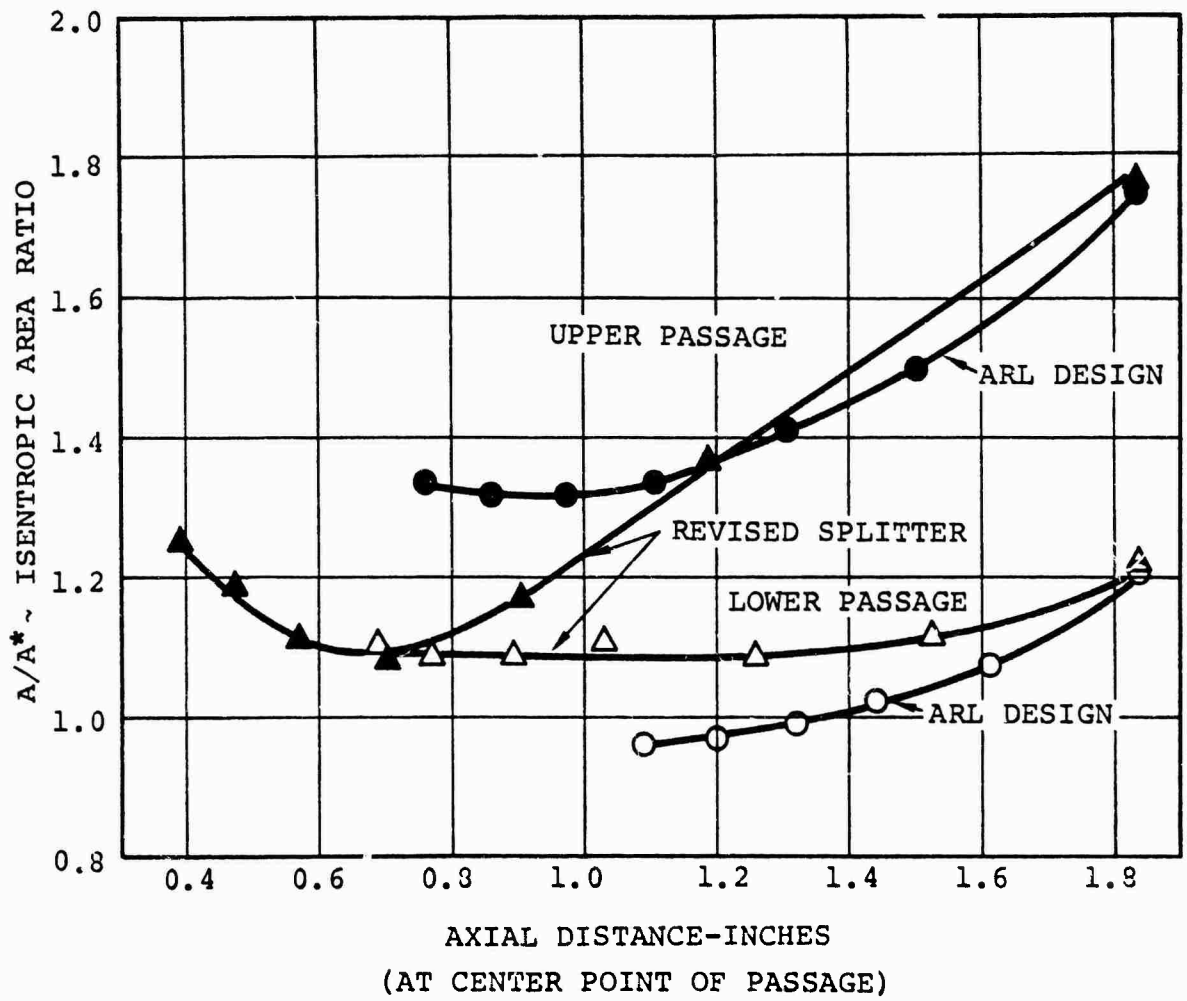


Figure 34. Area Distributions for Modified Splitter Passages (Increased Length).

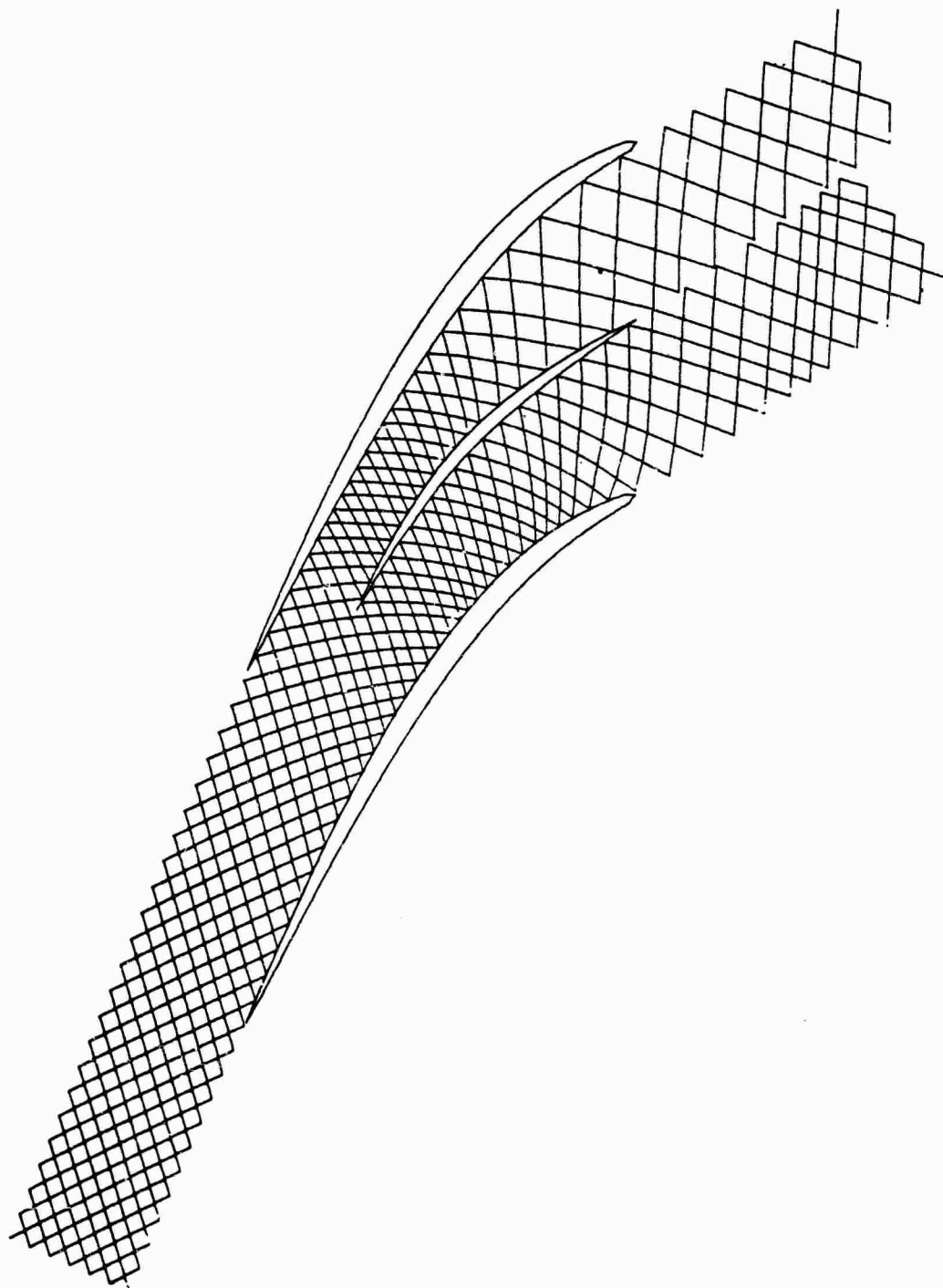


Figure 35. Grid System for Converging Cascade With a Modified Splitter Configuration (Increased Length).

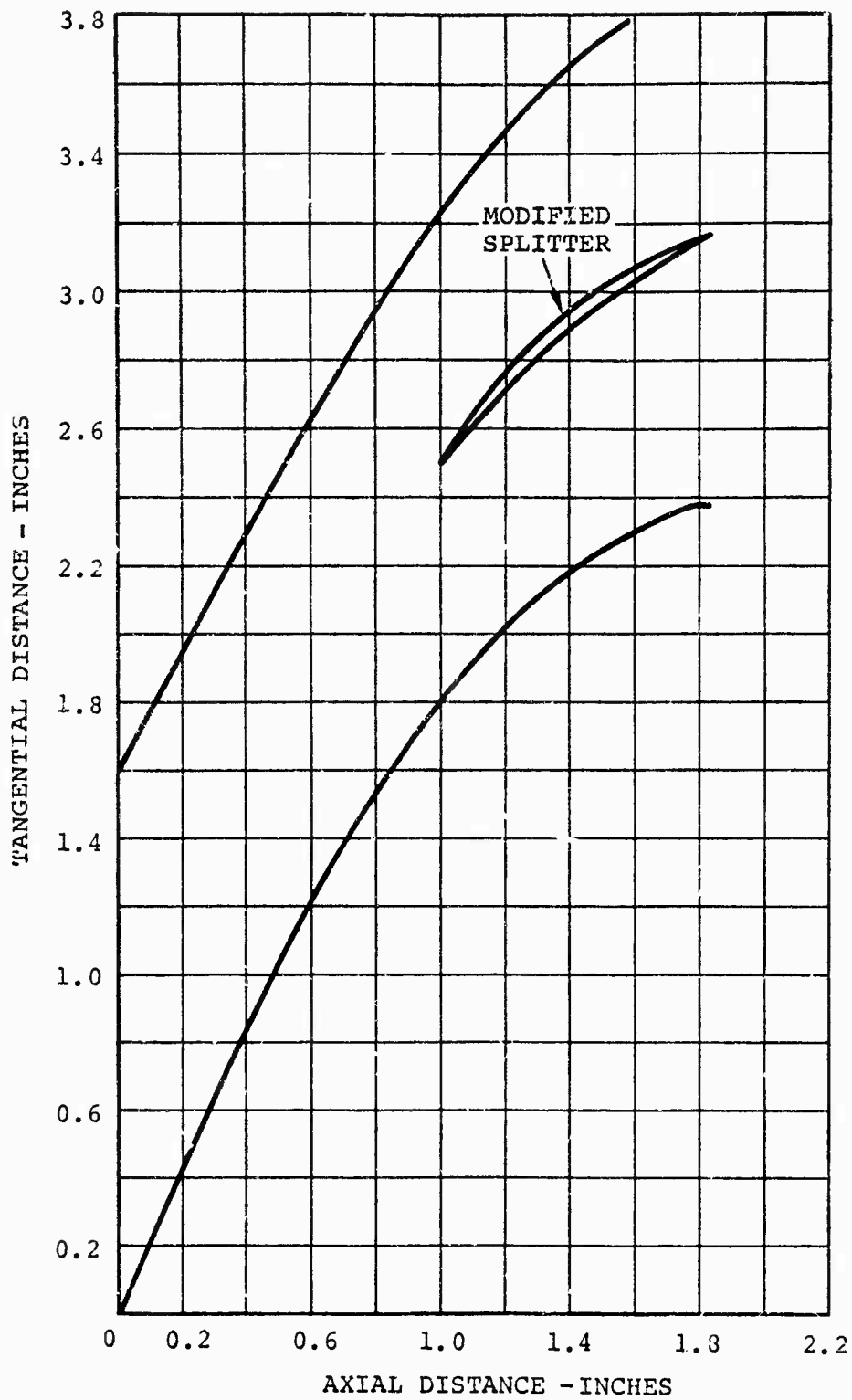


Figure 36. Modified Splitter for Cascade (Shortened Splitter).

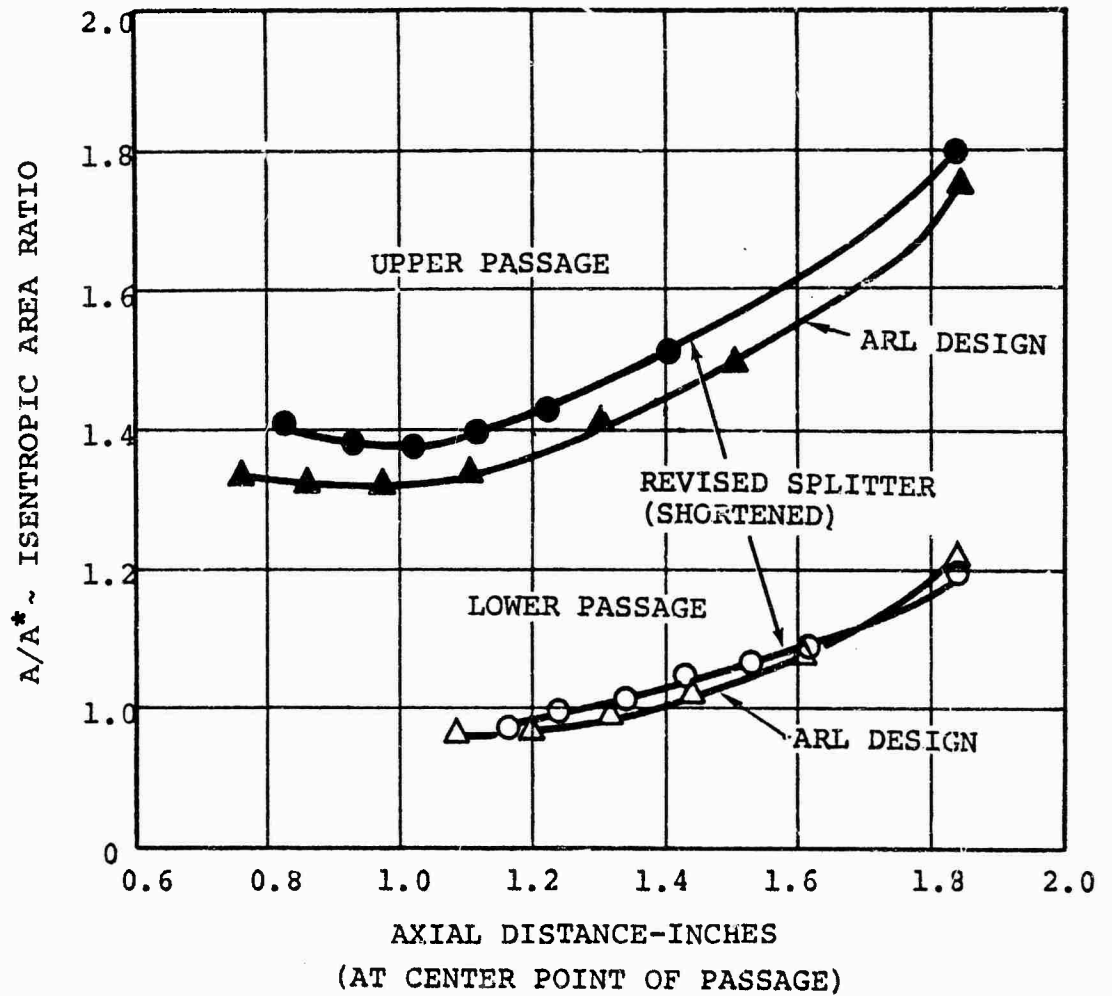


Figure 37. Area Distribution for Modified Splitter Passages (Shortened Splitter).

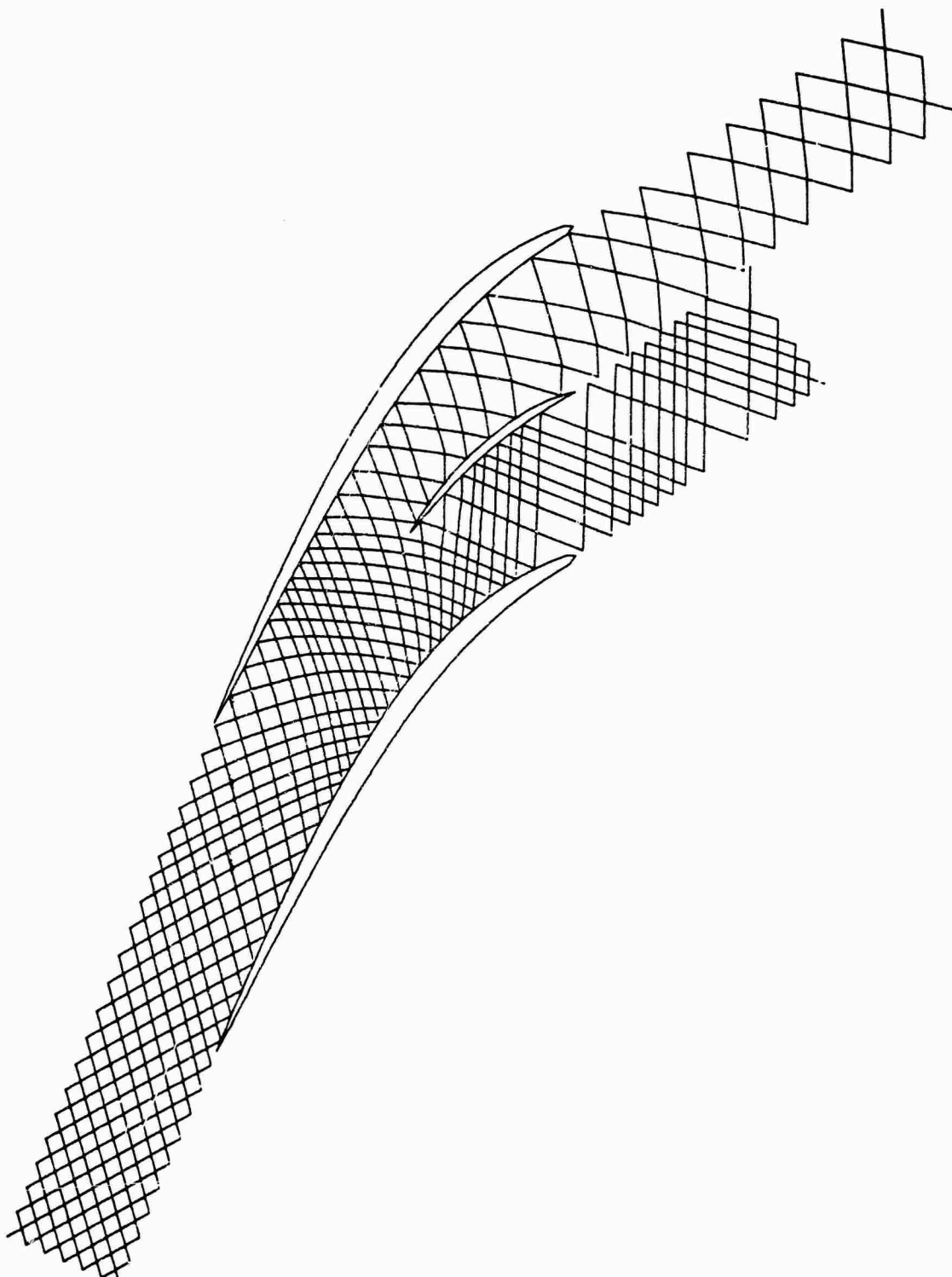
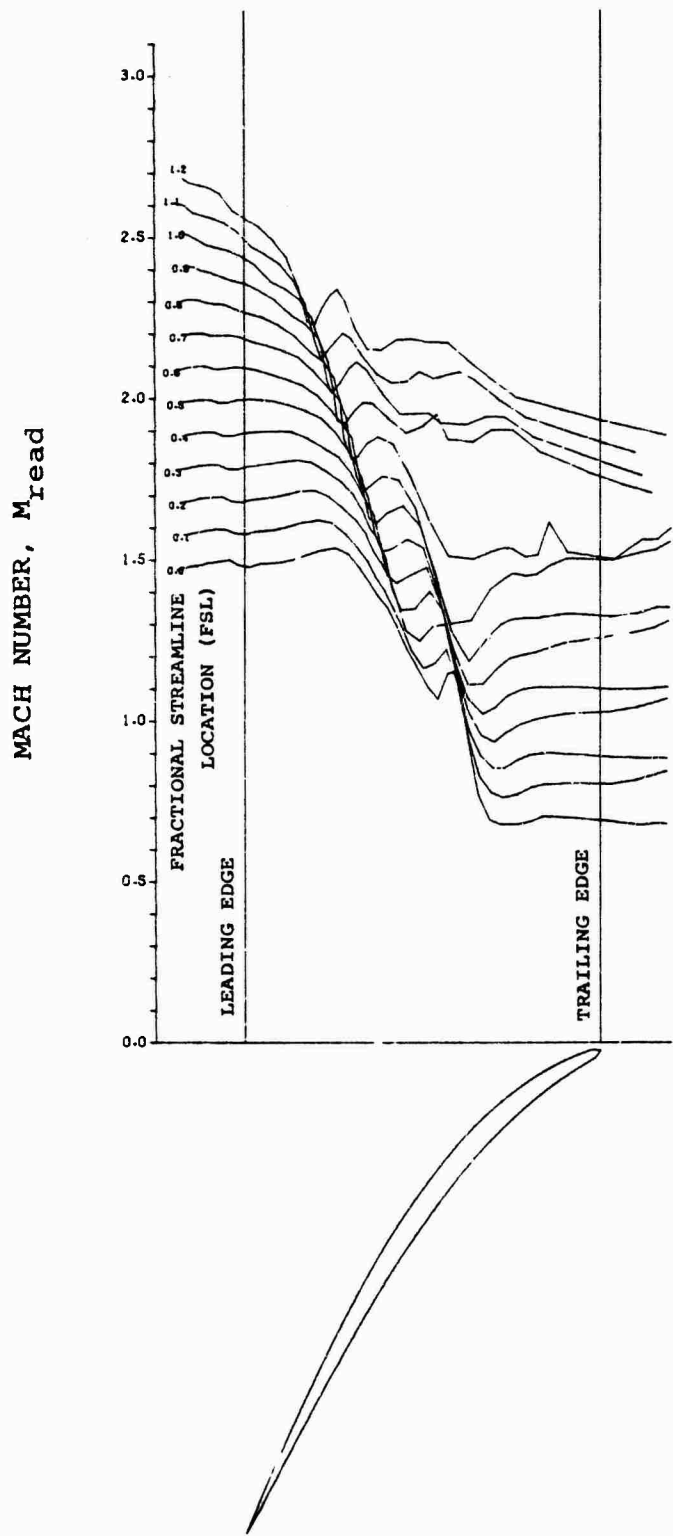


Figure 38a. Grid System for Converging Cascade With a Modified Splitter Configuration (Shortened Splitter).



$$M = M_{\text{read}}^{\text{-FSL}}$$

Figure 38b. Streamline Mach Number Distribution for Converging Cascade With a Modified Splitter Configuration (Shortened Splitter).

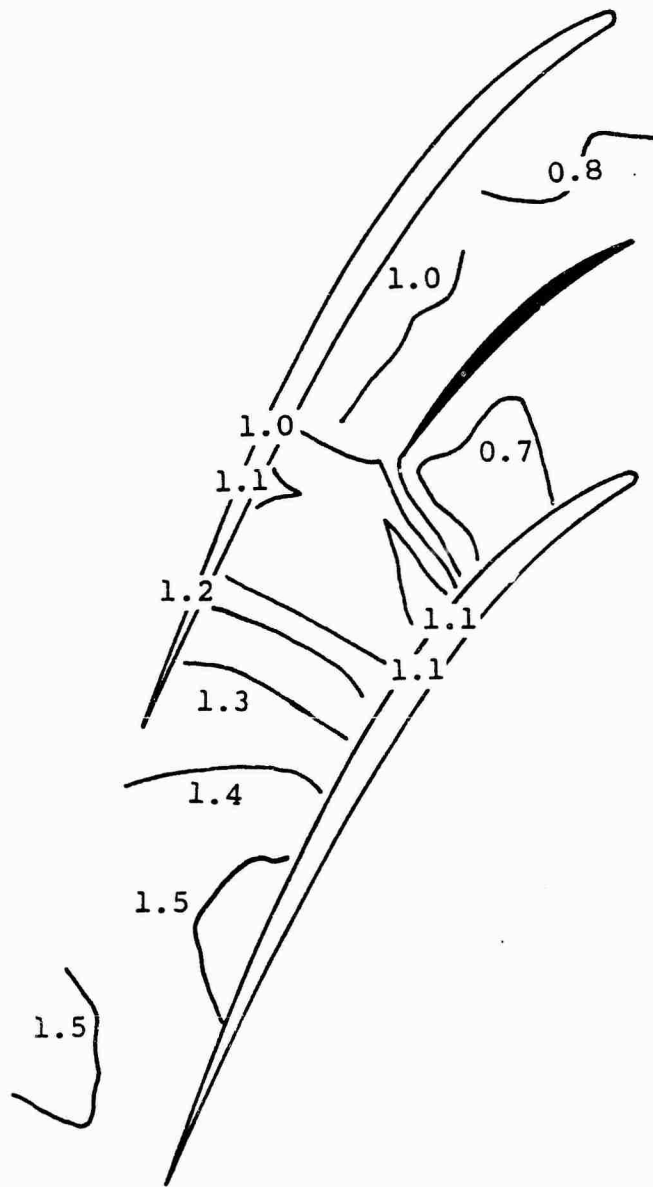


Figure 38c. Internal Mach Number Distribution for Cascade With Modified Splitter (Shortened Splitter).

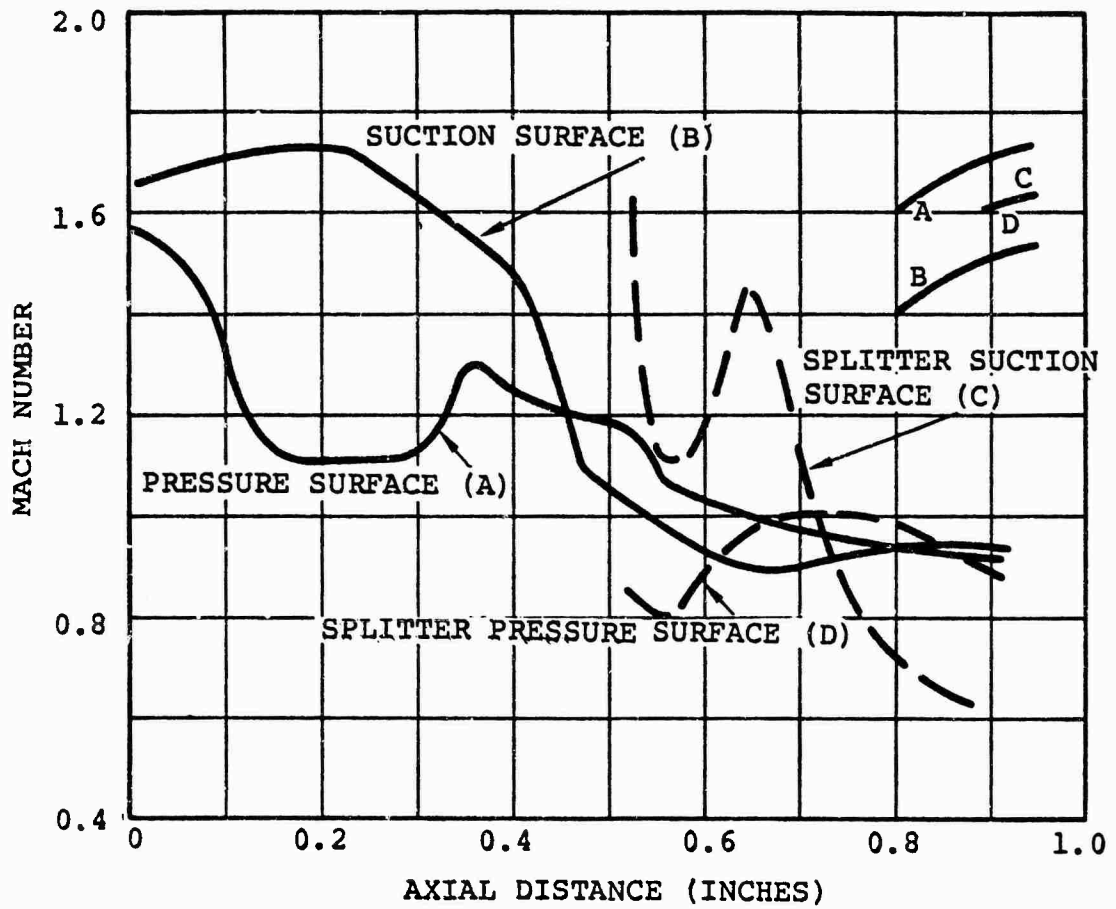


Figure 38d. Surface Mach Number Distribution for Cascade With Modified Splitter (Shortened Splitter).

#### SECTION IV

#### CONCLUSIONS

An inviscid calculation can be used to analyze fluid dynamic elements when viscous effects are sufficiently small to permit the flow to be dominated by pressure forces. When viscous effects are very low, good calculated predictions of pressure distributions can be obtained. This has been observed to be the case for most low-speed cascade data. As viscous effects become more prominent, the inviscid calculation does not accurately predict the effects of boundary layer growth and increased losses on the pressure distributions within the cascade. However, even when viscous effects are large, an inviscid calculation can be used to identify regions of high loading and to provide an insight to the major sources of high losses.

When a splitter vane is added to the cascade, the system becomes more complex. Viscous effects that caused only modest disagreements between calculated and experimental velocity distributions in the plain cascade are now largely responsible for establishing the flow capacity of the passages on each side of the splitter. Areas of high loss reduce the local flow capacity and cause flow shifts relative to the splitter that are not predicted analytically. As a result, the splitter incidence and surface velocity distributions are not accurately predicted.

To obtain a completely satisfactory modeling of the flow in the high-turning, transonic cascade will probably require a method that includes both local viscous effects and full recognition of the three-dimensionality of the problem.

## REFERENCES

1. Dodge, Paul R., "A Non-Orthogonal Numerical Method for Solving Transonic Cascade Flows," ASME 76-GT-63.
2. Dodge, Paul R., "A Transonic Relaxation Method for Cascade Flow Systems," presented at the von Karman Institute for Fluid Dynamics, Lecture Series 59, "Transonic Flow in Turbomachinery," May, 1973.
3. Holtman, R. L., G. D. Huffman, R. B. McClure, and G. T. Sinnet, "Test of a Supersonic Compressor Cascade (Vol. I)," ARL 72-0170, Vol. I, December 1972.
4. Dodge, Paul R., "The Use of a Finite Difference Technique to Predict Cascade, Stator, and Rotor Deviation Angles and Optimum Angles of Attack," ASME Paper No. 73-GT-10.
5. Griepentrog, H., "Shock Wave Boundary Layer Interaction in Cascades," in AGARDograph No. 164 on "Boundary Layer Effects in Turbomachines," J. Surugue, Editor, December 1972.
6. McDonald, P. W., "The Computation of Transonic Flow through Two-Dimensional Gas Turbine Cascades," ASME Paper No. 71-GT-89.
7. Holtman, R. L., R. B. McClure, and G. T. Sinnet, "Test of a Supersonic Compressor Cascade with Splitter Vanes," ARL 73-0142, December 1973.

## LIST OF SYMBOLS

|          |   |
|----------|---|
| A        | area  |
| AVR      | axial velocity-density ratio  |
| b        | streamtube height normal to plane of calculation                                |
| C        | chord length  |
| M        | Mach number   |
| P        | pressure  |
| q        | velocity head   |
| $t_m$    | maximum blade thickness   |
| (X,Y)    | coordinates of axial-tangential coordinate system                               |
| $\alpha$ | angle of attack, $\beta-\gamma$   |
| $\beta$  | flow angle with respect to axial direction                                      |
| $\beta'$ | blade angle with respect to axial direction                                     |
| $\gamma$ | blade stagger angle with respect to axial direction, or ratio of specific heats |
| $\delta$ | deviation angle, $\beta_{TE}-\beta'_{TE}$                                       |
| $\theta$ | turning angle, $\beta_1-\beta_2$  |
| $\rho$   | density   |
| $\sigma$ | cascade solidity  |
| $\psi$   | stream function   |

Subscripts

|    |                                |
|----|--------------------------------|
| 1  | upstream                       |
| 2  | downstream                     |
| l  | lower streamtube               |
| s  | static conditions              |
| S  | splitter                       |
| t  | total or stagnation conditions |
| TE | trailing edge                  |
| u  | upper streamtube               |
| X  | axial projection               |